

University of Nebraska - Lincoln

DigitalCommons@University of Nebraska - Lincoln

Architectural Engineering – Dissertations and
Student Research

Architectural Engineering and Construction,
Durham School of

Spring 5-2012

ELECTROMAGNETIC HARVESTING TO POWER ENERGY MANAGEMENT SENSORS IN THE BUILT ENVIRONMENT

Evans Sordiashie

University of Nebraska-Lincoln, sord.evans@huskers.unl.edu

Follow this and additional works at: <https://digitalcommons.unl.edu/archengdiss>



Part of the [Architectural Engineering Commons](#)

Sordiashie, Evans, "ELECTROMAGNETIC HARVESTING TO POWER ENERGY MANAGEMENT SENSORS IN THE BUILT ENVIRONMENT" (2012). *Architectural Engineering – Dissertations and Student Research*. 18. <https://digitalcommons.unl.edu/archengdiss/18>

This Article is brought to you for free and open access by the Architectural Engineering and Construction, Durham School of at DigitalCommons@University of Nebraska - Lincoln. It has been accepted for inclusion in Architectural Engineering – Dissertations and Student Research by an authorized administrator of DigitalCommons@University of Nebraska - Lincoln.

ELECTROMAGNETIC HARVESTING TO POWER ENERGY MANAGEMENT
SENSORS IN THE BUILT ENVIRONMENT

by

Evans Sordiashie

A THESIS

Presented to the Faculty of
The Graduate College at the University of Nebraska
In Partial Fulfillment of Requirements
For the Degree of Master of Science

Major: Architectural Engineering

Under the Supervision of Professor Mahmoud Alahmad

Lincoln, Nebraska

May, 2012

ELECTROMAGNETIC HARVESTING TO POWER ENERGY MANAGEMENT SENSORS IN THE BUILT ENVIRONMENT

Evans Sordiashie, M.S.

University of Nebraska, 2012

Adviser: Mahmoud Alahmad

Recently, a growing body of scholarly work in the field of energy conservation is focusing on the implementation of energy management sensors in the power distribution system. Since most of these sensors are either battery operated or hardwired to the existing power distribution system, their use comes with major drawbacks. Battery maintenance and associated labor costs can make implementing sensors very expensive. Although hardwired sensors require very little post-installation maintenance, any energy savings they may procure is offset by the amount of energy expended during the course of the sensors normal operation. In response to these energy challenges, this thesis proposes an electromagnetic harvesting device that powers such sensor technologies by scavenging low electromagnetic field energy. First, the quantities of magnetic flux densities around common current carrying conductors in the built environment are estimated according to the equivalent amount of power that can be generated. Then, a prototype of the harvesting device for scavenging low magnetic flux is designed and developed. Finally, the device is evaluated for real-world implementation using a novel prototype board.

ACKNOWLEDGEMENT

I would like to thank my adviser, Dr. Mahmoud Alahmad, for his continued support and presence as a source of advice, guidance, and assistance during my academic career.

I would also like to extend my appreciation to my research colleague, Timothy Wisnieski for his continued support throughout this research.

DEDICATION

I would like to dedicate this work to my wonderful family who are my inspiration, my happiness, and my source of energy.

GRANT INFORMATION

This project is funded and sponsored by the Durham School of Architectural Engineering and Construction.

TABLE OF CONTENTS

GRANT INFORMATION.....	v
LIST OF FIGURES	viii
LIST OF TABLES.....	ix
INTRODUCTION	1
1.1 Motivation.....	1
1.2 Problem Formulation	3
1.3 Research Goals.....	6
1.4 Thesis Overview	7
BACKGROUND	8
2.1 Energy Harvesting System.....	8
2.1.1 Energy Sources	8
2.1.2 Converting Processes	11
Photovoltaic Harvesting.....	12
Thermogenerator.....	12
Piezoelectric Harvester	12
RF Energy Harvester (Rectenna)	13
Electromagnetic Harvester.....	13
2.1.3 Load	14
2.2 Related Work	14
AN OVERVIEW OF ELECTROMAGNETICS & TRANSFORMERS	21
3.1 Introduction.....	21
3.2 Overview of Electromagnetics.....	21
3.2.1 Biot-Savart Law	22
3.2.2 Ampere's Law and Magnetic Flux Density	24
3.2.3 Ferromagnetic Materials	25
3.3 An Overview of Electrical Transformers.....	27
3.3.1 Current Transformers (CT)	30
3.3.2 Transformer Core Saturation	34
RESEARCH OBJECTIVE, METHODOLOGY, AND DESIGN	36
4.1 Introduction.....	36
4.2 Research Objective and Methodology	36
4.3 The Design Process.....	40

4.3.1 Design Calculations	41
RESULTS AND DISCUSSION	49
5.1 Introduction.....	49
5.2 Electromagnetic Energy Around Current Carrying Conductors	50
5.3 Induced and DC Output Voltages	52
5.4 Core Size, Versus Magnetic Flux and Input Load Current	55
5.6 Simulation vs. Experimental Results	62
5.7 Discussion	63
TECHNICAL CHALLENGES, BENEFITS AND OPPORTUNITIES.....	65
6.1 Introduction.....	65
6.2 Challenges.....	65
6.3 Benefits	66
6.4 Opportunities	67
CONCLUSION AND RECOMMENDATIONS.....	69
7.1 Future Research	70
APPENDICES	71
Appendix A.....	71
Appendix A.1: Wire Properties Table for Winding Conductors (50)	71
Appendix B	72
Appendix B.1: Specifications of AMCC-4 Core	72
Appendix B.2: Winding Schematic Drawings of AMCC-4 Core.....	73
Appendix C	74
Appendix C.1: MATLAB Programming Codes	74
REFERENCES	100

LIST OF FIGURES

Figure 1.1: US Net Electricity Generation by Energy Source for 2011.....	2
Figure 1.2: CO ₂ Emissions from Fossil Fuels Due to Electricity Generation in 2009 (3).	3
Figure 1.3: Conceptual Diagram of the Energy Harvesting Device in the Electrical System	6
Figure 2.1: Components of Energy Harvesting Systems	8
Figure 2.2: Summary of Potential Energy That Can Be Harvested from Humans (30)	11
Figure 2.3: Available Magnetic Field Harvesting Products.....	14
Figure 2.4: Multiturn Coil on a Magnetic Core Around A Current Carrying Conductor (42)	17
Figure 2.5: Rectangular Coil Near a Current Carrying Conductor (42)	17
Figure 2.6: Measured Induced Voltages From (42).....	19
Figure 3.1: Electric Current Relationship with Magnetic Field, Biot-Savart (1).....	22
Figure 3.2: Magnetic Field Around Current Carrying Conductor of Finite Length	23
Figure 3.3: Domain Alignment in Ferromagnetic Materials.....	26
Figure 3.4: A Simplified Diagram of an Electric Transformer (5)	28
Figure 3.5: Simple Transformer Circuit.....	29
Figure 3.6: Simplified Circuit Diagram of a Current Transformer	31
Figure 3.7: Complete Circuit Diagram of a Current Transformer with a Bridge Rectifier.....	32
Figure 3.8: Current Transformer Core and Window Area.....	33
Figure 4.1: Standard Metal Boxes Used in Electrical Wiring Systems (Table 314.16 (A), NEC 2008)	37
Figure 4.2: Energy Harvesting Device Core Specifications (proposed design).....	41
Figure 4.3: Cross-Sectional Area of the Core	41
Figure 4.4: Core Window Area.....	42
Figure 4.5: Circuit Diagram of the Energy Harvesting Device.	44
Figure 4.6: Voltage Doubler Circuit	47
Figure 4.7: Voltage Regulator Incorporated into the Voltage Doubler Circuit	47
Figure 5.1: Magnetic Flux Density Around a 10 A Current Carrying Conductor	50
Figure 5.2: A Cut Through Section of Magnetic Flux Density Around a 10 A Current Carrying Conductor.....	51
Figure 5.3: Magnetic Flux Density for Different Currents from 1-20 A	52
Figure 5.4: Induced Voltages per Primary Load Input (Watts)	53
Figure 5.5: Induced Voltages per Primary Load Currents (A).....	53
Figure 5.6: A Combination Plot of Induced Voltage Against Primary Input Load and Radial Distances from MPL (300 turns of #25 Secondary Winding)	54
Figure 5.7: A Combination Plot of Induced Voltage Against Primary Input Load and Radial Distances from MPL (500 Turns of #25 Secondary Winding)	54
Figure 5.8: DC Output Voltages per Primary Input Load Currents.....	55
Figure 5.9: Core Cross Section vs. Available Magnetic Flux Density	56
Figure 5.10: Core Cross Section Vs. Primary Input Current	56
Figure 5.11: Combination Plot of Cross Sectional Area vs. Primary and Radial Distances.....	57
Figure 5.12: Prototype Energy Harvesting device made from AMCC-4 Core.	58
Figure 5.13: Board for Energy Harvesting Experiments	58

Figure 5.14: Schematic Diagram of the Experimental Board	60
Figure 5.15: Experimental Induced Voltages with AMCC-4 Core.....	61
Figure 5.16: Experimental Induced Voltages with AMCC-4	61
Figure 5.17: Comparison of Simulated and Experimental Induced Voltages.....	62

LIST OF TABLES

Table 1.1: Power Consumption Data for Some Common Energy Monitoring Sensors	4
Table 2.1: Magnetic Field Energy Harvesting for Different Core Configurations (41)	16
Table 3.1: Relative Permeabilities of Common Ferromagnetic Materials (46)	27
Table 4.1: Sensor Energy Demand Specifications.....	40
Table 5.1: Simulated and Experimentally Measured Induced Voltages ($r = 8\text{mm}$).....	62

Chapter 1

INTRODUCTION

The efficient management of our energy needs in the built environment requires that we carefully account for each trickle of energy we consume. Recently, engineers have been using efficient energy management sensors as a way to monitor energy and accomplish energy control tasks. Unfortunately, these sensor technologies use energy in the performance of such tasks. This thesis focuses on electromagnetic harvesting as a way to power wireless energy monitoring sensors in the built environment. Energy can be saved if sensors are powered by free electric energy scavenged from the built environment. This research looks into creating an effective energy management system that both utilizes an ambient energy source and reduces costs through low maintenance requirements.

1.1 Motivation

This chapter presents the motivation for this research as well as an overview of the various chapters of the research. Since the oil crisis of the 1970s, novel ways to conserve energy have continued to be a top research priority for energy scholars in the United States. Population growth coupled with an insatiable quest for newer electronic technologies has led to a demand for electricity that will surely continue to grow. Unfortunately, it is not yet clear if we are prepared to keep up with this increasing demand in the future. The World Energy Outlook estimates a 76% increase in electricity

use between the years of 2007 to 2030 with an average yearly growth rate of 2.5% (1). However, the demand for electricity has exceeded power transmission growth by 25% since 1982 (2). This is very alarming considering the fact that some 2 billion people currently have no access to electricity (1). Moreover, about 20% of the total CO₂ emissions in the U.S. result from electricity generation alone (3). Figures 1.1 and 1.2 give the U.S. electricity generation by source and equivalent CO₂ emissions from fossil fuels. Since just a little over 13% of our electricity needs are currently generated from renewable energy sources, carbon emissions will continue to endanger the health of the planet for years to come.

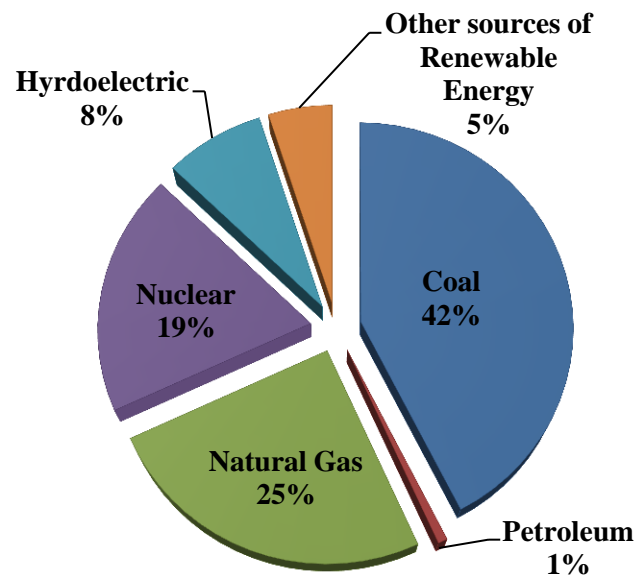


Figure 1.1: US Net Electricity Generation by Energy Source for 2011
Jan, (Source: Energy Information Administration (EIA), Electric Power Monthly, January 30, 2012, Table 1.1), (4).

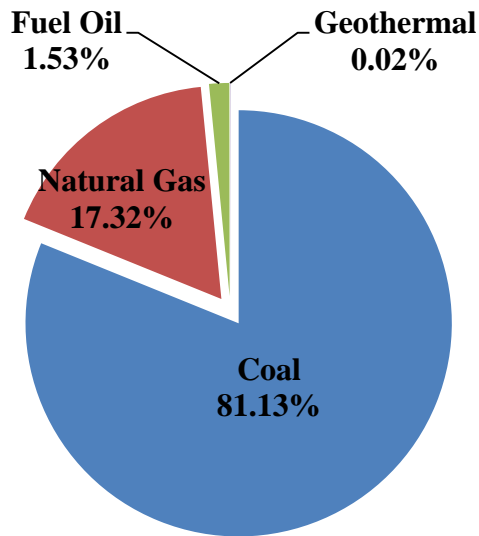


Figure 1.2: CO₂ Emissions from Fossil Fuels Due to Electricity Generation in 2009 (3).

While it should be noted that some scholars have found the relationship between global warming and carbon emissions debatable (5), (6), (7), it is well agreed that our natural resources are being depleted for energy generation.

1.2 Problem Formulation

As part of the effort to curb the rate at which our natural resources are being depleted, it is very important that we not only look for ways to generate energy from renewable sources but also to lower our own energy usage. This means efficiently managing our energy usage both at the residential and commercial level as well as in the built environment as a whole. Recent technologies (8), (9), (10) are focusing on monitoring energy at the node level to conserve energy in the built environment. A node

or outlet is any point in the electrical distribution system at which current is drawn to power electric equipment (11). Real-time energy consumption data can be collected by attaching sensor monitoring devices to these nodes. This has been accomplished in a variety of ways in the prior literature. The investigators in (8), for example, attached wireless sensors to every node in the electrical distribution system for energy monitoring and conservation purposes. However, the sensors themselves consume some energy during normal operation.

Generally, sensors are either battery operated, hardwired from the existing electrical system or are both battery operated and hardwired. Such configurations ensure that the sensor continues to operate during power outages. In a hardwired system, some of the conserved energy will in turn be reused by the sensors during operation. This means that more actual energy will be conserved if the sensors do not draw energy from the existing electrical system. The lifespan of batteries in battery operated sensors last about 9 months in duration. Table 1.1 shows the power consumption data for some common energy monitoring sensors.

Table 1.1: Power Consumption Data for Some Common Energy Monitoring Sensors

Wireless Product	Current Consumption			Battery Voltage	Power Consumption
	Transmission mode	Reception mode	Sleep mode		
RCS-S09U Universal ISM Band FSK Transceiver Module (12)	15mA - 26mA	11mA - 15mA	0.3 μ A	2.2V-3.8V	33mW - 78mW

G-Link 2.4 GHz Wireless Accelerometer Node (Micro Strain) (13)	25mA	25mA	0.5mA	3.7V	92.5mW
IMOTE2 (Crossbow) (14)	33mA	33mA	390 μ A	3.2V-4.5V	127.05mW
XBEE Zigbee/802.15. 4 Modules (DigiInternational) (15)	50mA	50mA	10 μ A	2.8V-3.4V	155mW
DataBridge wireless I/O modules (16)	37mA - 120mA	37mA - 120mA	< 100uA	2.7V –3.6V	116.55mW - 378mW
Apex and Apex LT Modules (17)	170mA	37mA	5 μ A	2.1V-3.6V	105.45mW - 484.5mW
Lt Series Transceiver Module (18)	12mA - 14mA	12mA - 14mA	11.5 μ A-20 μ A	2.1V-3.6V	34.2mW - 39.9mW
Si4420 Universal ISM Band FSK Transceiver (19)	13mA - 26mA	11mA -15mA	0.3 μ A	2.2V-5.4V	41.8mW - 98.8mW

Batteries for battery operated sensors require periodic replacement after they lose all of their energy. Calculations for the total replacement costs must therefore include not only the cost of the batteries but also any additional labor requirements. An average home containing 30 nodes equipped with such sensors will thus be quite expensive to maintain.

As a way to tackle the power demand of these energy management sensors, this thesis proposes the use of electromagnetic energy harvesting to supply their power needs. Figure 1.3 is a conceptual diagram of the proposed energy harvesting method for supplying power to the sensors.

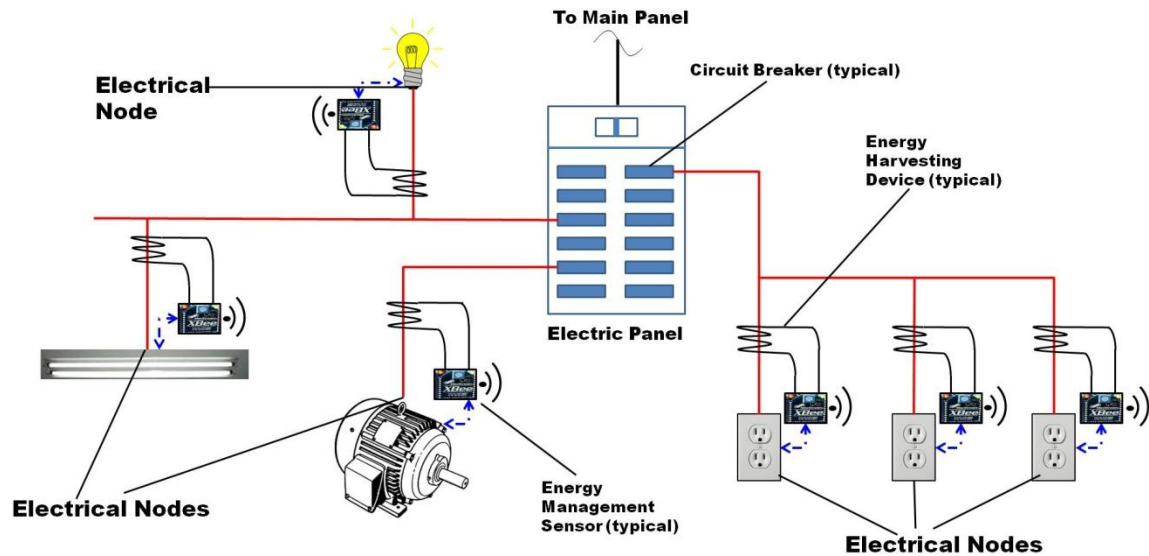


Figure 1.3: Conceptual Diagram of the Energy Harvesting Device in the Electrical System

1.3 Research Goals

One of the goals of this research is to develop a "free" energy source that can power energy management sensors in the built environment. Achievement of this goal will not only increase energy conservation in the built environment but also reduce sensor related maintenance costs. Thus, sensors will eventually be energy neutral and able to operate for an indefinite amount of time.

A second goal of this research is to investigate and determine if electromagnetic energy harvesting is a viable energy source for generating power for other low-powered devices. Electromagnetic harvesting will reduce human dependence on batteries to meet the energy requirements of low-powered devices in the built environment. In fact, it may even make low powered devices autonomous so that they could be employed in hazardous or inaccessible locations in the built environment. It should also be mentioned that one of the related benefits of using the proposed device is that it is an eco-friendly solution, and, with widespread use, may reduce pollution caused by battery disposal

landfills. Last but not least, it is hoped that the proposed work will promote innovations in the built environment that lead to increased energy conservation. This research will open doors to enable the design and manufacturing of future sensor products for electrical energy conservation that incorporate this energy harvesting technology.

1.4 Thesis Overview

The remaining sections of this thesis are broken into 7 major chapters. Chapter 2 gives background information on energy harvesting systems, definitions, and descriptions of common energy harvesting methods, related research and the objectives of this thesis. Chapter 3 gives an overview of electromagnetics and the theory of transformer basics. Chapter 4 describes the research objective, methodology and design. Chapter 5 provides a simulation of and gives experimental data on the proposed energy harvesting device. Chapter 6 summarizes some of the technical challenges involved with use of the device and possible future applications of the device. Finally, Chapter 7 concludes with a review of the information presented in this thesis.

Chapter 2

BACKGROUND

Chapter 2 introduces the definitions, terms, energy harvesting methods and related work that form the foundation for the work presented in this thesis. This chapter will also discuss the proposed work.

2.1 Energy Harvesting System

Energy harvesting systems are made up of three basic components: The energy source, energy scavenger (active component) and external electrical circuit. Figure 2.1 shows a typical energy harvesting system.

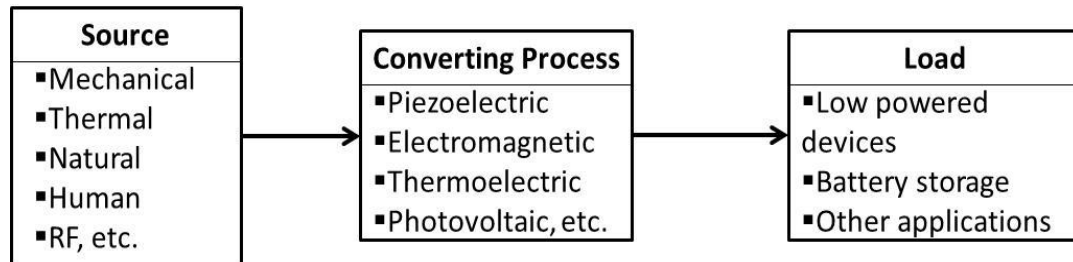


Figure 2.1: Components of Energy Harvesting Systems

In order to harvest useful electrical energy, these three basic components must be in place at all times. The following section gives a summary of common energy sources.

2.1.1 Energy Sources

The most common energy harvesting sources are natural (solar, wind, ocean, etc) energy, mechanical energy, radio frequency (RF), and human (physical) energy (20),

(21). Other types of energy sources include thermoelectricity (temperature variations) and electromagnetic energy.

Sources of natural energy include solar, wind, ocean waves, and water movements. Energy derived from these sources is mostly called renewable energy. Close to 13% (see Chapter 1) of the total electrical energy generated in the United States comes from renewable sources. Of these sources, conventional hydroelectric energy is the leading supplier or provider. The production of hydroelectricity involves using the gravitation pull of water to turn a generator powered turbine. China is currently the world's leading producer of conventional hydroelectricity followed by Canada and the United States, respectively (22).

Recently, solar and wind power are becoming popular sources of energy to harvest. Energy from light (solar power) is directly converted to electrical energy using solar cells (photovoltaic cells). Sunlight is the major source of light for most solar power generation plants. Some common smaller applications of solar power are portable hand calculators, wrist watches and street lights (23). Wind power is generated through the conversion of energy from a fast moving wind source. Wind turbines, which are typically designed with two or three blades mounted on a shaft from a rotor, capture wind energy (through a spinning action) to generate electricity (24). In order to generate large quantities of energy using this source, power companies have to mount hundreds of individual wind turbines over a widely spaced area. Places in which such mass power can be generated are called wind farms. Wind farms may be located in both onshore and offshore areas.

Mechanical energy is created by the motion or vibrations from machines, mechanical stress and strain from high-pressure motors, manufacturing machines, and other related rotational activities (25). In general, harvesting devices for vibrational sources fall in three main categories: electrostatic, piezoelectric and electromagnetic (26). Small, self-powered devices that use mechanical harvesting are known as micro-electromechanical systems (MEMS), (26), (27).

RF energy is another energy harvesting source that can be broadcast radios, public telecommunication services and other dedicated RF devices (28). The energy harvesting device (rectenna) is able to convert the RF energy into direct current (21). RF energy is inversely proportional to distance and therefore drops as the distance from a source is increased.

Humans generate energy that is a combination of mechanical and thermal energy derived from bodily activities. Running, walking, and other movements produce kinetic energy that can be converted into power. In (29) for example, energy generated from walking was used to harvest electrical energy by the piezoelectric method. In the past, hand-cranked radios and other similar devices were powered by human movement. A summary by Starner of the potential energy that can be harvested from humans is shown in Figure 2.2 (30).

Temperature differences between two points can also be used to generate electrical energy. This is commonly known as thermoelectricity. Thermoelectricity is the direct conversion of a temperature difference into electricity. The device used to generate thermoelectricity is called a thermogenerator (21). Thermoelectricity is referred to in some texts as the “Peltier-Seebeck effect” named after Thomas Seebeck who discovered

electric current flow between the junctions of two different metals at different temperatures.

<i>Activity</i>	<i>Kilocal/hr</i>	<i>Watts</i>
sleeping	70	81
lying quietly	80	93
sitting	100	116
standing at ease	110	128
conversation	110	128
eating meal	110	128
strolling	140	163
driving car	140	163
playing violin or piano	140	163
housekeeping	150	175
carpentry	230	268
hiking, 4 mph	350	407
swimming	500	582
mountain climbing	600	698
long distance run	900	1,048
sprinting	1,400	1,630

Figure 2.2: Summary of Potential Energy That Can Be Harvested from Humans

(30)

Electromagnetic fields are becoming a viable source for energy harvesting. While it is not a naturally available source of energy, it does occur around existing power distribution lines. Using Faraday's law of induction, an electromotive force (emf) is induced in an inductor (coil) placed in a magnetic field. Electricity from Faraday's principle is generated by relative movement of the inductor coil in a permanent magnetic field or an inductor placed in a changing magnetic field.

2.1.2 Converting Processes

Ambient energy exists all around us and can be transformed into a useful energy source. This section gives a brief summary of some commonly available energy harvesting methods.

Photovoltaic Harvesting

The photovoltaic (PV) effect is the process through which a photovoltaic cell (solar cell) converts light into electricity. Photons traveling to the surface of photovoltaic cells are absorbed and their energy transferred to make electricity. Solar power is the most common source of light energy harvesting due to its high power density (31). In addition to natural solar light, indoor fluorescent and tungsten lamp illuminations are also potential sources for harvestable light energy. Much less energy can be harvested from indoor environments compared to outdoor environments since less electricity can be generated by PVs with decreasing light irradiance (24).

Thermogenerator

A thermogenerator is a device that generates electricity by converting the temperature difference between two points, a process known as the thermoelectric effect. Thermogenerators are usually attached to bodies or devices which have a comparable temperature difference in relation to their surrounding environment. A good example of the thermoelectric effect is a wrist watch powered by electricity generated from body heat (32).

Piezoelectric Harvester

Quartz crystals have the ability to generate electricity when pressure is applied to them (33). This process is known as the piezoelectric effect or piezoelectricity. In principle, piezoelectricity involves the accumulation of electric charges in solid materials when mechanical stresses are applied to them. Apart from pressure, other kinetic schemes, such as strain, stress, and distortion, can also be applied to piezoelectric materials to generate electricity. Conversely, a mechanical deformation (shrinking or

expansion) is produced when an electric field is applied to piezoelectric materials. Commonly used piezoelectric materials are ceramics. Some useful applications are ceramic resonators, ceramic bandpass filters, ceramic discriminators, ceramic traps, SAW filters, and buzzers (34).

RF Energy Harvester (Rectenna)

The rectenna is the harvesting device used to scavenge power from RF energy (21). It consists of a receiving antenna and a rectifier circuit which converts RF or microwave power into useful DC power (35). The five main components of a rectenna are an antenna, input low-pass filter, rectifying diode, output filter, and resistive load (36). Design and experiments of a high-conversion-efficiency rectenna are found in (36).

Electromagnetic Harvester

From Faraday's law of induction, an induced electromotive force is generated in an inductor (conductor) placed in a magnetic field. This principle is also called electromagnetic induction. The conductor typically takes the form of a coil and electricity is generated by either the relative movement of the coil and the magnet, or via a stationary coil in a changing magnetic field. The converse of this principle is also true. Thus, a magnetic field is generated around a conductor carrying electrical current. The research proposed herein focuses on generating electrical energy by exploiting this combined principle. A magnetic field is generated around current carrying conductors in the built environment. This magnetic field is used in this research to produce electricity for the purposes of supplying energy to energy management sensors. Since the sensors are located close to the electrical nodes, the electromagnetic field generated around the current carrying conductors becomes an ideal source for energy harvesting.

2.1.3 Load

Common use of energy harvesting application is for supplying power to low powered devices. These devices are mostly low powered sensors used in remote or hazardous locations for system monitoring. Table 1.1 in Chapter 1 lists some of these sensors. In harvesting systems where power generated is not constant, battery storage systems are incorporated to store power during peak times to be used later. This is common with photovoltaic systems which typically incorporate batteries for power storage during the day to be used later at night (24). Other common applications of energy harvesting are solar powered calculators and lamps, thermal powered wrist watches, etc. The next section reviews some of the related research in electromagnetic energy harvesting which is the proposed harvesting method of this research.

2.2 Related Work

Several designs for magnetic field harvesting have been proposed in the prior art. Some of the currently available products that harvest energy from electromagnetic fields include the power donut (37) and power line sensor (38), shown in Figure 2.3.



Power donut (24)



power line sensor (25)

Figure 2.3: Available Magnetic Field Harvesting Products

The majority of these designs focus on high voltage (HV) transmission lines that have currents in excess of 50A. The authors of (39) propose a microcontroller controlled electromagnetic energy harvesting system for harvesting energy from a single HV transmission line with current between 65A and 130A. The system comprises a toroid magnetic power generator setup, voltage multiplier, DC-DC boost converter and microcontroller. An adaptive algorithm is incorporated into the microcontroller to adjust the duty cycle of the converter so that it achieves maximum output power. The magnetic field energy harvesting setup is able to boost 1V AC and can store power at 58mW for 65A flowing through the HV single conductor.

In (40), D. Pimentel et al. presents power management techniques for energy harvesting systems. They introduce Harvesting Aware Power Management (HAPM) strategies for Energy Harvesting Systems (EHS) that keep devices operating in an energy neutral mode. The authors consider the advantages and disadvantages of three different methods of HAPM: Duty Cycling, Dynamic Voltage, or Frequency Scaling and Maximum Power Point Tracking. The authors conclude that dynamic or adaptive power management is the best choice for energy harvesting systems (2010).

Rohit Moghe et al. (41) study the electric and magnetic field energy harvesting for wireless sensor networks in power system applications. Their work begins with a market survey on the power consumption of a selection of wireless communication devices. Surveys on vibration, solar, and thermal based energy harvesting products are also presented along with information on energy harvesting methods in vibration, thermal, solar EM Wave and Magnetic Field Energy. Theoretical analysis of their electric-field harvesting shows a maximum harvested power of 95.2mW. Experimental testing of a

piezoelectric based energy harvesting device is also conducted revealing that up to $108.24\mu\text{W}$ can be harvested for a 1000A current carrying conductor. Experimental testing for magnetic field energy harvesting conducted by Rohit Moghe et al. for various core and winding configurations is shown in Table 2.1(41). The maximum power generated is found to be 257mW (2009).

Table 2.1: Magnetic Field Energy Harvesting for Different Core Configurations

(41)

Type of Coil	No. of turns	O.C. Voltage at 200A Primary current (V)	O.C. Voltage at 1000A Primary Current (V)	Max. Harvestable Power (mW)
Rogowski Coil	18	0.03	0.16	8
28AWG wire wound on a Wooden Core	200	0.24	1.21	29.8
28AWG wire wound on a hollow semi cylindrical Silicon Steel Core	250	0.37	1.77	210.2
28AWG wire wound on a Flux Concentrator	300	0.50	2.64	257
Flux Concentrator Connected to a Transformer	300	12.5	70.6	225

Rashed H. Bhuiyan et al. propose an energy coupler for scavenging energy from current carrying conductors to power wireless sensors in electrical systems (42). Their device uses a magnetic core with an air gap in between layers. The core material presented in their work is a mu-metal of cylindrical form. Figures 2.4 and 2.5 show the diagrams for the core configuration used in their theoretical analysis (2010).

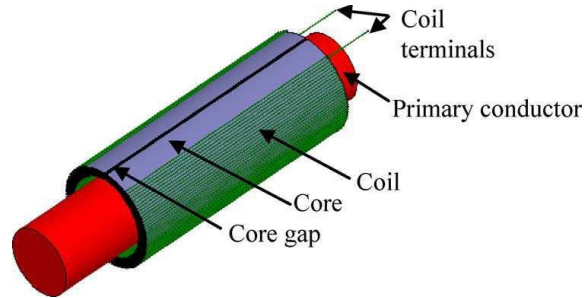


Figure 2.4: Multiturn Coil on a Magnetic Core Around A Current Carrying Conductor (42)

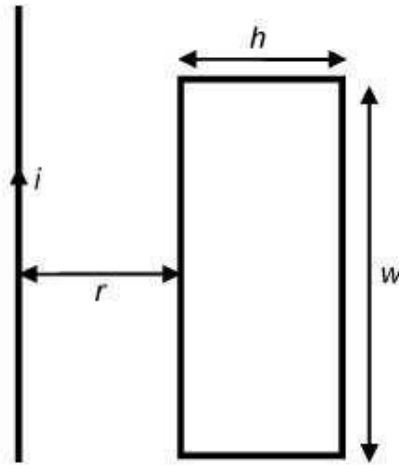


Figure 2.5: Rectangular Coil Near a Current Carrying Conductor (42)

The voltage induction equation is given as (42):

$$V = N\mu_0\mu_r wfI \ln\left(1 + \frac{h}{r}\right)$$

Where N – number of turns wound around the magnetic core, μ_0 and μ_r are the permeability of free space and relative permeability of the core, w and h are the width and height of the core, f is the operating frequency, r is the distance from the current carrying conductor and I is the root mean square (rms) magnitude current in the current carrying conductor. A prototype of the coupler is built and tested in an experiment setup with a board consisting of eight parallel 200 W light bulbs, 120V, 60 Hz supply main (42). Multiple turns of the primary conductor are passed through the opening of the coupler each carrying 13.5A. The energy coupler is shown to be capable of producing 10mW of DC power to a 50 Ω . The authors estimated a higher power to be generated by the coupler with conductors carrying currents in excess of 1000 A (2010).

Except for the work presented in (42), no research to the author's knowledge looks at harvesting electromagnetic energy from low current drawing conductors. Moreover, the research presented in (42) uses multiple primary turns to generate an ample amount of power. The highest voltage induced was approximately 1.5V AC for 5 primary turns and 280 turns of secondary winding for 13.5A current in the primary conductors (42). However, even though the energy coupler in (42) has praiseworthy features such as its ease of use and miniature size, the low current range in the built environment (typical, 1-30A) can reduce its capacity to generate power. This is due to the fact that not enough magnetic flux can be transferred to secondary windings for power generation with the configuration of the proposed energy coupler. Figure 2.6 shows a graph of measured induced voltages from Bhuiyan et al. (42). For practical applications, a single primary turn will typically be used in the energy coupler. From the graph in Figure

2.6 it can be seen that the amount of voltage induced for a single primary turn is a little over 0.2V for 280 turns with a primary current of 13.5A. This makes the coupler presented ideal for high current drawing conductors.

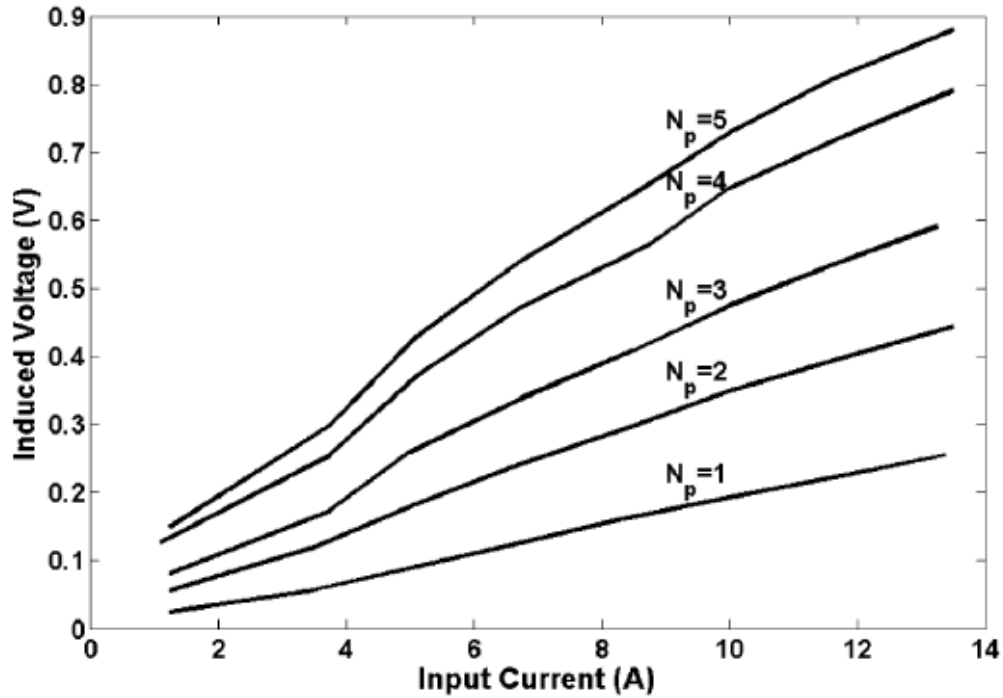


Fig. 11. Measured induced voltages versus currents (I) with number of turns (N_p) of the primary current conductor as a parameter. Parameters: $w = 50$ mm, $n = 8$, $T = 1.25$ mm, $N = 280$, $l_g = 1$ mm, $d = 0.1016$ mm, $f = 60$ Hz, and $\mu_r = 10^5$.

Figure 2.6: Measured Induced Voltages From (42)

The harvesting device proposed in this research uses only a single primary current carrying conductor with multiple secondary windings from 200 to 500 turns. The core used in the research is an amorphous material designed at a reduced size to better scavenge magnetic energy. The core material has a saturation flux density of 1.56 T (43) and a rectangular cross-sectional area. Theoretical analysis used is based on design of current transformers. In order to effectively harvest ample amounts of energy, the available magnetic flux around the current carrying conductors (1-30A) in the built

environment is theoretically analyzed and simulated. The equivalent voltage that can be induced from this available magnetic flux is also analyzed and simulated for a given magnetic core. Magnetic flux and voltages induced is also simulated for various loads at electrical nodes. Simulation of the cross-sectional area of a magnetic core against the voltage induction is done with variable parameters to include the load consumed at the nodes, the current flowing through the primary conductor, and the proximity of the current carrying conductor to the core. Experimental testing is done with an already available standard amorphous core and the results are then compared with the theoretical simulation.

Since the design of the proposed energy harvesting device is based on the electrical transformer, this next chapter gives an overview of transformer basics and current transformer design.

Chapter 3

AN OVERVIEW OF ELECTROMAGNETICS & TRANSFORMERS

3.1 Introduction

Electromagnetic energy harvesting applies the theory of electromagnetism and principles of electric transformer design basics. Electric current flowing to the nodes where energy management sensors are located generates a magnetic field around the current carrying conductor. This magnetic field serves as the main energy source for the proposed electromagnetic energy harvesting device. To estimate amount of available magnetic field strength around the nodes and the equivalent amount of power that can be generated, this chapter offers a review on electromagnetics and transformer basics.

3.2 Overview of Electromagnetics

Electromagnetics involve the theory and application of electric and magnetic fields. Any electric charge in motion has an associated magnetic field. Maxwell's equations are the set of fundamental equations that govern electromagnetics (44). These equations are combination of Faraday's, Ampere's and Gauss' laws (44). For a complete presentation of electromagnetic theory and derivation of Maxwell equations, the reader is referred to references (44) and (45). To estimate the available magnetic field around current carrying conductors for energy harvesting, this section focuses on Boit-Savart law, Ampere's law and ferromagnetic materials.

3.2.1 Biot-Savart Law

Biot and Savart discovered that a conductor carrying a steady current produces a force on a magnet. They developed an equation that gives the magnetic field at some point in space in terms of the current that produces the field. Figure 3.1 shows an illustration of the Biot-Savart law. Thus for a steady current I flowing through the conductor dl , the magnetic field dH at a point P has the following properties:

- The vector dH is perpendicular to both dl and to the unit vector \hat{R} directed from the element dl to the point P .
- The magnitude of dH is inversely proportional to R^2 , where R is the distance from the element dl to the point P .
- The magnitude of dH is proportional to the current I and to the length dl of the element.
- The magnitude of dH is proportional to $\sin\theta$, where θ is the angle between the vectors dl and \hat{R} .

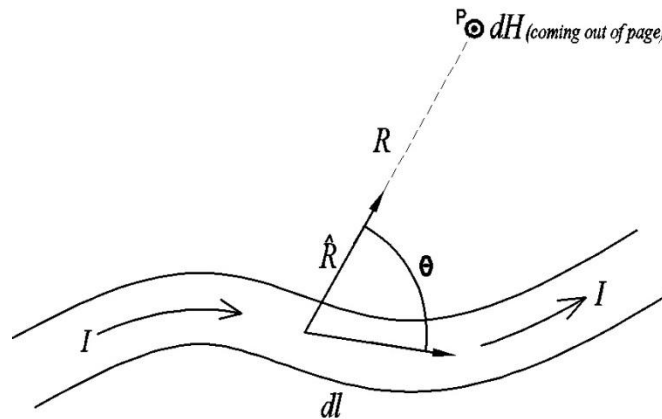


Figure 3.1: Electric Current Relationship with Magnetic Field, Biot-Savart (44)

The differential form of Biot - Savart is given by equations 1, 2:

$$dH = \frac{I}{4\pi} \cdot \frac{dl \times \hat{R}}{R^2} \quad 1$$

The total magnetic field H due to a conductor of finite length l carrying a current I is,

$$H = \frac{I}{4\pi} \cdot \int_l \frac{dl \times \hat{R}}{R^2} \quad 2$$

Derivation of magnetic field around a finite length linear conductor

Figure 3.2 shows a conductor of finite length carrying a current in the upward direction.

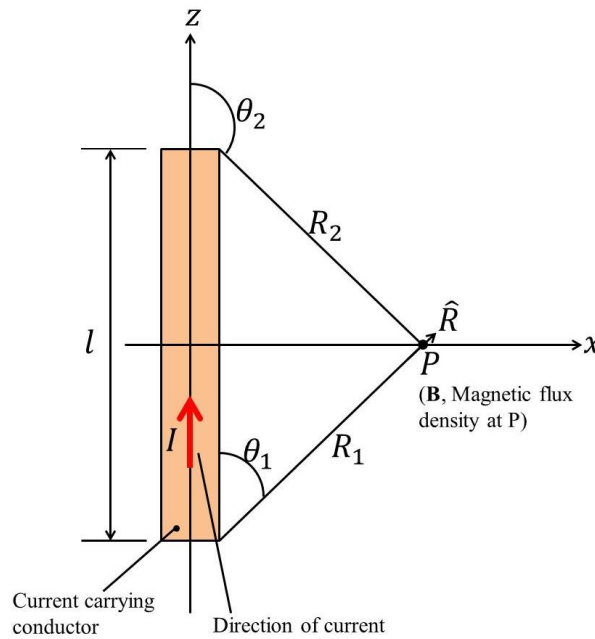


Figure 3.2: Magnetic Field Around Current Carrying Conductor of Finite Length

The integration of equation 2 for a current carrying conductor of length l is stated as:

$$H = \frac{I}{4\pi} \cdot \int_{-l/2}^{l/2} \frac{dl \times \hat{R}}{R^2} \quad 3$$

$$dl = dz \hat{z} \quad 4$$

$$dl \times \hat{R} = dz(\hat{z} \times \hat{R}) \quad 5$$

$\hat{z} \times \hat{R} = \sin\theta \hat{\psi}$, where $\hat{\psi}$ is the unit vector normal to the plane determined by z and R

when they are drawn from a common point.

$$H = \hat{\psi} \frac{I}{4\pi} \cdot \int_{-l/2}^{l/2} \frac{\sin\theta}{R^2} dz \quad 6$$

Expressing R and z in terms of θ and substituting;

$$R^2 = \frac{r^2}{\sin^2\theta}, \quad z = -r \frac{\cos\theta}{\sin\theta}, \quad dz = \frac{r}{\sin^2\theta} d\theta$$

Therefore,

$$H = \hat{\psi} \frac{I}{4\pi} \cdot \int_{\theta_1}^{\theta_2} \frac{\sin^3\theta}{r^2} \cdot \frac{r}{\sin^2\theta} d\theta = \hat{\psi} \frac{I}{4\pi} \cdot \int_{\theta_1}^{\theta_2} \frac{\sin\theta}{r} d\theta \quad 7$$

$$H = -\frac{I}{4\pi r} (\cos\theta_2 - \cos\theta_1) \hat{\psi} \quad 8$$

Expressing $z = -\frac{l}{2}, \frac{l}{2}$ in terms of θ_1 and θ_2 ;

$$\cos\theta_1 = \frac{l/2}{\sqrt{r^2 + \left(\frac{l}{2}\right)^2}}, \quad \cos\theta_2 = \frac{-l/2}{\sqrt{r^2 + \left(\frac{l}{2}\right)^2}},$$

$$H = \frac{I}{4\pi r} \cdot \frac{2l}{\sqrt{4r^2 + l^2}} \hat{\psi} = \frac{Il}{2\pi r \sqrt{4r^2 + l^2}} \hat{\psi} (\text{A/m}) \quad 9$$

Biot – Savart law due to surface and volume distributions are expressed as follows (44):

$$H = \frac{I}{4\pi} \cdot \int_S \frac{J_s \times \hat{R}}{R^2} ds \quad (\text{for surface current}) \quad 10$$

$$H = \frac{I}{4\pi} \cdot \int_V \frac{J \times \hat{R}}{R^2} dV \quad (\text{for volume current}) \quad 11$$

Where, J_s is the surface current density (A/m) and J is the volume current density in (A/m²), R is the distance vector between surface or volume and an observation point of interest where magnetic field is being determined (m).

3.2.2 Ampere's Law and Magnetic Flux Density

Ampere's circuital law states that the line integral of a magnetic field H, around a closed path is equal to the current traversing the surface bounded by that path (44), (45).

Ampere's law in equation form is given by:

$$\oint_C \mathbf{H} \cdot d\mathbf{l} = I \quad 12$$

Where C denotes the contour of close path.

The sign convention for the direction of the contour C path follows the right – hand rule.

Thus if the direction of I is aligned with the direction of the thumb of the right hand, then the direction of the contour C should be chosen along that of the other four fingers.

Therefore, given the direction of current flow in a current carrying conductor, the magnetic field close contour around the conductor will follow the right – hand rule.

The magnetic flux density B and field intensity H are related by (44), (45);

$$B = \mu H \text{ (T)} \quad 13$$

Where, μ is the magnetic permeability property of the medium through which the field penetrates. This is usually denoted in text as μ_0 for most dielectric materials and metals except for ferromagnetic materials. $\mu_0 = 4\pi \times 10^{-7} \text{ (N/A}^2\text{)}$, (44).

For a current carrying wire conductor of finite length l shown in Figure 3.2, the magnetic flux density is given by:

$$B = \mu H = \mu \cdot \frac{Il}{2\pi r \sqrt{4r^2 + l^2}} \hat{\psi} \text{ (T)} \quad 14$$

For an infinitely long wire, $l \gg r$

$$B = \frac{\mu I}{2\pi r} \hat{\psi} \text{ (T)} \quad 15$$

3.2.3 Ferromagnetic Materials

The medium or material for transfer of electromagnetic energy for electricity should exhibit magnetic properties. These materials are called ferromagnetic materials.

Ferromagnetic materials are basically materials that have the ability to attract a magnet.

Some common ferromagnetic materials are iron, nickel, cobalt, alnico and an alloy of aluminum-nickel-cobalt. From earlier discussions, the flow of electric charge has an associated magnetic field. The magnetic field comes from the motion of electrons in the atoms of these materials. In addition, each electron spins when in motion. Ferromagnetic materials exhibit a long-range ordering property at the atomic level which causes the unpaired electron spins to line up parallel with each other in a region called a domain (45). Figure 3a shows this alignment phenomenon. Magnetic field is intense in each

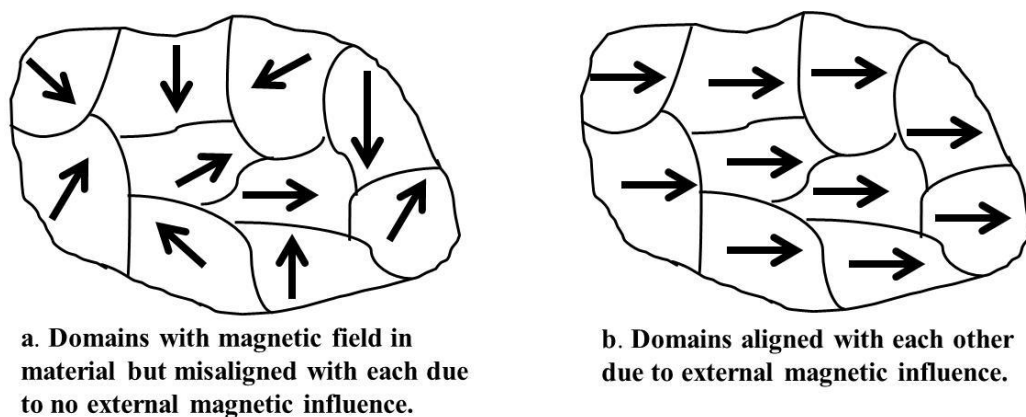


Figure 3.3: Domain Alignment in Ferromagnetic Materials

domain but the material as whole is not magnetized due to random orientations of domains (45), (50). However, an external influence of a magnetic field on a ferromagnetic material can cause the domains to line up with each other to cause magnetization. This is illustrated in Figure 3b. The magnetic field is then increased across the material by a factor called its relative permeability. Relative permeability is the ratio of permeability of a material to that of a vacuum at the same magnetic field strength (45). Table 3.1 gives the relative permeabilities of some common ferromagnetic materials.

Table 3.1: Relative Permeabilities of Common Ferromagnetic Materials (46)

Material	Relative Permeability(μ_r)
Cobalt	250
Nickel	600
Iron	6,000
Superalloy(5% mo,79% Ni)	107
Steel (0.9 C)	100
Silicon iron (4% si)	7,000
Permalloy(78.5% Ni)	100,000
Fe ₃ O ₄ (Magnetite)	100
Ferrites	5,000
Mumetal (75% Ni, 5% Cu, 2% Cr)	100,000
Permendur	5,000

Soft iron is used in electromagnetic applications like transformer cores, motors and temporary magnets. The next section is a summary on transformer basics and how electromagnetic energy is used to generate electricity.

3.3 An Overview of Electrical Transformers

This section looks at the basic working principle of transformers and the relevant equations for their design. A transformer is an electrical device that transfers energy from one circuit to another by electromagnetic induction (47). The key components of a transformer are a primary coil (winding), a secondary coil (winding) and a core material

that supports both windings. In addition, the core also acts as the medium for magnetic coupling between the primary and secondary windings. Thus, this can be said to be the medium for energy transfer. A simplified diagram of a transformer is shown in Figure 3.4.

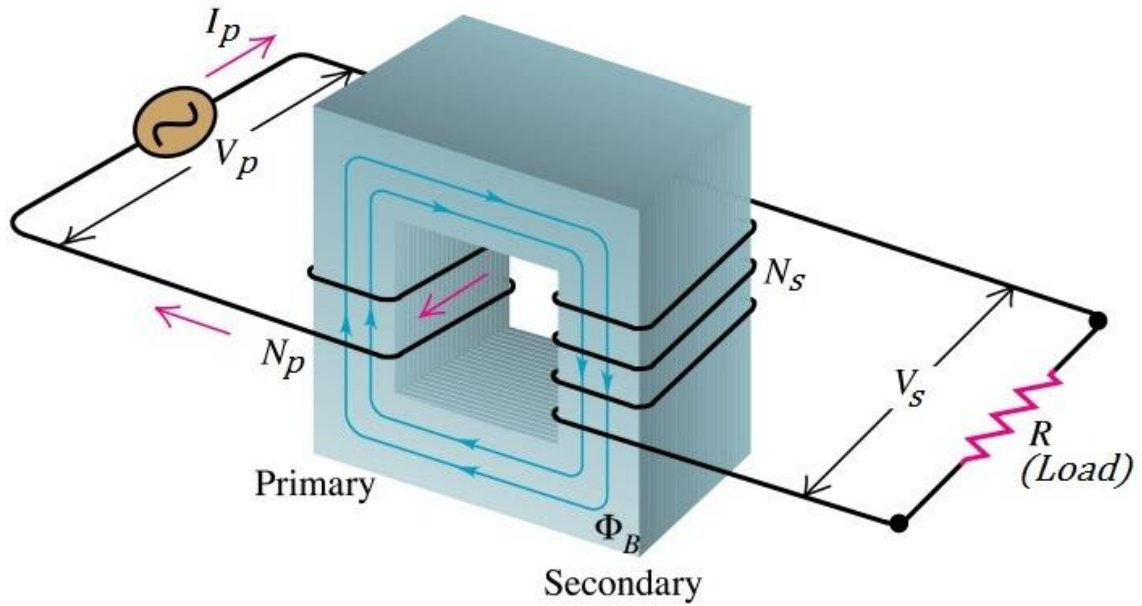


Figure 3.4: A Simplified Diagram of an Electric Transformer (5)

Faraday's law of induction is the basic law of electromagnetism relating to the operating principles of transformers. The law states that, time varying magnetic fields can produce an electric current in a closed loop (44). In other words, any coil of wire in a changing field of magnetic field will cause a voltage (electromotive force, emf) to be induced in the coil. The change can be a relative movement of either magnetic source or the coil. This is expressed in equation form as (44), (45):

$$\mathcal{E} = -N \frac{d\phi}{dt} = -N \frac{d}{dt} \int_s \mathbf{B} \cdot d\mathbf{s}$$

Where, \mathcal{E} induced emf, B magnetic field strength, N number of coil turns, s surface area of the inductor and ϕ magnetic flux density.

Conventional transformers are either used to step up or down voltage from a primary side to the secondary side winding. A simple transformer circuit is shown in Figure 3.5. They are constant power devices which means, the product of the primary voltage and current is the same as the product of the secondary voltage and current. The ideal transformer equations are:

$$|Primary\ power| = I_p V_p = |Secondary\ power| = I_s V_s$$

$$\frac{V_s}{V_p} = \frac{N_s}{N_p} = \frac{I_p}{I_s} \quad 17$$

V_p Primary side voltage, V_s Secondary Voltage, N_p Primary turns, N_s Secondary turns, I_p Primary current, I_s Secondary current.

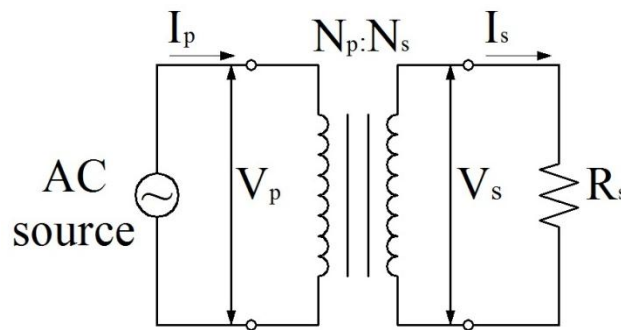


Figure 3.5: Simple Transformer Circuit

In practical transformers however, material properties of core plays an important role. The cores are selected so as not to saturate under low magnetic flux. Thus transformers are designed with cores of high permeabilities. The design principle is based on estimating the total component losses and performing an iterative process to get a balance between output performance and geometry of the core. The losses are copper

losses of the windings and losses of the core material (49). Practical transformers are designed by using equation 18 (49).

$$\frac{W_A(A_c)^{\frac{2(\beta-1)}{\beta}}}{(MLT)l_m^{(2/\beta)}} \left[\left(\frac{\beta}{2} \right)^{-\left(\frac{\beta}{\beta+2} \right)} + \left(\frac{\beta}{2} \right)^{\left(\frac{2}{\beta+2} \right)} \right]^{-\left(\frac{\beta+2}{\beta} \right)} = \frac{\rho I_{tot}^2 \lambda_1^2 K_{fe}^{\left(\frac{2}{\beta} \right)}}{4K_u(P_{tot})^{\left(\frac{\beta+2}{\beta} \right)}} \quad 18$$

Where, ρ effective wire resistivity, I_{tot} total rms winding current, referred to primary, λ_1 applied primary volt-sec, P_{tot} Allowed total power dissipation, K_u winding fill factor, β core loss exponent, K_{fe} core loss coefficient, A_c core cross-sectional area, W_A core window area, l_m magnetic path length, MLT mean length per turn of winding.

The terms on the left hand side of equation 18 are dependent on core geometry and that on the right hand side depend on the specifications of application (output voltage, current). Complete derivation of equation 18 and other related equations are found in (49) and (50).

3.3.1 Current Transformers (CT)

Harvesting electromagnetic flux around current carrying conductors through conventional voltage transformer design will require the current carrying conductors to be wound around transformer cores. This will involve modification of existing electrical wiring systems and also can be difficult to achieve with solid conductors. The current transformer (CT) is therefore the suitable choice to harvest energy from the magnetic flux around current carrying conductors. This section looks at the main theoretical equations used for designing current transformers.

Current transformers are used in high-power circuits where large currents are involved. They are mostly used in monitoring current of conductors or cables in AC power circuits (50). Figure 3.6 shows a circuit diagram of a simplified current transformer used to monitor line currents.

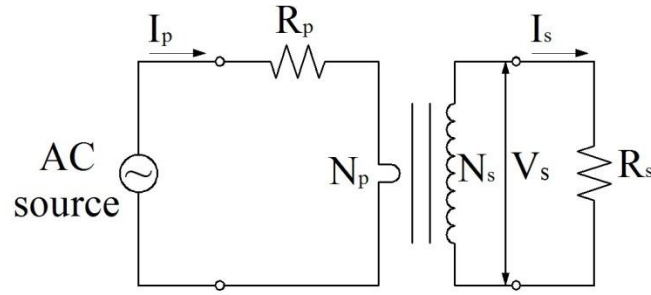


Figure 3.6: Simplified Circuit Diagram of a Current Transformer

Lists of predominant equations for designing current transformers are included below.

Application specific equations (50):

$$\frac{I_p}{I_s} = \frac{N_s}{N_p}, N_p = 1$$

$$\frac{I_p}{I_s} = N_s \quad 19$$

$$I_s = \frac{V_s}{R_s} \text{ (A)} \quad 20$$

I_p Primary current, I_s secondary current, N_p primary turns, N_s secondary turns, V_s secondary load voltage, R_s secondary load resistance.

For an output DC load R_o , at the secondary side, a bridge rectifier will be required to convert the secondary voltage from AC to DC voltage. Figure 3.7 shows the circuit diagram of a bridge rectifier incorporated into the secondary side of the CT.

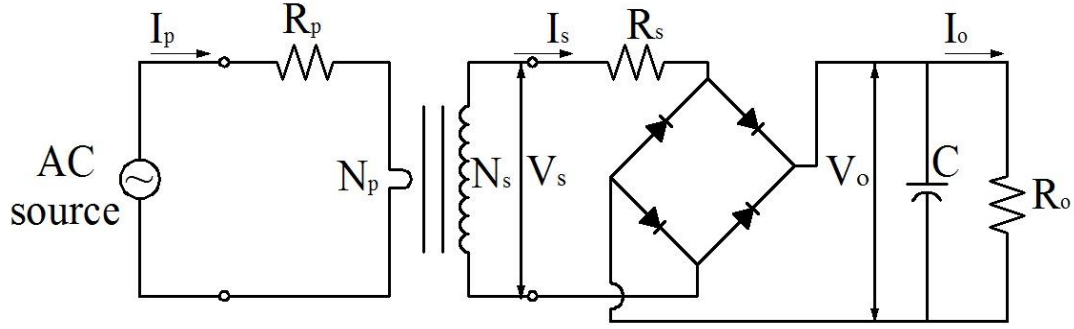


Figure 3.7: Complete Circuit Diagram of a Current Transformer with a Bridge Rectifier

Secondary winding resistance R_s

$$R_s = MLT (N_s) \left(\frac{\mu\Omega}{cm} \right) (10^{-6}) (\Omega) \quad 21$$

MLT is mean length per winding turn

and the output load voltage, V_o

$$V_o = I_o (R_o) \quad 22$$

The Secondary voltage V_s is calculated using equation 23

$$V_s = V_o + V_d \text{ (Volts)} \quad 23$$

Where, V_d is diode voltage drop

Total secondary output power, P_o

$$P_o = I_s V_s \text{ (watts)} \quad 24$$

Core Geometry Equations (50):

Figure 3.8 illustrates current transformer core geometry parameters. The window area W_a is a through rectangular hole in the core material.

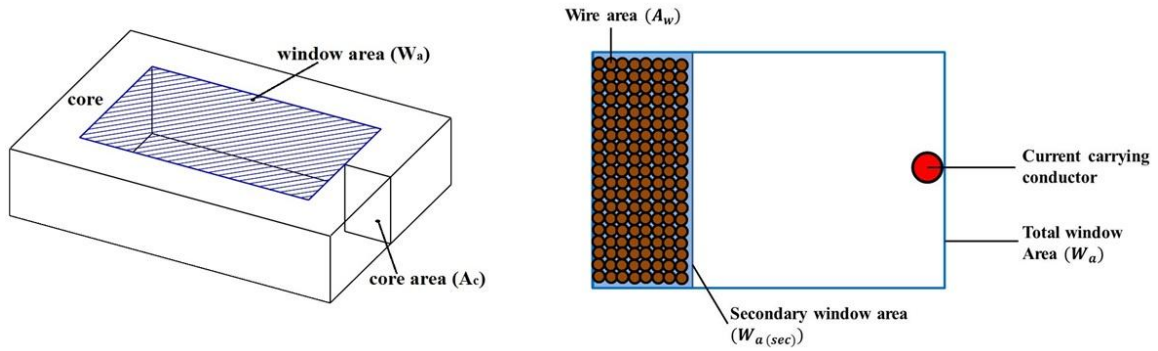


Figure 3.8: Current Transformer Core and Window Area

Core cross sectional area A_c

$$A_c = \frac{V_s(10^4)}{K_f B_{ac} f N_s} (\text{cm}^2) \quad 25$$

K_f is Waveform factor (4 for square wave and 4.44 for sinusoidal wave), (50). B_{ac} is

Operating Magnetic flux density, f is Operating frequency,

Effective window area, $W_{a(eff)}$

$$W_{a(eff)} = W_a S_3 (\text{cm}^2) \quad 26$$

W_a is Core window area, S_3 Effective window area constant (ratio of usable window area to window area), typical value of S_3 is 0.873 (31).

Secondary window area, $W_{a(sec)}$

$$W_{a(sec)} = \frac{W_{a(eff)}}{2} (\text{cm}^2) \quad 27$$

Wire area, A_w

$$A_w = \frac{W_{a(sec)} S_2}{N_s} (\text{cm}^2) \quad 28$$

S_2 is wire lay fill factor (ratio of wound area to usable window area), typical value of S_2 is 0.61 (50).

Table A.1, (50) in the appendix shows various wire areas (A_w) and corresponding AWG wire for winding. The general rule for wire selection is that when calculated, the wire area should not fall within 10% of the listed value in the wire table, otherwise the next smaller size should be selected. The design of other special CTs are found in (50).

3.3.2 Transformer Core Saturation

Transformer performance is limited by the amount of magnetic flux that can be contained in the core. Ferromagnetic cores tend to saturate after a certain level of magnetic flux. This further increase of the magnetic field flux after saturation will not result in a proportional increase in induced voltage. Saturation causes distortion of the wave shape of the primary current or voltage to secondary windings. This results in what is called harmonics in transformers. Harmonics are the distortions in wave shape of secondary side AC voltages. Common indication of harmonics in transformers is increase in temperature of during operation.

In order to avoid harmonics in transformers, material of cores should have high permeabilities. Saturation is also based on the core size, the number of coil turns, as well as the voltage and current in the windings. To improve the permeability of the cores, cut-cores are often used in most transformer applications.

The small size of the energy harvesting device requires a core material that will not saturate under the magnetic flux generated by the operating current. The typical operating current target range for this research is 1-20A. The magnetic core material

proposed for the energy harvesting device is Metglas allow 2605SA1. Metglas 2605SA1 has a high saturation flux density of 1.56 T (51) which is very high compared to the maximum magnetic flux for the target 1-20A. Simulations of magnetic flux generation from various currents are discussed in Chapter 5. The next chapter gives the objectives of this research and explains the methodology involved. The design process of the proposed energy harvesting device is illustrated in a case study.

Chapter 4

RESEARCH OBJECTIVE, METHODOLOGY, AND DESIGN

4.1 Introduction

Developing a miniature power supply that has a limited source of energy (electromagnetic field) requires in-depth design considerations. Apart from the size and source of energy being a limitation, the minimum required amount of power that can be generated also depends largely on these limitations. This minimum amount of power should be able to power the sensor to enable continual operation. Therefore, a careful design has to balance the aforementioned limitations whilst also meeting the required minimum output power. This chapter discusses the main objectives, methodology, and design considerations that must be taken into account to meet such a goal.

4.2 Research Objective and Methodology

The main objectives and methodology of the research can be summarized as follows:

- [1] To develop and design a small electromagnetic energy harvesting device that will fit into the standard electrical node boxes in Figure 4.1 (52). The most common sizes of boxes used for wiring electrical nodes are 95mm by 50mm by 90mm and 100mm sq. by 38mm. Therefore, the size of the harvesting device shall meet the existing form factor of standard boxes for electrical nodes without any modification to the electrical wiring system.

Box Trade Size			Minimum Volume		Maximum Number of Conductors* (arranged by AWG size)						
mm	in.		cm ³	in. ³	18	16	14	12	10	8	6
100 × 32	(4 × 1¼)	round/octagonal	205	12.5	8	7	6	5	5	5	2
100 × 38	(4 × 1½)	round/octagonal	254	15.5	10	8	7	6	6	5	3
100 × 54	(4 × 2⅛)	round/octagonal	353	21.5	14	12	10	9	8	7	4
100 × 32	(4 × 1¼)	square	295	18.0	12	10	9	8	7	6	3
100 × 38	(4 × 1½)	square	344	21.0	14	12	10	9	8	7	4
100 × 54	(4 × 2⅛)	square	497	30.3	20	17	15	13	12	10	6
120 × 32	(4⅞ × 1¼)	square	418	25.5	17	14	12	11	10	8	5
120 × 38	(4⅞ × 1½)	square	484	29.5	19	16	14	13	11	9	5
120 × 54	(4⅞ × 2⅛)	square	689	42.0	28	24	21	18	16	14	8
75 × 50 × 38	(3 × 2 × 1½)	device	123	7.5	5	4	3	3	3	2	1
75 × 50 × 50	(3 × 2 × 2)	device	164	10.0	6	5	5	4	4	3	2
75 × 50 × 57	(3 × 2 × 2¼)	device	172	10.5	7	6	5	4	4	3	2
75 × 50 × 65	(3 × 2 × 2½)	device	205	12.5	8	7	6	5	5	4	2
75 × 50 × 70	(3 × 2 × 2¾)	device	230	14.0	9	8	7	6	5	4	2
75 × 50 × 90	(3 × 2 × 3½)	device	295	18.0	12	10	9	8	7	6	3
100 × 54 × 38	(4 × 2⅛ × 1½)	device	169	10.3	6	5	5	4	4	3	2
100 × 54 × 48	(4 × 2⅛ × 1⅞)	device	213	13.0	8	7	6	5	5	4	2
100 × 54 × 54	(4 × 2⅛ × 2⅛)	device	238	14.5	9	8	7	6	5	4	2
95 × 50 × 65	(3¾ × 2 × 2½)	masonry box/gang	230	14.0	9	8	7	6	5	4	2
95 × 50 × 90	(3¾ × 2 × 3½)	masonry box/gang	344	21.0	14	12	10	9	8	7	4
min. 44.5 depth	FS — single cover/gang (1¾)		221	13.5	9	7	6	6	5	4	2
min. 60.3 depth	FD — single cover/gang (2⅜)		295	18.0	12	10	9	8	7	6	3
min. 44.5 depth	FS — multiple cover/gang (1¾)		295	18.0	12	10	9	8	7	6	3
min. 60.3 depth	FD — multiple cover/gang (2⅜)		395	24.0	16	13	12	10	9	8	4

*Where no volume allowances are required by 314.16(B)(2) through (B)(5).

Figure 4.1: Standard Metal Boxes Used in Electrical Wiring Systems (Table 314.16 (A), NEC 2008)

Method :

- Develop a method for designing a small electric current transformer by balancing key parameters – the core size, primary energy source, and output performance.
The primary source will be the magnetic field generated around a conductor carrying 1-20A in a 120V system. This will be mainly based on transformer design basics and theories.
- Propose and produce design drawings of a small current transformer for electromagnetic energy harvesting. The design drawing will be generated in CAD and shall be a shop working drawing standard.

- Coordinate with the electric transformer manufacturing company to manufacture the proposed design.

[2] Develop a method for estimating the electromagnetic field strength around the current carrying conductors and the equivalent amount of power that can be generated by the energy harvesting device using theoretical equations.

Method :

- Estimate the amount of magnetic field strength around the current carrying conductors. This will be based on the theory of electromagnetics and use MATLAB tools.
- Use theoretical equations for transformer design basics to estimate the equivalent amount of power that can be generated from the magnetic field above. This will be done with MATLAB tools.

[3] Build a prototype board made up of typical electrical nodes and run experiments with the proposed energy harvesting device. The board will have a 120V- 20A electrical distribution wiring system with an energy management sensor at the node. Typical loads such as light and plug loads will be used in the experiments.

Method:

- Design an electric distribution layout with a 120V- 20A rated conductor comprised of 5 nodes (2 lighting nodes with 2 switching nodes and 3 - 120V duplex nodes).

- Build the prototype board from the design layout. An energy management sensor will be attached to one of the nodes.
- The energy harvesting device will be mounted on the current carrying conductor at a node and hard wired to the energy management sensor. A re-chargeable battery shall be incorporated into the board for storing generated power during periods in which the sensors are idle.
- Two additional low powered devices (LED and USB power outlets) shall be mounted on the board for demonstration purposes and hard wired to the energy harvesting device.

[4] Investigate potential challenges and other useful applications. These challenges will be in relation to:

- Design limitations,
- Code violations and
- Practical implementation.

A list of other low power devices in the built environment will also be presented.

The next section explains the design process behind the creation of the energy harvesting device.

4.3 The Design Process

To illustrate design process, this section presents a case study to design the proposed energy harvesting device. The theoretical design approach is based on that of a CT. The various parameters for design and operation are given as follows:

- Sensor energy specifications (current consumption, battery voltage, average power consumption) are shown in Table 4.1.
- Energy harvesting device output voltage, 5V DC.
- Diode voltage drop is 2V DC.
- The core size specifications (height, Length, width, window size) are shown in Figure 4.2.
- Operating primary current range is 1-20A rms and a voltage of 120 V AC rms.
- Operating frequency, sine wave 60Hz.
- Operating current carrying conductor size is #12 AWG.

Table 4.1: Sensor Energy Demand Specifications

Sensor	Current Consumption			Battery Voltage	Average Power Consumption
	Transmission mode	Reception mode	Sleep mode		
XBEE Zigbee/802.15. 4 Modules (15)	50mA	50mA	10 μ A	2.8V-3.4V	155mW

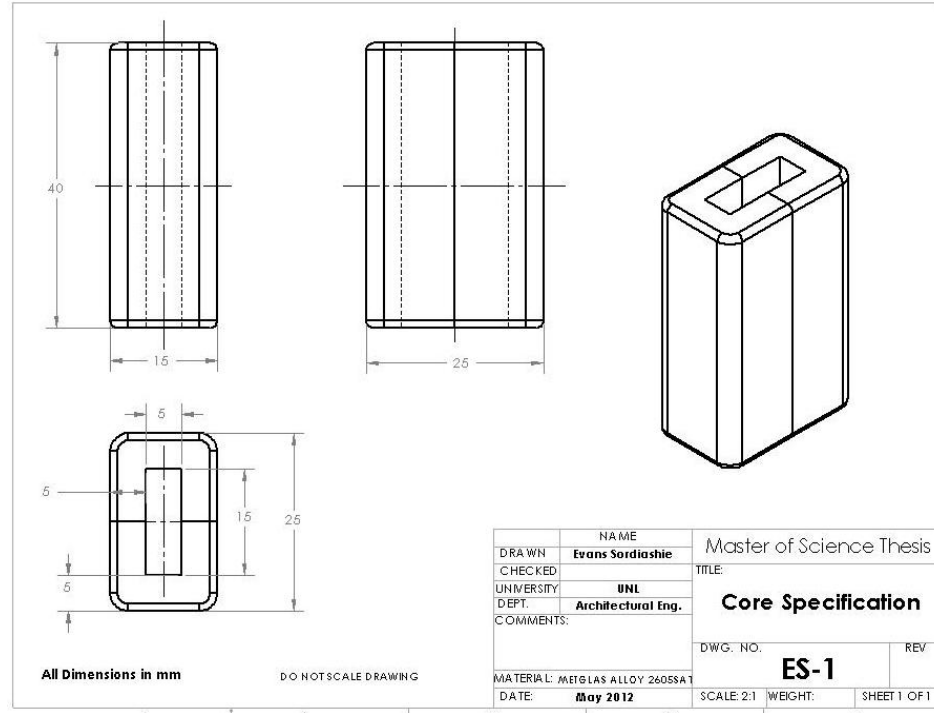


Figure 4.2: Energy Harvesting Device Core Specifications (proposed design)

4.3.1 Design Calculations

A cross sectional area of the core from equation 25 in Chapter 3 is given by;

$$A_c = \frac{V_s(10^4)}{K_f B_{ac} f N_s} (cm^2)$$

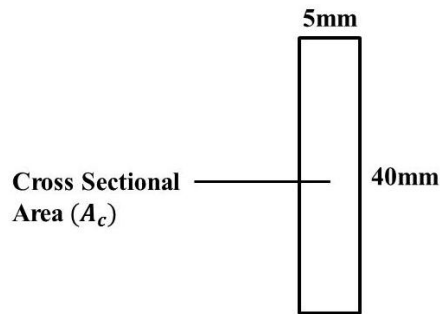


Figure 4.3: Cross-Sectional Area of the Core

From the core geometry in Figure 4.3,

$$\text{Core height, } l = 40\text{mm} = 40 \times 10^{-3} \text{ m}$$

$$A_c = (5 \times 40)\text{mm}^2 = 2 \text{ cm}^2$$

Distance from current carrying conductor to magnetic path length r , as shown in Figure 4.4 is

$$r = \left(\frac{5}{2} + 4\right) = 6.5 \text{ mm} = 6.5 \times 10^{-3} \text{ m}$$

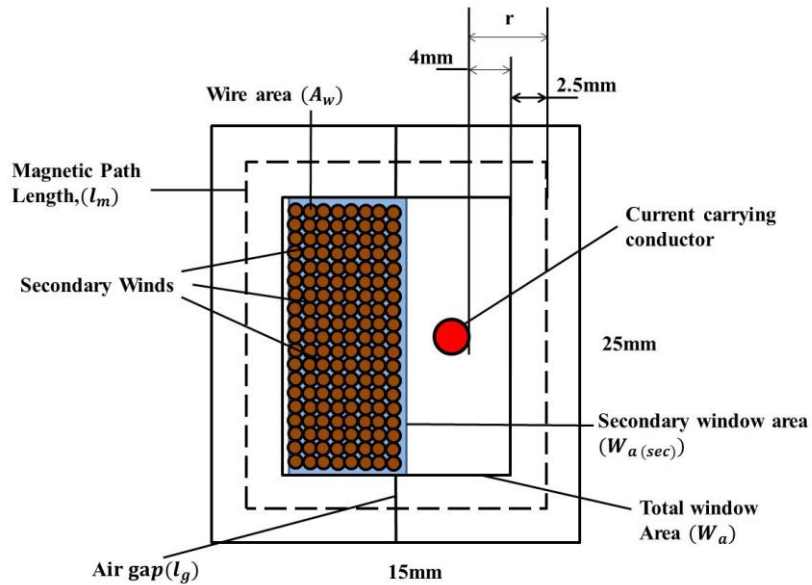


Figure 4.4: Core Window Area

Finding permeability of core

$$\text{Permeability of free space } \mu_o = 4\pi \times 10^{-7} \text{ H/m}$$

$$\text{Permeability of Metglas material, } \mu_m = 3000 \text{ H/m}$$

$$\text{Air gap between cut cores, } l_g = 120 \times 10^{-6} \text{ m}$$

Magnetic path length, $l_m \cong 2 (20 + 10) = 60 \times 10^{-3} m$

Overall relative permeability of Core assembly μ_r is given by (50);

$$\mu_r = \frac{\mu_m}{1 + \mu_m \left(\frac{l_g}{l_m} \right)}$$

$$\mu_r = \frac{3000}{1 + 3000 \left(\frac{120 \times 10^{-6}}{60 \times 10^{-3}} \right)} = 428.57$$

Finding magnetic field strength

Operating primary current, $I_p = 10 A (rms)$

Magnetic field strength generated by $10 A$ flowing through conductor is given by equation 14;

$$B_{ac} = \frac{\mu_0 \mu_r I_p l}{2\pi r \sqrt{4r^2 + l^2}} (T)$$

Where, $\mu = \mu_0 \mu_r$, effective permeability of core assembly.

$$B_{ac} = \frac{4\pi \times 10^{-7} \times 428.57 \times 10 \times (40 \times 10^{-3})}{2\pi \times 6.5 \times 10^{-3} \times \sqrt{4 \times (6.5 \times 10^{-3})^2 + (40 \times 10^{-3})^2}} (T)$$

$$B_{ac} = 0.1254 T$$

Finding total secondary winding

Diode and secondary winding resistance voltage drop, $V_d \cong 3 V$.

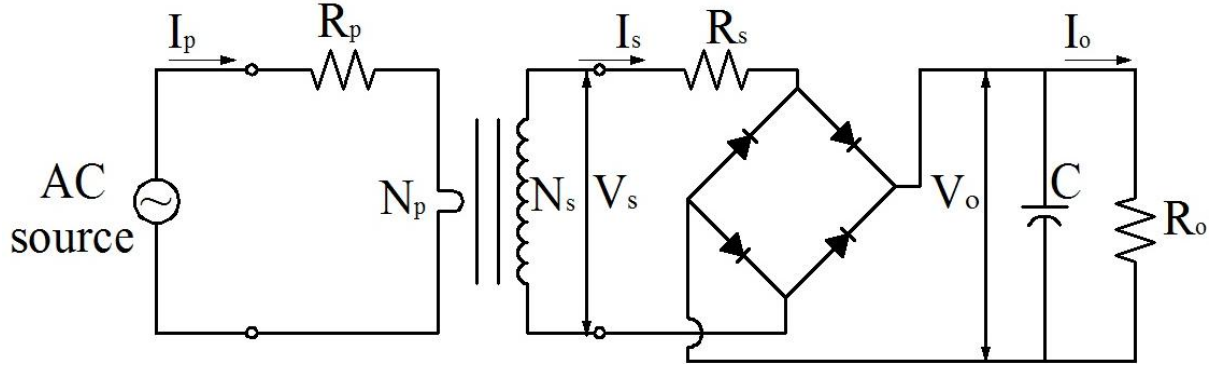


Figure 4.5: Circuit Diagram of the Energy Harvesting Device.

Expected output voltage is $V_o = 5\text{ V DC}$

Output load current is 50 mA ,

Corresponding output load resistance R_o is,

$$R_o = \frac{V_L}{I_o} = \frac{3.4}{50} = 68\Omega, V_L \text{ is actual sensor voltage requirement.}$$

Total secondary voltage, V_s is given by;

$$V_s = V_o + V_d$$

$$V_s = 5 + 3 = 8\text{ V(rms)}$$

Primary turns, $N_p \cong 1$

Waveform factor for sine wave, $K_f = 4.44$

Operating frequency, $f = 60\text{ Hz}$

Total Secondary winding N_s , is given by;

$$N_s = \frac{V_s(10^4)}{K_f B_{ac} f A_c} = \frac{8 \times 10^4}{4.44 \times 0.1254 \times 60 \times 2} = 1197.3$$

$$N_s \cong 1200 \text{ turns}$$

Finding conductor size for winding

Total window area as shown in Figure 4.4 is,

$$W_a = 15 \times 5 = 75 \text{ mm}^2 = 0.75 \text{ cm}^2$$

Effective window area $W_{a(eff)}$, available for winding (both primary and secondary) is,

$$W_{a(eff)} = W_a \times S_3, \quad S_3 \text{ is effective window area constant. Typical value of } S_3 \text{ is } 0.873 \text{ (50).}$$

$$W_{a(eff)} = 0.75 \times 0.873 = .655 \text{ cm}^2$$

Secondary window area, $W_{a(sec)}$ is,

$$W_{a(sec)} = \frac{W_{a(eff)}}{2} \text{ (cm}^2\text{)}$$

$$W_{a(sec)} = \frac{0.655}{2} = 0.327 \text{ cm}^2$$

Cross sectional area A_w of the conductor for winding is given by;

$$A_w = \frac{W_{a(sec)} \times S_2}{N_s}, \quad S_2 \text{ is the fill factor or the wire lay, for usable window area. Typical}$$

value of S_3 is 0.61 (50).

$$A_w = \frac{0.327 \times 0.61}{1200} = 0.000166 \text{ cm}^2$$

Table A.1 (50) in appendix A shows various wire areas (A_w) and corresponding AWG wire for winding. The corresponding AWG conductor for the winding is selected to be # 36.

The corresponding winding resistance is calculated using equation 21.

$$R_s = MLT (N_s) \left(\frac{\mu\Omega}{cm} \right) (10^{-6})$$

MLT is the average perimeter of the cross sectional area of core before and after windings has been added. This is estimated as:

$$MLT = \frac{(40 + 5) \times 2 + (40 + 5) \times 2 \times 1.4 - 0.355}{2} \quad (mm)$$

Where, 140% is allowed for increase in perimeter for windings and 0.355mm is allowed for wrapper thickness on windings.

$$MLT = 10.8 \quad (cm)$$

$$R_s = 10.8 (1200)(13608)(10^{-6}) = 176.36\Omega$$

The winding resistance is very high compared to the load resistance (68Ω). To reduce this resistance, 500 turns of #25 AWG winding will be used for the secondary winding.

This will also increase the current output of the harvesting device because of the constant power principle of the transformer. The new induced voltage V_s , is calculated using equation 25.

$$V_s = \frac{N_s \times K_f \times B_{ac} \times f \times A_c}{(10^4)} = 3.34 \text{ V (rms)}$$

The new winding resistance is,

$$R_s = 10.8 (500)(1062)(10^{-6}) = 5.73\Omega$$

An AC to DC voltage doubler (multiplier) is used to boost up the new voltage. Figure 4.6 shows a circuit of the voltage doubler.

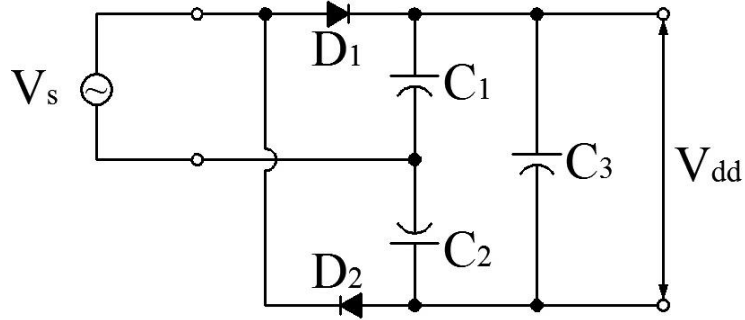


Figure 4.6: Voltage Doubler Circuit

The doubled voltage V_{dd} is calculated with equation 29

$$V_{dd} \cong 2 \times V_s \text{ peak} = 2\sqrt{2} \times V_s (\text{rms}) \quad 29$$

$$V_{dd} \cong 2\sqrt{2} \times 3.34 = 9.45 \text{ V (DC)}$$

To reduce and stabilize V_{dd} voltage for sensor operation voltage (2.8-3.4V DC) a voltage regulator is incorporated into the circuit. This is shown in Figure 4.7.

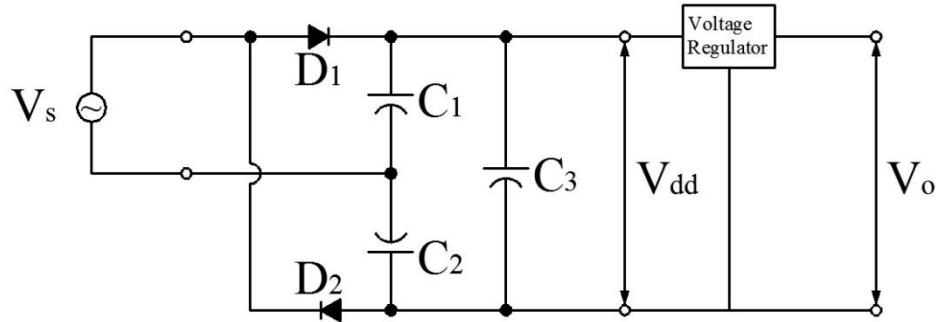


Figure 4.7: Voltage Regulator Incorporated into the Voltage Doubler Circuit

A summary of the final design specifications are as follows:

- Operating current carrying conductor, #12 AWG

- Primary turn, 1
- Average operating primary current , 10 A rms
- Operating frequency, sine wave 60Hz.
- Operating flux density, 0.1254 T
- Harvesting device size and specifications; Magnetic Material (Metglas alloy 2605SA1, High Saturation Flux Density (1.56 T)), Window area, W_a , 0.75 cm², Magnetic path length, $l_m \cong 6\text{cm}$, (see Figure 4.2).
- Winding conductor, # 25 AWG, 500 turns.
- Output voltage for sensor, 3.3V DC
- Output Load Resistance, $\sim 68\Omega$
- Voltage regulator, LM2937 rated at 3.3 V DC
- Diode D_1 , D_2 (IN4003), C_1 C_2 C_3 ,(1 μ F rated at 100V)

This concludes the design process. The core size in Figure 4.2 is proposed core geometry for this research. The geometry will fit into typical node boxes (95mm by 50mm by 90mm or 100mm sq. by 38mm) in the built environment. In addition, management sensors can be directly mounted on the harvesting device at the node.

However, due to long manufacturing lead time for the proposed core of energy harvesting device, a smaller standard core readily available is used for prototyping and experiment. The core used is Amorphous Metal C Core #4 (AMCC-4). Detail specifications of the AMCC-4 core are provided in chapter 5.

Chapter 5

RESULTS AND DISCUSSION

5.1 Introduction

The main objective of this research is to design an electromagnetic harvesting device that will draw energy from available electromagnetic field around current carrying conductors at electrical nodes to generate power for energy management sensors. The size of this harvesting device is also a key objective as the device should fit into boxes at the electrical nodes without affecting the form factor of the boxes. To achieve these goals, it is very important to estimate the electromagnetic energy around typical current conductors in the built environment. With estimates of magnetic fields available, further estimates of equivalent voltage to be induced can be successfully done in relation to the size of the energy harvesting device core. The cross sectional area, A_c of the core needs to be carefully selected to prevent magnetic flux saturation but yet fit into typical boxes of nodes. This chapter presents simulation results and discusses the available electromagnetic energy around typical current carrying conductors in the electrical distribution system. All simulations are done with MATLAB software tools. Refer to Appendix C for the related programming codes.

The proposed core size in Figure 4.2 is not a standard core size available on the market. This means that a core must be customized for the proposed energy harvesting device. The manufacturing lead time to produce such a core is estimated to be 3 to 5 months (53). In addition, since only a few cores are needed for experiments and testing,

the initial cost will be high. To resolve this problem, a standard small size core is used in the simulations and experiments. Appendix B gives the winding specifications for the AMCC-4 core. All the results in this thesis are therefore based on the AMCC-4 core. This chapter also includes results from actual experiments conducted with an AMCC-4 core prototype energy harvesting device.

5.2 Electromagnetic Energy Around Current Carrying Conductors

Figures 5.1 and 5.2 show simulations of magnetic flux density around a current carrying conductor. Magnetic flux density reduces radially with increasing distances away from the conductor. This validates the Biot – Savart law which basically gives magnetic flux density around the conductor to be directly proportional to the current flowing through the conductor and inversely proportional to the distance of that point from the conductor.

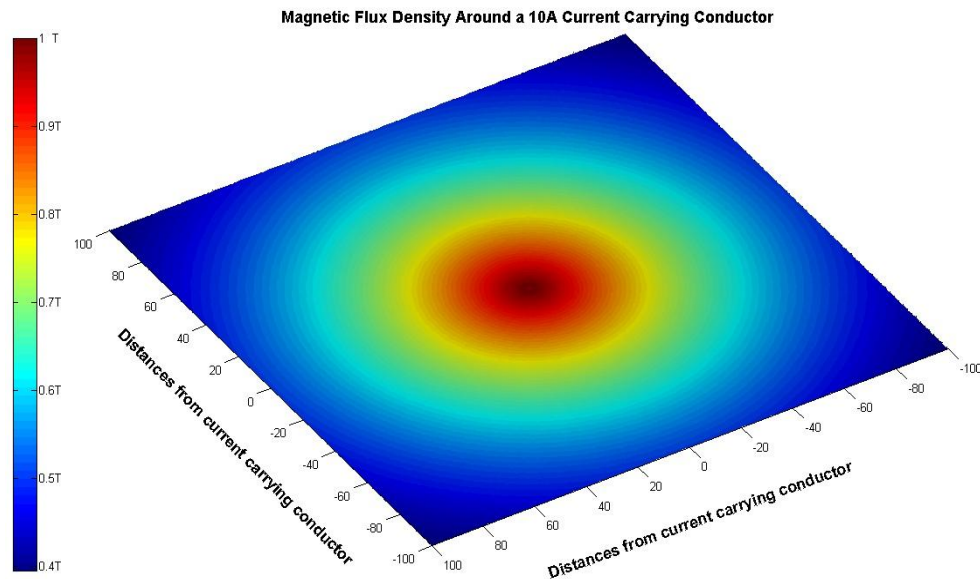


Figure 5.1: Magnetic Flux Density Around a 10 A Current Carrying Conductor

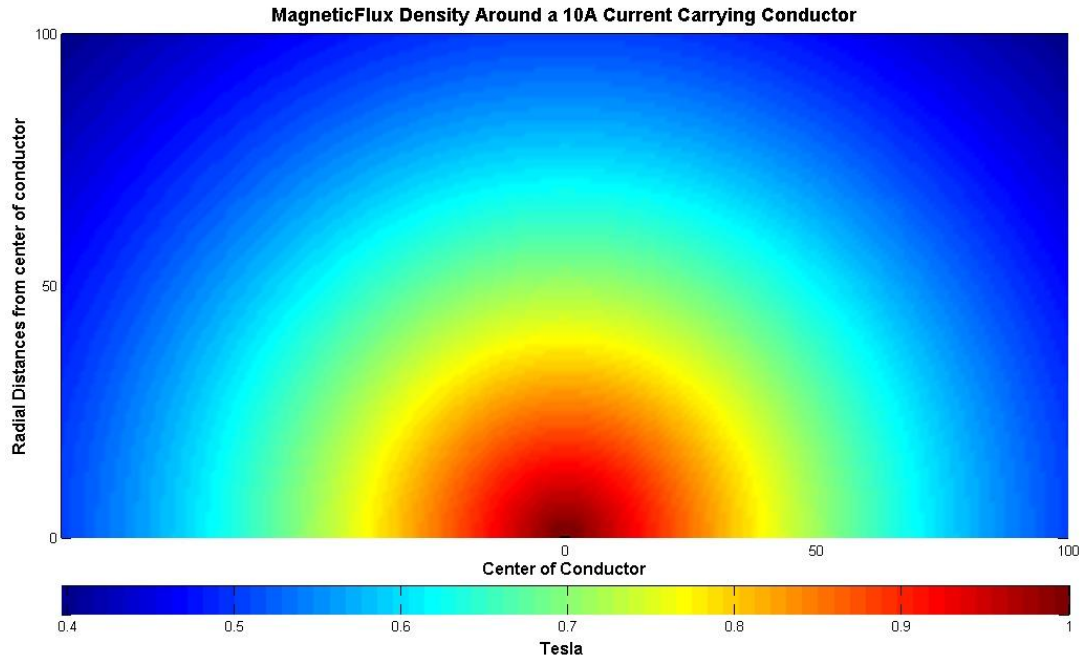


Figure 5.2: A Cut Through Section of Magnetic Flux Density Around a 10 A Current Carrying Conductor

Figure 5.3 shows theoretical result of electromagnetic flux density around a common current carrying conductor in the built environment. The conductor is #12 AWG and the current carrying capacity is 1-20A.

The magnetic flux density on the graph (see Figure 5.3) is calculated using permeability of free space ($\mu_0 = 4\pi \times 10^{-7} \text{ H/m}$) and equation 14. To estimate magnetic flux that can be harvested for power generation, the relative permeability (μ_r) of the core has to be calculated as was done in the case study in chapter 4. Magnetic flux density around current carrying conductor decreases with increasing radial distances from the conductor. The simulation on the graph (see Figure 5.3) shows a radial distance of 2mm to 30mm from the current carrying conductor.

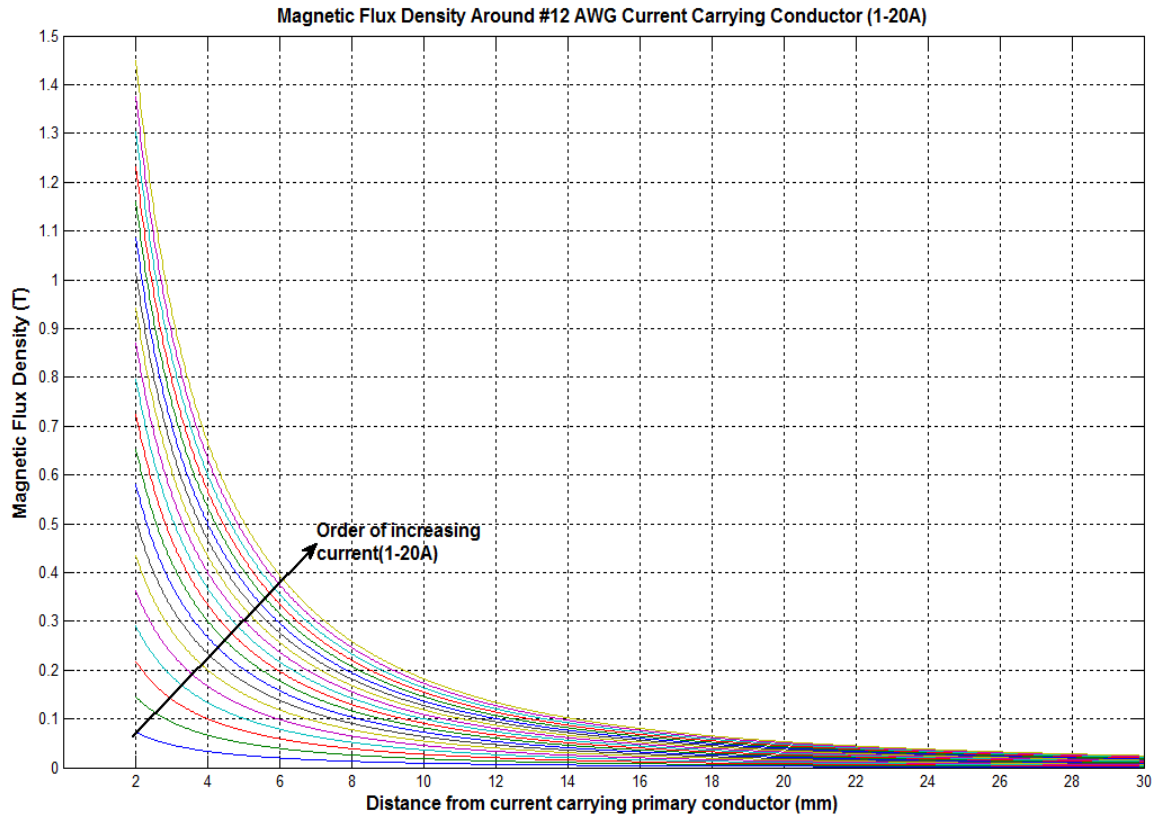


Figure 5.3: Magnetic Flux Density for Different Currents from 1-20 A

5.3 Induced and DC Output Voltages

The electric voltages that can be generated from corresponding primary load input (in watts) are shown in Figure 5.4. The voltages are generated using the AMCC-4 core. Each graph shows 5 different plots. The plots correspond to the voltages generated at radial distances from current carrying conductor to the magnetic path line (MPL, see Figure 4.4). The MPL is the length of an average magnetic field line around the interior of the core (49). The location of this field line is approximated to be at the center of the core as shown in Figure 4.4 (49). Figure 5.5 shows corresponding voltages for primary input current.

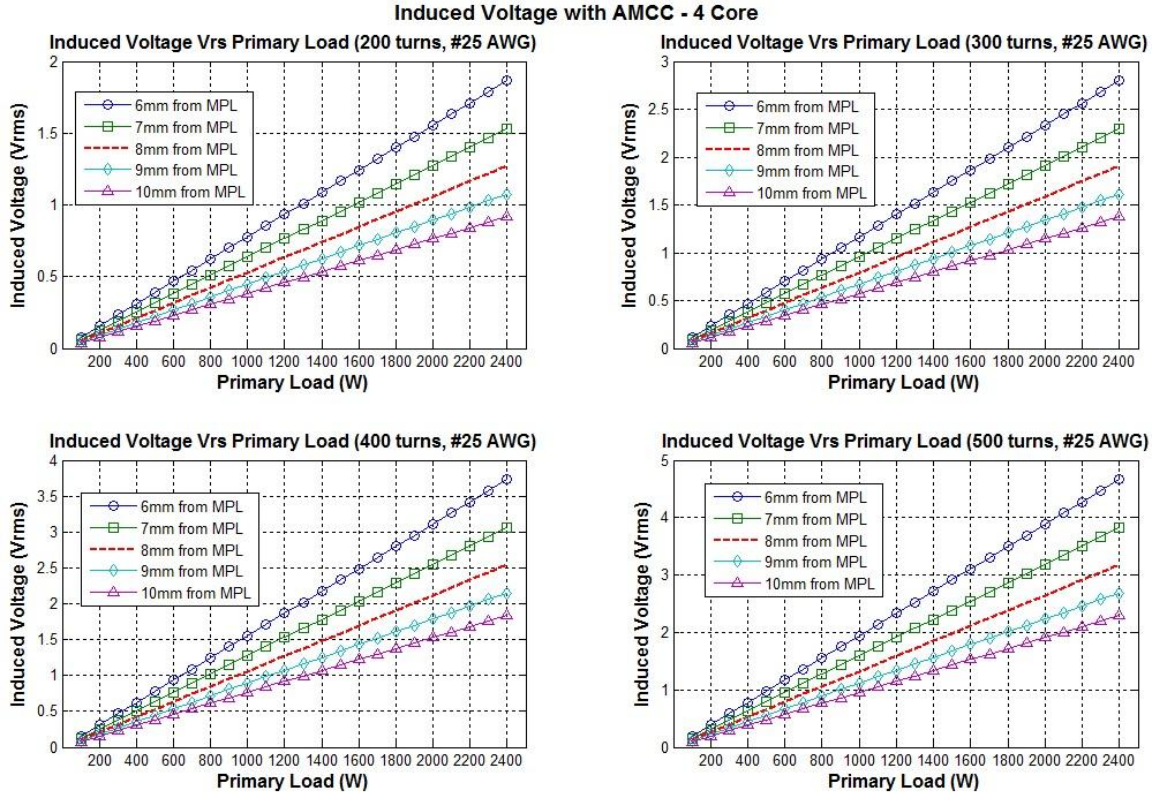


Figure 5.4: Induced Voltages per Primary Load Input (Watts)

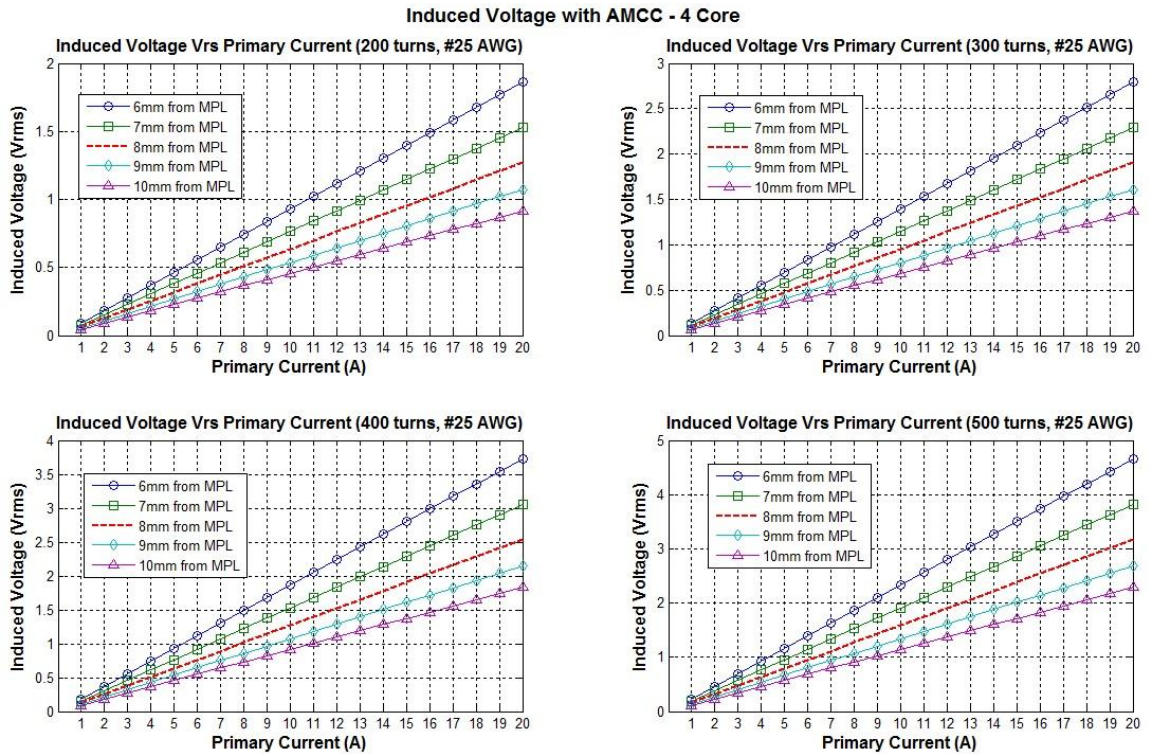


Figure 5.5: Induced Voltages per Primary Load Currents (A)

Figure 5.6 and 5.7 shows the voltages induced for a given load (watts) or current (A) and radial distances from current carrying conductor to MPL. The windings used on the AMCC-4 core for these simulations are 300 and 500 turns respectively.

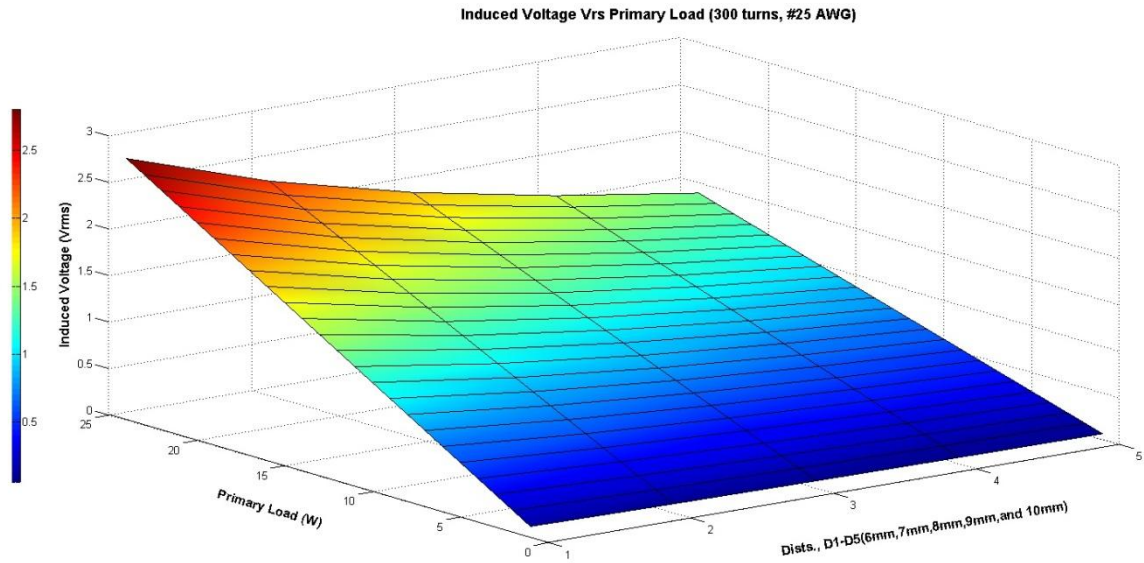


Figure 5.6: A Combination Plot of Induced Voltage Against Primary Input Load and Radial Distances from MPL (300 turns of #25 Secondary Winding)

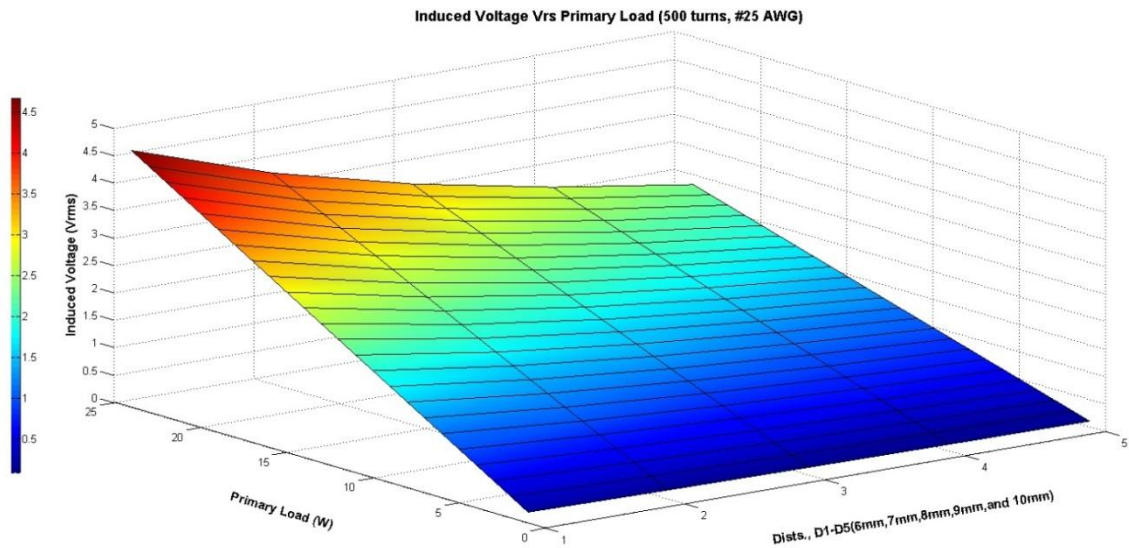


Figure 5.7: A Combination Plot of Induced Voltage Against Primary Input Load and Radial Distances from MPL (500 Turns of #25 Secondary Winding)

Most energy sensors use DC voltages during operation. Simulated voltages in Figure 5.5 are converted to DC component by incorporating an AC to DC bridge rectifier. A 0.5V voltage drop is allowed for the conversion from AC to DC. Figure 5.8 shows the DC voltage simulations.

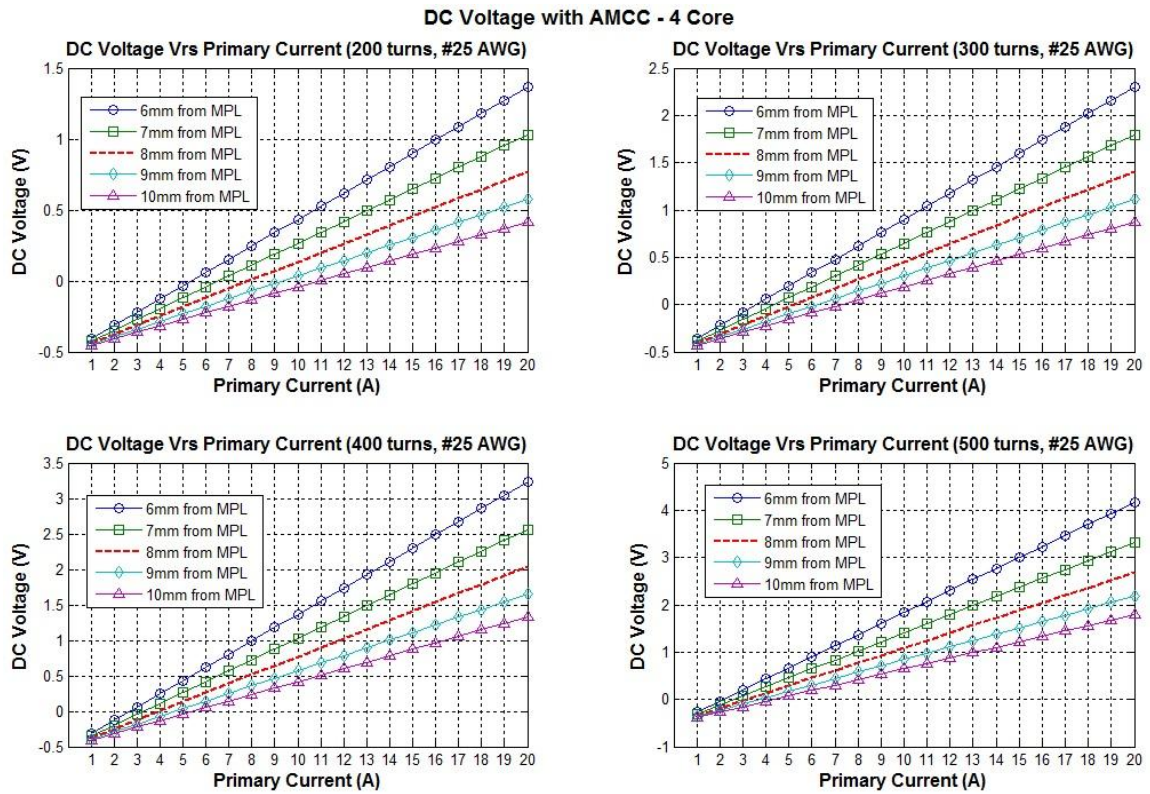


Figure 5.8: DC Output Voltages per Primary Input Load Currents

5.4 Core Size, Versus Magnetic Flux and Input Load Current

As one of the key objectives of the research, estimating the size of the core of energy harvesting device was very important. The size of the core basically translates to the cross sectional area of the core. Figure 5.9 shows a simulation of cross section estimation for a given magnetic flux density. The expected output voltages with a specific number of secondary windings on the core are also given. Corresponding graph for core cross section and primary input current is also shown in Figure 5.10.

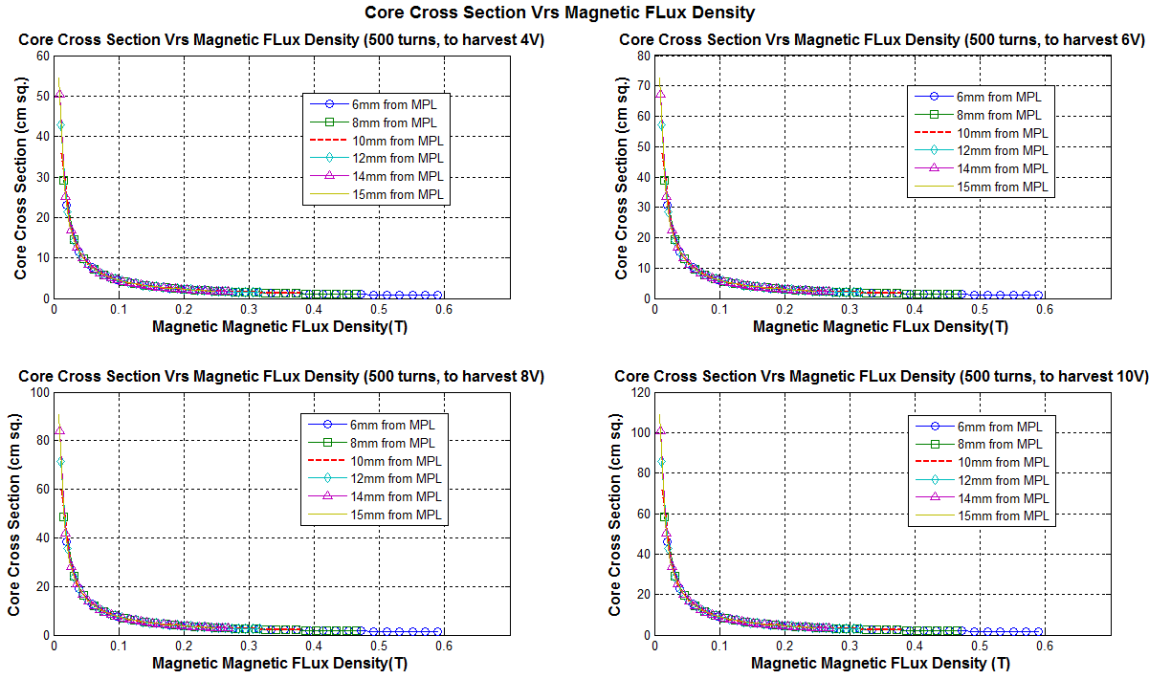


Figure 5.9: Core Cross Section vs. Available Magnetic Flux Density

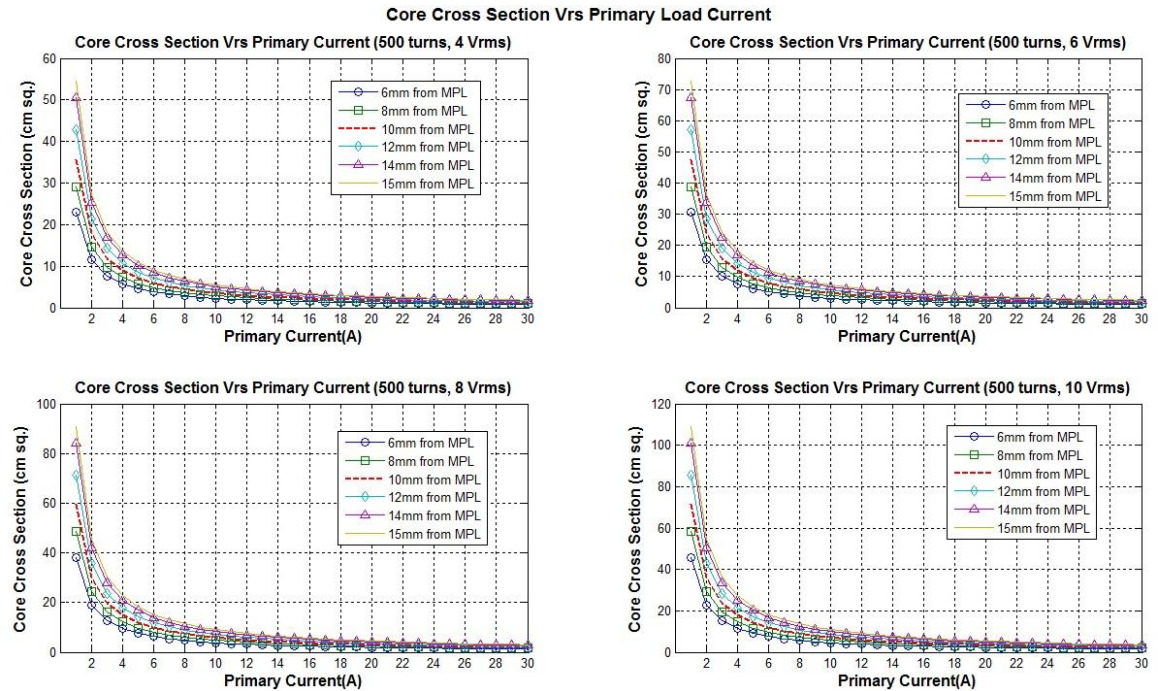


Figure 5.10: Core Cross Section Vs. Primary Input Current

To analyze how radial distances and input primary current affect the cross sectional area of the core of harvesting device, a combination plot is presented with radial distances and primary currents as inputs. This is shown in Figure 5.11.

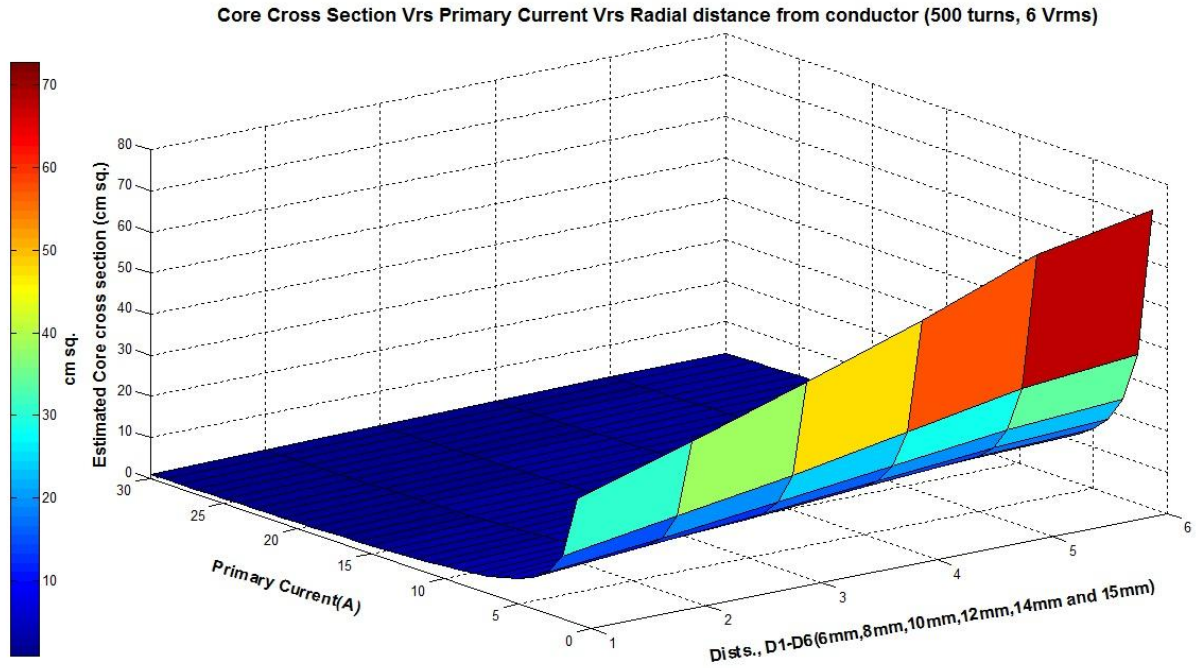


Figure 5.11: Combination Plot of Cross Sectional Area vs. Primary and Radial Distances

5.5 Experimental Results

To validate results from simulations, a prototype energy harvesting device is built with an AMCC-4 with windings, 200, 300, 400 and 500. Figure 5.12 shows an image of the AMCC-4 with the leads of the various windings. Except for the black colored, each lead corresponds to a number of windings. A circuit diagram of the windings is presented in Appendix B2.

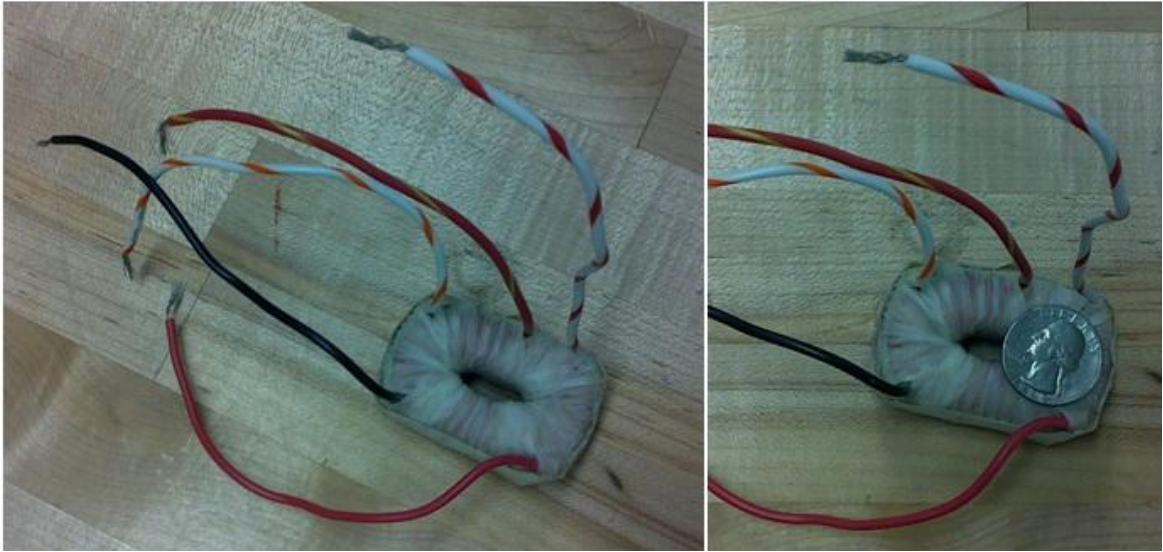


Figure 5.12 Prototype Energy Harvesting device made from AMCC-4 Core.

The board used for experiments is in Figure 5.13. The board is made up of some typical nodes in the built environments and rated for 120 V. The harvesting device is mounted on

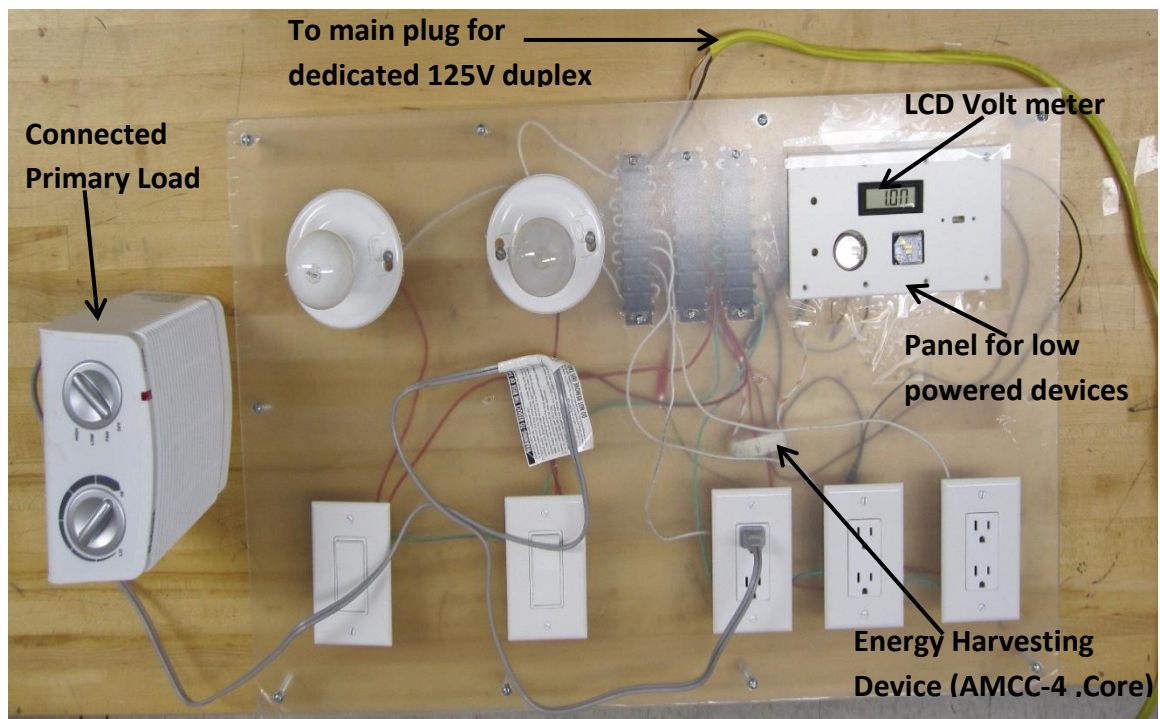


Figure 5.13: Board for Energy Harvesting Experiments

a current conductor on the board as shown in Figure 5.13. The board consists of duplex receptacles, lamp sockets and switches and low powered devices. A main plug for dedicated duplex receptacle is also included to supply power to the board.

The following are part inventory used in building the board for experiments.

- 1) Plastic platform
- 2) 3 duplex receptacles rated at 125 V.
- 3) 2 lamp holders rated at 120 V with connecting switches.
- 4) All conductors are #12 AWG (single phase, Neutral and Ground)
- 5) Low powered devices (energy sensors, USB outlet, LED lights, LED light)
- 6) DC bridge voltage multiplier (Diode D1, D2 (IN4003), C1 C2 C3 , 1μ F rated at 100V)
- 7) Voltage regulator, LM2937 rated at 3.3 V DC, LCD voltage display meter
- 8) 3V DC Chargeable Li-ion battery
- 9) #12 AWG main electric plug connector for a dedicated duplex receptacle rated at 125V.

Figure 5.14 shows a schematic diagram of the board used for experiment. The following steps are used to take measurements from the board.

- a. The main plug is plugged into a dedicated duplex receptacle rated at 120/125V.
- b. A multimeter is connected to the leads of the harvesting device installed on the current carrying conductor on the board.
- c. Various sizes of loads (lamps, small size heaters, etc.) are connected to the nodes (lamp socket, receptacles) on the board.

- d. The loads are turn on and induced voltage measurements are recorded from the multimeter. The sizes of the loads are also recorded. This step is repeated for various loads up to a combined total of 2400 W and also for different winding turns of the harvesting device.
- e. The recorded induced voltage measurements are plotted against corresponding connected loads for the different windings on the harvesting device.
- f. The main plug is disconnected from the dedicated duplex receptacle to conclude the experimental process.

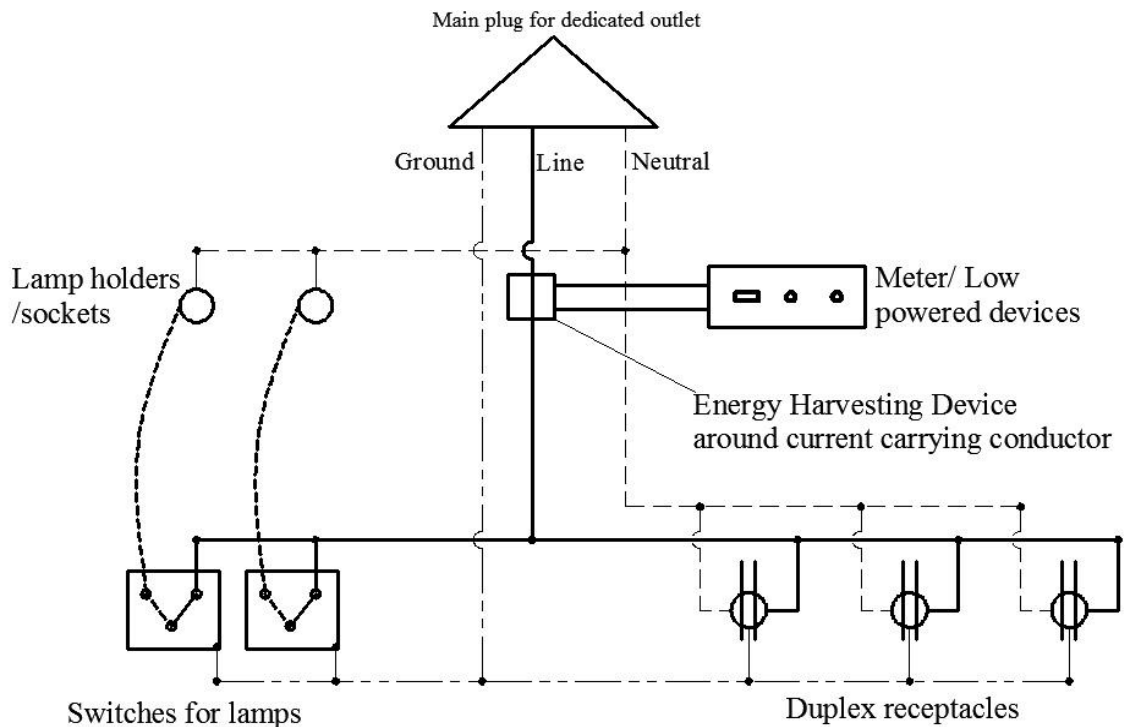


Figure 5.14: Schematic Diagram of the Experimental Board

Figure 5.15 and 5.16 show plotted measurements from experiments with different winding configurations for the AMCC-4 harvesting device.

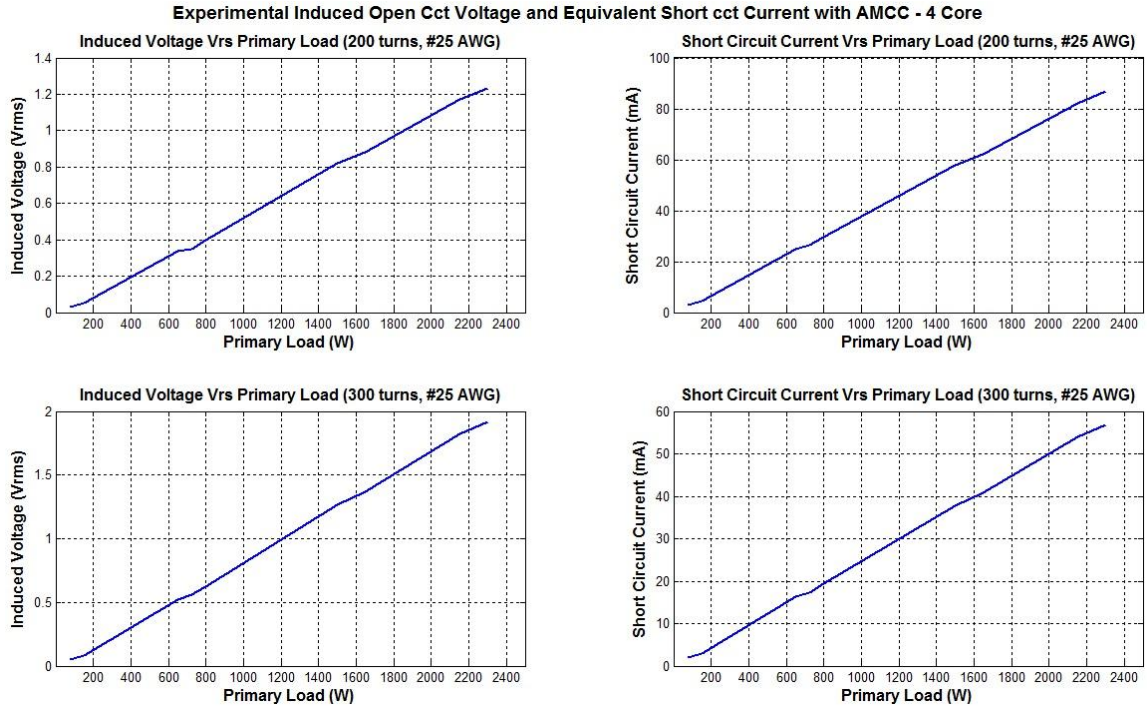


Figure 5.15: Experimental Induced Voltages with AMCC-4 Core

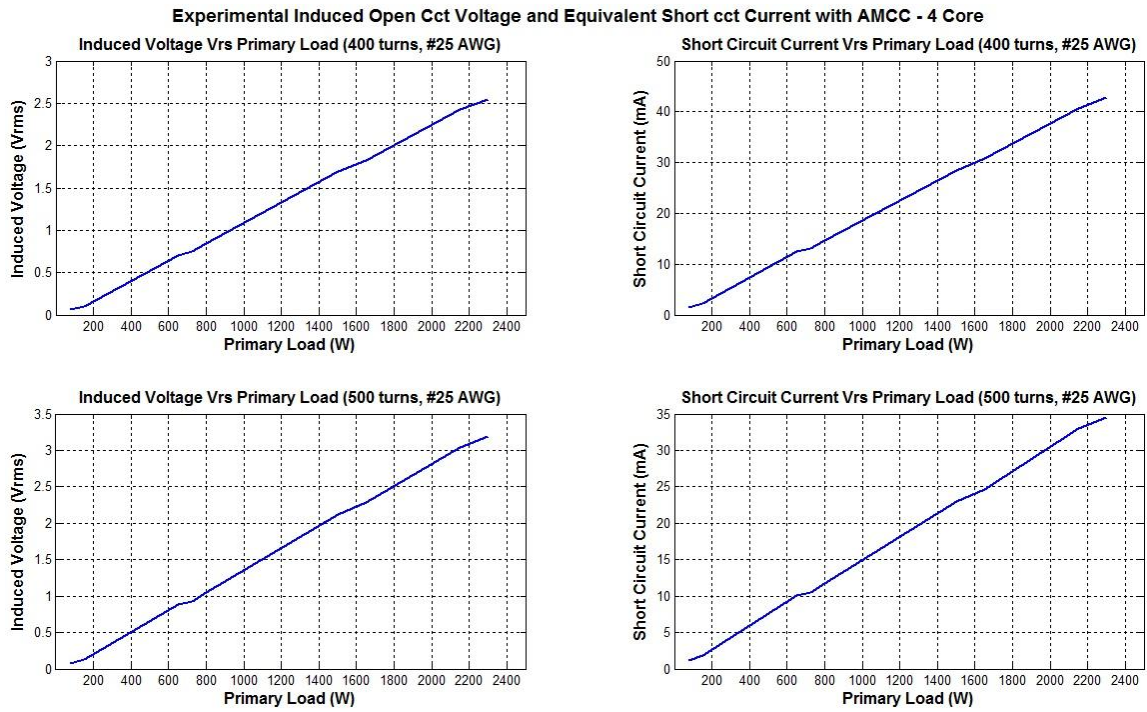


Figure 5.16: Experimental Induced Voltages with AMCC-4

5.6 Simulation vs. Experimental Results

A comparison between simulated and experimental induced voltages for various turns of secondary windings is shown in Figure 5.17. Experimental measurement are plotted with a black line and labeled on each graph.

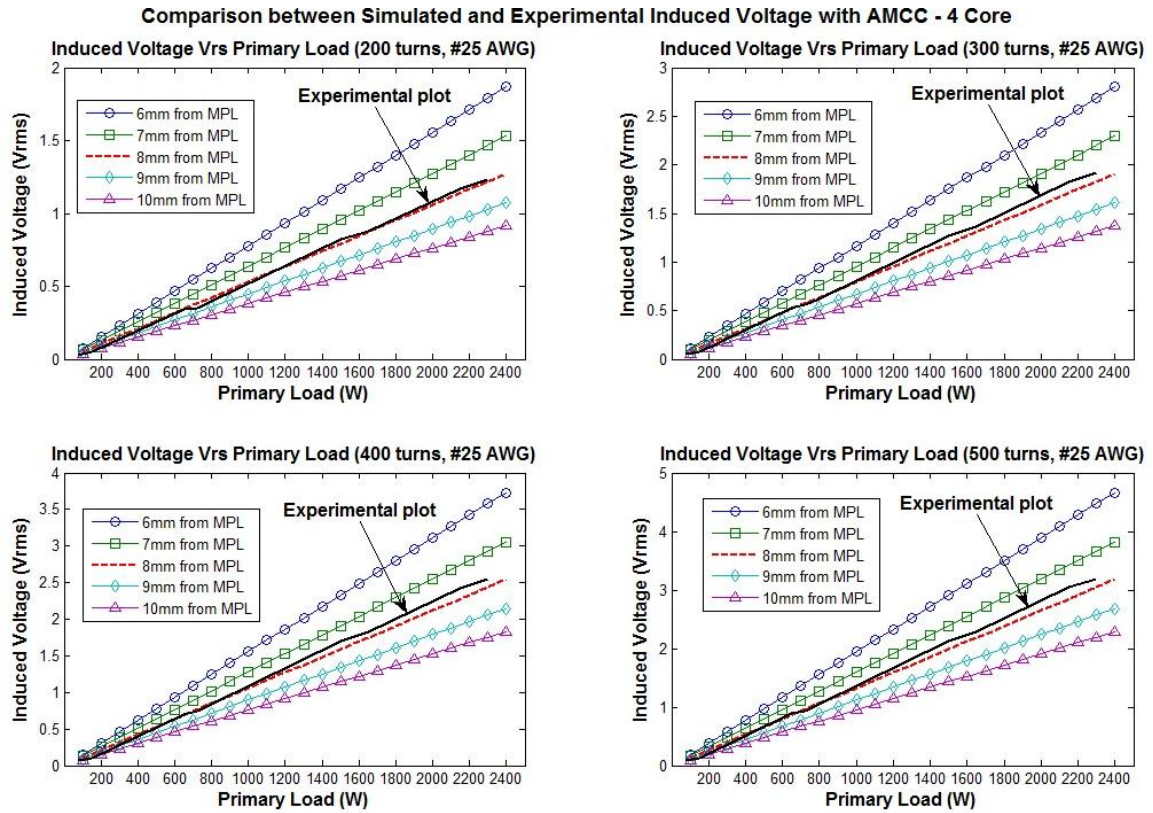


Figure 5.17: Comparison of Simulated and Experimental Induced Voltages

Table 5.1: Simulated and Experimentally Measured Induced Voltages ($r = 8\text{mm}$)

Primary Load (Watts)	Induced Voltages (V rms)							
	200 Turns		300 Turns		400 Turns		500 Turns	
	Simulated	Measured	Simulated	Measured	Simulated	Measured	Simulated	Measured
150	0.08	0.05	0.12	0.08	0.16	0.10	0.20	0.13
650	0.34	0.34	0.52	0.52	0.69	0.70	0.86	0.89
800	0.42	0.40	0.64	0.62	0.85	0.84	1.06	1.05
1500	0.80	0.82	1.19	1.27	1.59	1.70	1.99	2.12
1650	0.87	0.88	1.31	1.37	1.75	1.83	2.19	2.28
2150	1.14	1.17	1.71	1.82	2.28	2.43	2.85	3.04
2300	1.22	1.23	1.83	1.92	2.44	2.55	3.05	3.19

Table 5.1 shows the values of simulated and measured induced voltages from experiments. The voltages are tabulated according to the sizes of loads drawing current at the electrical nodes. Simulated and measured voltages correspond to an 8mm radial distance from the primary current carry conductor to the MPL. The measurements and simulations are also tabulated according to the number of winding turns on the AMCC-4 core.

5.7 Discussion

The objective of this research is to design an energy harvesting device to scavenge electromagnetic energy in the built environment for the purposes of supplying power to energy management sensors. The average power requirement of energy management sensors is 2V – 6 VDC and 12 – 170 mA DC. The amount of power generated depends on the proximity of the current carrying conductor to the MPL. A comparison between the simulation and experimental results indicate that the current carrying conductor is approximately 8mm in proximity from the MPL. With this proximity, simulation and experimental results show a little over 3VAC can be generated with an AMCC-4 core with 500 turns of #25 AWG. An equivalent short circuit current of 34mA AC was measured in laboratory experiments. Using a bridge voltage doubler or multiplier, the induced 3VAC can be boosted up to 6VDC to be feed into a voltage regulator and stabilized for sensor input.

The AMCC-4 was used in the simulation and experiments since it was the smallest available cut core on the market with the preferred magnetic permeability for this research.

The AMCC-4 core has a cross section of 1.11 cm^2 which is much smaller than that of the proposed core in the case study in Chapter 4. The height of the AMCC-4 core is only 15mm and hence able to enclose a much smaller length of the current carrying conductor which is very essential in the power generation process. With the proposed core in Figure 4.2 of cross sectional areas 2 cm^2 and a height of 40mm, a lot more energy can be harvested. This core size will also fit in most boxes of electrical nodes.

An estimate of the amount of the magnetic flux densities around current carrying conductors in the built environment for power generation show an average of 0.25 T can be scavenged at a radial distance of 8mm from a conductor carrying 20A. An equivalent of 3VAC can be generated from this magnetic flux density. This means that for high current drawing nodes in the building electrical system, a much higher voltage can be induced with the proposed energy harvesting device. The material property of the proposed core has a saturation flux density of 1.56 T which is much higher to prevent the core from saturating.

The prototype board used in the experiments contained a typical electrical wiring system design. The loads used for testing were incandescent lamps and small size (wattage) heaters. To utilize power generated at all times, a rechargeable battery is included in the board setup to store energy when power is not being used by the energy management sensor. This board also displays an energy management sensor alongside LEDs connected to output power from the energy harvesting device. The next chapter looks at some of the technical challenges as well as potential future applications of this research.

Chapter 6

TECHNICAL CHALLENGES, BENEFITS AND OPPORTUNITIES

6.1 Introduction

Originally, electrical node boxes were designed to contain electrical cables and splice connectors. Node boxes come in various sizes as shown in NEC table 314.6(A) in Figure 4.1. With the exception of the node boxes, most electrical distribution cables are hidden in enclosed spaces within the built environment. Even though the proposed harvesting device is intended to supply power to energy management sensors in the built environment, other low powered devices can also be supplied with similar harvested power. This chapter examines some of the technical challenges associated with the design of the harvesting device, benefits that may be derived as a result of its use, as well as related future opportunities.

6.2 Challenges

Article 314.71 of the National Electrical Code (NEC) (52) states that pull and junction boxes and handhole enclosures shall provide adequate space and dimensions for conductor installation. Installing energy harvesting devices to power the sensor devices in the boxes of the nodes will reduce the allowable space required by the NEC.

Moreover, in order to power other low powered devices that are not necessarily located at the electrical nodes, access to current carrying conductors in the conduits will

be a limitation to scavenging magnetic flux density. Another limitation is mounting of harvesting device on current carrying conductors. That is, in order to scavenge for magnetic flux, the current carrying conductor must be mounted through the opening in the harvesting device (unlike other current transformers which can be clipped on to the conductor).

In applications where the energy demand of the sensors is less than the quantity generated, energy storage devices (chargeable batteries) have to be incorporated in the installation setup. If the energy scavenged is of an amount lower than the required power, then a back-up chargeable battery must be added to supplement the power requirement. This battery can be recharged with scavenged power during periods in which the energy management sensor is idle.

6.3 Benefits

This research has the potential to create a much more sustainable built environment and thus greatly benefit society. Because the energy source (magnetic field) is in close proximity to the energy management sensor, generated power can be directly applied to the sensor at its location. The ultimate goal of replacing batteries or supplying power to the hardwired energy management sensors with free perpetual energy can be achieved. This will save money in terms of the cost of batteries and all but eliminate the labor costs associated with battery replacement. Even with the limited amount of energy harvested, rechargeable batteries can be used in place of conventional batteries. Power generated by the energy harvesting device will continuously replenish used up energy from the batteries and thus prolong life of batteries.

Furthermore, electricity usage is ultimately maximized since there is additional capture when current is drawn through existing conductors. Thus, the magnetic field located around the current carrying conductors is put to efficient use.

Finally, one of the great advantages of using this device is that it can serve as a potential energy supply for common low powered devices such as motion sensors, phone chargers and some wall clocks in the built environment. Recent power outlet technologies (54), (55), (56) that feature a USB outlet for powering low powered devices up to 5VDC can be powered from this energy harvesting device when that node is drawing power. However, in this case it should be noted that the node will have to draw current in excess of 10A. Wall clocks typically mounted on hallway corridors walls can be powered with an energy harvesting device installed on current carrying conductors powering the lamps in the hallway. In order to constantly supply power to such a clock, a rechargeable battery backup can be incorporated and replenished from time to time by the harvesting device. Motion sensors in corridor hallways that are hardwired or battery operated can also be connected in a similar configuration.

6.4 Opportunities

The proposed energy harvesting device is potentially useful in a variety of other applications than the ones stated in this thesis. For example, if the device is permanently incorporated into the node boxes of the electrical system, power can be harvested for USB outlets. These outlets are currently being integrated into some newer power outlets (57). Therefore, the proposed energy harvesting device would therefore eliminate the need to hardwire these USB outlets to the existing electrical system.

This harvesting device may also be developed into an addressable sensor. That is, the harvesting device can be integrated with a transceiver circuit which will notify a parent transceiver whenever current is drawn at a node. The transceiver integrated with the harvesting device has a unique identification code that can also be used as an alerting system.

Finally, these harvesting devices may be mounted around high current drawing conductors. The harvested power could be channeled to a battery bank to power emergency lighting systems during power outages or other emergency situations.

The final chapter summarizes the whole research and presents the conclusion and recommendations for future work.

Chapter 7

CONCLUSION AND RECOMMENDATIONS

Four objectives were accomplished in this research. First, available magnetic flux was estimated around common current carrying conductors in the built environment. The Biot-Savart law's theoretical equation for estimating the magnetic flux of a given current flowing through a conductor is used to achieve this objective. Second, a comparison of the simulated induced voltages to the experimentally measured values proved accurate Faraday's law of induction. Using theoretical equations for current transformers derived from Faraday's law of induction, an estimate for the average voltages that can be induced from the magnetic flux on the current carrying conductors is given. Third, a harvesting device is designed that is small enough to fit into typical nodes of boxes in the electrical power distribution system in the built environment. It should be noted that due to manufacturing lead time, the prototype harvesting device used for experimenting and simulation is not of the proposed design shape. Thus, the geometry of the harvesting device used for experiments will not fit into a typical node box. Finally, a board was built for the purpose of experimenting with the prototype energy harvesting device. Experimental measurements reveal that an average of 2 V - 3V rms (equivalent short circuit current , 20 mA -40mA) can be induced from magnetic flux around current conductors in the built environment.

Based on a comparison of the experimental and simulated values, it is recommended that a prototype of the proposed design of the harvesting device be built and tested.

7.1 Future Research

Electromagnetic harvesting depends on a secondary ambient source of energy. Thus in order to harvest energy through the electromagnetic converting process, a changing magnetic flux density field must first be established. In the proposed researched, this field is generated when alternating current flows through electrical conductors in the built environment. In future research, investigations will be done to find out whether the harvesting operation affects the magnitude of current flowing through the primary conductor. A further investigation will be done to see if the type of primary load (resistive, inductive, capacitive) at a node in the electrical system has any relationship with magnetic flux density generation.

Another future research will be to investigate how much energy that can be scavenged from magnetic flux density in a given space volume. This investigation will also include harvesting electromagnetic energy around metallic conduits carrying electrical conductors in the built environment.

APPENDICES

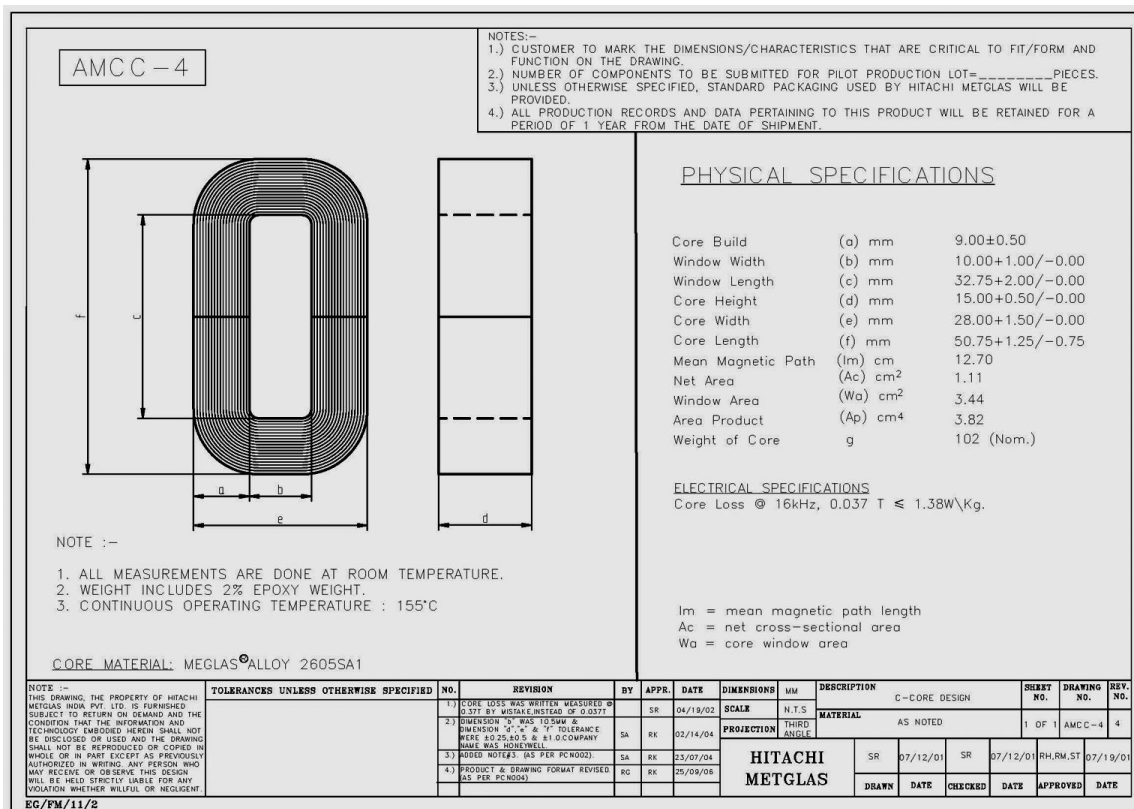
Appendix A

Appendix A.1: Wire Properties Table for Winding Conductors (50)


Wire Table												
AWG	Bare Area		Resistance $\mu\Omega/\text{cm}$ 20°C	Heavy Synthetics								
				Area		Diameter		Turns-Per		Turns-Per		Weight
	$\text{cm}^2(10^{-3})$	cir-mil		$\text{cm}^2(10^{-3})$	cir-mil	cm	Inch	cm	Inch	cm^2	Inch^2	
1	2	3	4	5	6	7	8	9	10	11	12	13
10	52.6100	10384.00	32.7	55.9000	11046.00	0.2670	0.105	3.9	10	11	69	0.46800
11	41.6800	8226.00	41.4	44.5000	8798.00	0.2380	0.094	4.4	11	13	90	0.37500
12	33.0800	6529.00	52.1	35.6400	7022.00	0.2130	0.084	4.9	12	17	108	0.29770
13	26.2600	5184.00	65.6	28.3600	5610.00	0.1900	0.075	5.5	13	21	136	0.23670
14	20.8200	4109.00	82.8	22.9500	4556.00	0.1710	0.068	6.0	15	26	169	0.18790
15	16.5100	3260.00	104.3	18.3700	3624.00	0.1530	0.060	6.8	17	33	211	0.14920
16	13.0700	2581.00	131.8	14.7300	2905.00	0.1370	0.054	7.3	19	41	263	0.11840
17	10.3900	2052.00	165.8	11.6800	2323.00	0.1220	0.048	8.2	21	51	331	0.09430
18	8.2280	1624.00	209.5	9.3260	1857.00	0.1090	0.043	9.1	23	64	415	0.07474
19	6.5310	1289.00	263.9	7.5390	1490.00	0.0980	0.039	10.2	26	80	515	0.05940
20	5.1880	1024.00	332.3	6.0650	1197.00	0.0879	0.035	11.4	29	99	638	0.04726
21	4.1160	812.30	418.9	4.8370	954.80	0.0785	0.031	12.8	32	124	800	0.03757
22	3.2430	640.10	531.4	3.8570	761.70	0.0701	0.028	14.3	36	156	1003	0.02965
23	2.5880	510.80	666.0	3.1350	620.00	0.0632	0.025	15.8	40	191	1234	0.02372
24	2.0470	404.00	842.1	2.5140	497.30	0.0566	0.022	17.6	45	239	1539	0.01884
25	1.6230	320.40	1062.0	2.0020	396.00	0.0505	0.020	19.8	50	300	1933	0.01498
26	1.2800	252.80	1345.0	1.6030	316.80	0.0452	0.018	22.1	56	374	2414	0.01185
27	1.0210	201.60	1687.0	1.3130	259.20	0.0409	0.016	24.4	62	457	2947	0.00945
28	0.8046	158.80	2142.0	1.0515	207.30	0.0366	0.014	27.3	69	571	3680	0.00747
29	0.6470	127.70	2664.0	0.8548	169.00	0.0330	0.013	30.3	77	702	4527	0.00602
30	0.5067	100.00	3402.0	0.6785	134.50	0.0294	0.012	33.9	86	884	5703	0.00472
31	0.4013	79.21	4294.0	0.5596	110.20	0.0267	0.011	37.5	95	1072	6914	0.00372
32	0.3242	64.00	5315.0	0.4559	90.25	0.0241	0.010	41.5	105	1316	8488	0.00305
33	0.2554	50.41	6748.0	0.3662	72.25	0.0216	0.009	46.3	118	1638	10565	0.00241
34	0.2011	39.69	8572.0	0.2863	56.25	0.0191	0.008	52.5	133	2095	13512	0.00189
35	0.1589	31.36	10849.0	0.2268	44.89	0.0170	0.007	58.8	149	2645	17060	0.00150
36	0.1266	25.00	13608.0	0.1813	36.00	0.0152	0.006	62.5	167	3309	21343	0.00119
37	0.1026	20.25	16801.0	0.1538	30.25	0.0140	0.006	71.6	182	3901	25161	0.00098
38	0.0811	16.00	21266.0	0.1207	24.01	0.0124	0.005	80.4	204	4971	32062	0.00077
39	0.0621	12.25	27775.0	0.0932	18.49	0.0109	0.004	91.6	233	6437	41518	0.00059
40	0.0487	9.61	35400.0	0.0723	14.44	0.0096	0.004	103.6	263	8298	53522	0.00046
41	0.0397	7.84	43405.0	0.0584	11.56	0.0086	0.003	115.7	294	10273	66260	0.00038
42	0.0317	6.25	54429.0	0.0456	9.00	0.0076	0.003	131.2	333	13163	84901	0.00030
43	0.0245	4.84	70308.0	0.0368	7.29	0.0069	0.003	145.8	370	16291	105076	0.00023
44	0.0202	4.00	85072.0	0.0316	6.25	0.0064	0.003	157.4	400	18957	122272	0.00020

Appendix B

Appendix B.1: Specifications of AMCC-4 Core



Appendix B.2: Winding Schematic Drawings of AMCC-4 Core



FROST MAGNETICS INC

~~3200 NORTH CENTRAL AVENUE, SUITE 200, CHICAGO, ILLINOIS 60641~~
~~800-541-5555 (TOLL FREE)~~

BLACK 0—1

RED 0—2

WHT/RED 0—3

RED/YEL 0—4

WHT/ORN 0—5

PART NO. FM-8361-A	
DATE 2-13-12 ENG. M7	
CUST. EVANS	
CUST. NO. SAME	
CU. LOSS	
FE LOSS	
TOTAL LOSSES	
VA	I _{EX}
LB	
SA	
ΔT	

CORE AMCC-4	WND	LEG	A _C (NET)	LC	VOL	FLUX DENS.	W/LB	WT (NET)
WDG. FORM Z-L-KAPTON PR.								
TERMINAL								
LEAD NO.	1-2-3-4-5							
VOLTAGE (O.C.)								
CURRENT								
WIRE	#25 SN							
O.D.								
C.M.								
CM/A								
WL								
T/L								
LAYERS								
TURN	0 + 200 → 300 + 400 → 500							
TAPS								
LAYER INS.								
WRAPPER	1-L DACRON							
FT/TURN								
TOTAL LENGTH								
OHMS/M								
DCR								
IR/% REG								
LB/M								
WEIGHT								
I ² R								
BUILD								

BUILD UP

Appendix C

Appendix C.1: MATLAB Programming Codes

```

%*****
%%%%%%%%%% This code was written by Evans Sordiashie %%%%%%%%%%
%*****
%% MATLAB Code developed for Master of Science Thesis, May 2012, UNL.%%

%%%%%%%%%%%%%%%%%%%%%%%%%%%%%%%%%%%%%%%%%%%%%%%%%%%%%%%%%%%%%%%%%%%%%%%%%
Title: Electromagnetic Harvesting to power Energy Management Sensors
%%%%%%%%%%%%%%%%%%%%%%%%%%%%%%%%%%%%%%%%%%%%%%%%%%%%%%%%%%%%%%%%%%%%%%%%%

%This MATLAB code is used to determine the following:

% 1. Plot Magnetic Field around a Current carrying conductor

%*****
clear all
close all
clc
%=====
% current carrying conductor conductor parameters
%=====
L = 100;                % length of conductor
mu0 = 4*pi*1e-7;        % magnetic permeability constant
N=100;                  % number of elements in current carrying
conductor
I=10;                   % current flowing through the conductor (A)
%=====
xC = zeros(1,N);        % xyz coordinates points on current conductor
yC = zeros(1,N);
zC = zeros(1,N);

%=====
%Discretizing conductor
%=====
dl=L/N; l(1)=dl/2;

for i=2:N,
    l(i) = (i-1)*dl + l(1);
end

zC = 1;

% length of each elemental conductor element
Lx = 0; Ly = 0; Lz= dl;

% Detector space(rectangular coordinates~xP, yP, zP) where B is
calculated
NP = 200;                % Detector points NP x N
xPmax = 100;              % Dimensions of detector space

```

```

yPmin = 0; yPmax = N;

xP = linspace(-xPmax,xPmax,NP);
yP = linspace(-yPmax,yPmax,NP);
[xxP yyP] = meshgrid(xP,yP);
Bx = zeros(NP,NP);By = Bx; Bz = Bx;

%=====
% Calculation of magnetic field B
%=====
for c = 1 : N
    rx = xxP;
    ry = yyP;
    rz = zC(c);
    r = sqrt(rx.^2 + ry.^2 + rz.^2);
    r2 = r.^2;
    Bx = Bx + (mu0*I./(4*pi))*Lz.*ry./r2;
    By = By + (mu0*I./(4*pi))*Lz.*rx./r2;
    Bz = Bz + 0;
end
B = sqrt(Bx.^2 + By.^2 + Bz.^2);
B = B./max(max(B)); % normalize B to 1

%=====
% Simulation of Magnetic field for given current I
%=====
%2-D Plot
%=====
figure(1)
pcolor(xxP,yyP,B);
colormap(jet)
shading interp;
axis equal;
axis([-xPmax xPmax 0 yPmax]);
xlabel('Center of Conductor','FontWeight','bold','FontSize',12);
ylabel('Radial Distances from center of conductor','FontWeight','bold'....
    , 'FontSize',12);
set(gca,'XTick',[0:50:100]);
set(gca,'YTick',[0:50:100]);
rectangle('Position',[-1 0 2 0.2],'FaceColor','k');
title('MagneticFlux Density Around a 10A Current Carrying Conductor',...
    'FontWeight','bold','FontSize',14)
h = colorbar('horiz');
set(h, 'XTick')
xlabel(h, 'Tesla')
%=====
%3-D View
%=====
figure(2)

surf(xxP,yyP,B,'FaceColor','interp',...
    'EdgeColor','none',...
    'FaceLighting','phong')
daspect([1 1 1])

```

```

axis tight
xlabel('Distances from current carrying
conductor','FontWeight','bold'...
      , 'FontSize',12, 'Rotation',-44);
ylabel('Distances from current carrying conductor',
'FontWeight','bold'...
      , 'FontSize',12, 'Rotation',19.5);
view(-122,36)
camlight left
colormap(jet)
% colorbar
title('Magnetic Flux Density Around a 10A Current Carrying
Conductor',...
      'FontWeight','bold','FontSize',14)
h = colorbar;
ylabel = get(h, 'YTickLabel');
T = repmat('T',length(ylabel),1);
ylabel = [ylabel T];
set(h, 'YTickLabel',ylabel);

%=====
%%%%%%%%%%%%%% End %%%%%%%%%%%%%%%
%=====

%%%%%%%%%%%%%%
%Title: Electromagnetic Harvesting to power Energy Management Sensors%%
%%%%%%%%%%%%%%

%This MATLAB code is used to determine the following:

% 1. Magnetic field strength around a conductor carrying 1-20A
% 2. Plot of magnetic field strength against currents
% 3. Plot of Induced voltage vrs primary conductor current (1-20A)
% 4. Plot of DC voltage vrs primary conductor current (1-20A)

%*****
% Electromagnetic Harvesting to power Energy Management Sensors

clear all
close all
clc

% parameters for current carrying conductor
L = 15; % length (mm) copper #12 AWG conductor
C = 2.05/2; % conductor average radius (mm), NEC Table 8

%=====
% Core properties
%=====
lm = 12.2e-2; %(m), Magnetic path length (from core data), AMCC-4 Core
lg = 120e-6; %(m), Air gap between cut cores(range 25-150 micro meter)
mu_m = 3000; % (H/m), permeability of core material (Amorphous, 2605)
mur = mu_m/(1 + mu_m *(lg/(lm))); % relative permeability of core
mu0 = 4e-7 * pi; % Magnetic permeability of free space or vacuum
mu = mu0 * mur;% (H/m), Effective permeability of core

```

```

%=====
% Calculating Magnetic Strength around current carrying conductor
%=====
Ip = 1:1:20; % Primary current range
I = Ip;
r = (C:.025:30); % radial distances from current carrying
conductor, 0.025 increments

B = zeros(1160,1); % Magnetic field Strength

for p = 1:20;
    for i = 1:1160;
        B(i,p) = (mu * I(p) * L * 1e-3)/(2*pi*r(i)*1e-3 *...
            sqrt(4*(r(i)*1e-3)^2 + (L*1e-3)^2));
    end
end

r1 = r(41:1160)'; % Selected radial distances
Bac = B(41:1160,1:20); % Corresponding magnetic field strength
H = [r1 Bac(41:1160,1:20)]; % Matrix of radial distances and magnetic
flux
%=====
% Plotting generated magnetic field against radial distance. Field
% generated for 1-20A
%=====
clf
figure(1)
plot(r1, Bac(:,1:20));
set(gca, 'XTick', 2:2:30)
set(gca, 'YTick', 0:0.1:1.5)
grid on
xlabel({'Distance from current carrying primary conductor (mm)'},...
    'FontWeight','bold','FontSize',12);
ylabel({'Magnetic Flux Density (T)'}, 'FontWeight','bold','FontSize',12);
title('Magnetic Flux Density Around #12 AWG Current Carrying Conductor (1-20A)',...
    'FontWeight','bold',...
    'FontSize',12);
%Create arrow
annotation1 = annotation(...
    'arrow',...
    [0.1795 0.312],[0.1441 0.3594],...
    'LineWidth',2);

% Create textbox
annotation2 = annotation(...
    'textbox',...
    'Position',[0.306 0.3363 0.2096 0.05516],...
    'LineStyle','none',...
    'FitHeightToText','off',...
    'FontSize',12,...

```

```

'FontWeight','bold',...
'String',{'Order of increasing current(1-20A)'}));

%=====
% Calculating induced Voltage
%=====
% Core Parameters
% %=====
Ac = 1.11;% Cross sectional area of core in cm.sq, AMCC-4 Core.

%Operating Parameters
%=====
Np = 1; % Number of turns of primary conductor ~1
f = 60; % output frequency in Hz
Kf = 4.44; % Waveform factor, sinewave.
%=====
% Magnetic field strength at (,6,7,8,9,10mm)from current carrying...
% conductor is used for calculation ~ approx. distance from magnetic
% path length(lm or MPL)

D = [Bac(201,:) ' Bac(241,:) ' Bac(281,:) ' Bac(321,:) ' Bac(361,:) '];
%=====
% Calculating induced voltages for various number of magnetic wire
% windings
% around core. Ns = 50, 100, 150, 200, 250, 300, 350, 400, 450, 500.
%=====
Ns = (50:50:500);
Vs = zeros(20,5);
for w = 1:5,
    for g = 1:20,
        for m = 1:10,
            Vs (g,w,m) = Ac * Kf * D(g,w) * f * Ns(m)/(1e4);
        end
    end
end
Vs;

%=====
%Plotting Induced Voltages against Primary Current (A) for 200, 300,
% 400, 500turns.
%=====

% figure (2)
jj = figure('Color',[1 1 1]);
subplot(2,2,1)
plot1=plot (Ip, Vs(:, :, 4));
set(plot1(1), 'LineWidth',1.0, 'Marker', 'o');
set(plot1(2), 'LineWidth',1.0, 'Marker', 'square')
set(plot1(3), 'LineWidth',2.0, 'LineStyle', '--');
set(plot1(4), 'LineWidth',1.0, 'Marker', 'diamond');
set(plot1(5), 'LineWidth',1.0, 'Marker', '^');
set(gca, 'XTick',1:1:20)
grid on
xlabel({'Primary Current (A)'}, 'FontWeight', 'bold', 'FontSize', 12);

```



```

ylabel({'Induced Voltage (Vrms)'}, 'FontWeight', 'bold', 'FontSize', 12);

title({'Induced Voltage Vrs Primary Current (200 turns, #25 AWG)'}, ...
      'FontWeight', 'bold', 'FontSize', 12);
legend('6mm from MPL', '7mm from MPL', '8mm from MPL', '9mm from
MPL', '10mm from MPL')

set(legend, ...
     'Position', [0.1469791666666665 0.750053049452929 0.113125
0.144132653061225], ...
     'FontSize', 10);

subplot(2,2,2)
plot1=plot (Ip, Vs(:, :, 6));
set(plot1(1), 'LineWidth', 1.0, 'Marker', 'o');
set(plot1(2), 'LineWidth', 1.0, 'Marker', 'square')
set(plot1(3), 'LineWidth', 2.0, 'LineStyle', '--');
set(plot1(4), 'LineWidth', 1.0, 'Marker', 'diamond');
set(plot1(5), 'LineWidth', 1.0, 'Marker', '^');
set(gca, 'XTick', 1:1:20)
grid on
xlabel({'Primary Current (A)'}, 'FontWeight', 'bold', 'FontSize', 12);

ylabel({'Induced Voltage (Vrms)'}, 'FontWeight', 'bold', 'FontSize', 12);

title({'Induced Voltage Vrs Primary Current (300 turns, #25 AWG)'}, ...
      'FontWeight', 'bold', 'FontSize', 12);
legend('6mm from MPL', '7mm from MPL', '8mm from MPL', '9mm from
MPL', '10mm from MPL')

set(legend, 'Position', [0.6029166666666662 0.758343865779456 0.09625
0.125]);

subplot(2,2,3)
plot1=plot (Ip, Vs(:, :, 8));
set(plot1(1), 'LineWidth', 1.0, 'Marker', 'o');
set(plot1(2), 'LineWidth', 1.0, 'Marker', 'square')
set(plot1(3), 'LineWidth', 2.0, 'LineStyle', '--');
set(plot1(4), 'LineWidth', 1.0, 'Marker', 'diamond');
set(plot1(5), 'LineWidth', 1.0, 'Marker', '^');
set(gca, 'XTick', 1:1:20)
grid on
xlabel({'Primary Current (A)'}, 'FontWeight', 'bold', 'FontSize', 12);

ylabel({'Induced Voltage (Vrms)'}, 'FontWeight', 'bold', 'FontSize', 12);

title({'Induced Voltage Vrs Primary Current (400 turns, #25 AWG)'}, ...
      'FontWeight', 'bold', 'FontSize', 12);
legend('6mm from MPL', '7mm from MPL', '8mm from MPL', '9mm from
MPL', '10mm from MPL')

set(legend, 'Position', [0.159166666666666 0.282578559657006 0.09625
0.125]);

subplot(2,2,4)

```

```

plot1=plot (Ip, Vs(:, :, 10));
set(plot1(1), 'LineWidth', 1.0, 'Marker', 'o');
set(plot1(2), 'LineWidth', 1.0, 'Marker', 'square')
set(plot1(3), 'LineWidth', 2.0, 'LineStyle', '--');
set(plot1(4), 'LineWidth', 1.0, 'Marker', 'diamond');
set(plot1(5), 'LineWidth', 1.0, 'Marker', '^');
set(gca, 'XTick', 1:1:20)
grid on
xlabel({'Primary Current (A)'}, 'FontWeight', 'bold', 'FontSize', 12);

ylabel({'Induced Voltage (Vrms)'}, 'FontWeight', 'bold', 'FontSize', 12);

title({'Induced Voltage Vrs Primary Current (500 turns, #25 AWG)'}, ...
      'FontWeight', 'bold', 'FontSize', 12);
legend('6mm from MPL', '7mm from MPL', '8mm from MPL', '9mm from
MPL', '10mm from MPL')

set(legend, 'Position', [0.6091666666666654 0.294058151493739 0.09625
0.125]);

ha = axes('Position', [0 0 1 1], 'Xlim', [0 1], 'Ylim', [0
1], 'Box', 'off', 'Visible', 'off', 'Units', 'normalized', 'clipping' ,
'off');

text(0.5, 1, '\bf Induced Voltage with AMCC - 4
Core', 'HorizontalAlignment'...
, 'center', 'VerticalAlignment', 'top', 'FontWeight', 'bold', ...
'FontSize', 14);

%=====
%Calculating output DC Voltage
%=====
Vd = 0.5; % Diode voltage drop

Vo = zeros(20, 5);
for k = 1:5,
    for t = 1:20,
        for j = 1:10,
            Vo(t, k, j) = Vs(t, k, j) - Vd;
        end
    end
end
Vo;

%=====
%Plotting DC Voltages against Primary Current (A) for 200, 300, 400,
%500 turns
%=====

figure (3)
subplot(2, 2, 1)
plot1=plot (Ip, Vo(:, :, 4));
set(plot1(1), 'LineWidth', 1.0, 'Marker', 'o');
set(plot1(2), 'LineWidth', 1.0, 'Marker', 'square')
set(plot1(3), 'LineWidth', 2.0, 'LineStyle', '--');

```

```

set(plot1(4), 'LineWidth', 1.0, 'Marker', 'diamond');
set(plot1(5), 'LineWidth', 1.0, 'Marker', '^');
set(gca, 'XTick', 1:1:20)
grid on
xlabel({'Primary Current (A)'}, 'FontWeight', 'bold', 'FontSize', 12);

ylabel({'DC Voltage (V)'}, 'FontWeight', 'bold', 'FontSize', 12);

title({'DC Voltage Vrs Primary Current (200 turns, #25 AWG)'}, ...
      'FontWeight', 'bold', 'FontSize', 12);
legend('6mm from MPL', '7mm from MPL', '8mm from MPL', '9mm from
MPL', '10mm from MPL')

set(legend, ...
    'Position', [0.1469791666666665 0.750053049452929 0.113125
0.144132653061225], ...
    'FontSize', 10);

subplot(2,2,2)
plot1=plot (Ip, Vo(:, :, 6));
set(plot1(1), 'LineWidth', 1.0, 'Marker', 'o');
set(plot1(2), 'LineWidth', 1.0, 'Marker', 'square')
set(plot1(3), 'LineWidth', 2.0, 'LineStyle', '--');
set(plot1(4), 'LineWidth', 1.0, 'Marker', 'diamond');
set(plot1(5), 'LineWidth', 1.0, 'Marker', '^');
set(gca, 'XTick', 1:1:20)
grid on
xlabel({'Primary Current (A)'}, 'FontWeight', 'bold', 'FontSize', 12);

ylabel({'DC Voltage (V)'}, 'FontWeight', 'bold', 'FontSize', 12);

title({'DC Voltage Vrs Primary Current (300 turns, #25 AWG)'}, ...
      'FontWeight', 'bold', 'FontSize', 12);
legend('6mm from MPL', '7mm from MPL', '8mm from MPL', '9mm from
MPL', '10mm from MPL')

set(legend, 'Position', [0.6029166666666662 0.758343865779456 0.09625
0.125]);

subplot(2,2,3)
plot1=plot (Ip, Vo(:, :, 8));
set(plot1(1), 'LineWidth', 1.0, 'Marker', 'o');
set(plot1(2), 'LineWidth', 1.0, 'Marker', 'square')
set(plot1(3), 'LineWidth', 2.0, 'LineStyle', '--');
set(plot1(4), 'LineWidth', 1.0, 'Marker', 'diamond');
set(plot1(5), 'LineWidth', 1.0, 'Marker', '^');
set(gca, 'XTick', 1:1:20)
grid on
xlabel({'Primary Current (A)'}, 'FontWeight', 'bold', 'FontSize', 12);

ylabel({'DC Voltage (V)'}, 'FontWeight', 'bold', 'FontSize', 12);

title({'DC Voltage Vrs Primary Current (400 turns, #25 AWG)'}, ...
      'FontWeight', 'bold', 'FontSize', 12);

```

```

legend('6mm from MPL','7mm from MPL','8mm from MPL','9mm from
MPL','10mm from MPL')

set(legend,'Position',[0.159166666666666 0.282578559657006 0.09625
0.125]);

subplot(2,2,4)
plot1=plot (Ip, Vo(:, :, 10));
set(plot1(1), 'LineWidth', 1.0, 'Marker', 'o');
set(plot1(2), 'LineWidth', 1.0, 'Marker', 'square');
set(plot1(3), 'LineWidth', 2.0, 'LineStyle', '--');
set(plot1(4), 'LineWidth', 1.0, 'Marker', 'diamond');
set(plot1(5), 'LineWidth', 1.0, 'Marker', '^');
set(gca, 'XTick', 1:1:20)
grid on
xlabel({'Primary Current (A)'}, 'FontWeight', 'bold', 'FontSize', 12);

ylabel({'DC Voltage (V)'}, 'FontWeight', 'bold', 'FontSize', 12);

title({'DC Voltage Vrs Primary Current (500 turns, #25 AWG)'}, ...
'FontWeight', 'bold', 'FontSize', 12);
legend('6mm from MPL','7mm from MPL','8mm from MPL','9mm from
MPL','10mm from MPL')

set(legend,'Position',[0.609166666666665 0.294058151493739 0.09625
0.125]);

ha = axes('Position',[0 0 1 1], 'Xlim',[0 1], 'Ylim',[0
1], 'Box', 'off', 'Visible', 'off', 'Units', 'normalized', 'clipping' ,
'off');

text(0.5, 1, '\bf DC Voltage with AMCC - 4
Core', 'HorizontalAlignment'...
, 'center', 'VerticalAlignment', 'top', 'FontWeight', 'bold', ...
'FontSize', 14);

%=====
%%%%%%%%%% End %%%%%%%%%%
%=====

%%%%%%%%%
%%Title: Electromagnetic Harvesting to power Energy Management Sensors%
%%%%%%%%%

%This MATLAB code is used to determine the following:

% 1. Plot of Induced Voltage (Vrms) against Primary Load 100-2400(W)
% 2. Plot of Induced voltage vrs Primary Load vrs radial distance
%*****
clear all
close all
clc

% parameters for current carrying conductor

```

```

L = 15; % length (mm) copper #12 AWG conductor
C = 2.05/2; % conductor average radius (mm), NEC Table 8

%=====
% Core properties
%=====
lm = 12.2e-2; % (m), Magnetic path length (from core data), AMCC-4 Core
lg = 120e-6; % (m), Air gap between cut cores (range 25-150 micro meter)
mu_m = 3000; % (H/m), permeability of core material (Amorphous, 2605)
mur = mu_m / (1 + mu_m * (lg / (lm))); % relative permeability of core
mu0 = 4e-7 * pi; % Magnetic permeability of free space or vacuum
mu = mu0 * mur; % (H/m), Effective permeability of core

%=====
% Calculating Magnetic Strength around current carrying conductor
%=====
% Primary Load (Watts)
Rp = 100:100:2400;

% Primary Voltage (V rms)
Vp = 120;

Ip = Rp / Vp;

r = (C:.025:30); % radial distances from current carrying
conductor, 0.025 increments

B = zeros(1160,1);
for p = 1:24;
    for i = 1:1160;
        B(i,p) = (mu * Ip(p) * L * 1e-3) / (2*pi*r(i)*1e-3 * ...
            sqrt(4*(r(i)*1e-3)^2 + (L*1e-3)^2));
    end
end

%=====
% Selecting magnetic field strength values at radial distances from...
% current carrying conductor (1, 2, 3, 4, 5, 6, 7, 8, 9, 10mm ).
Current...
% range for #12 AWG conductor is 1 to 20A.
%=====

r1 = r(41:1160)'; % radial distances
Bac = B(41:1160,1:24); % Corresponding magnetic field strength
% H = [r1 B(41:1160,1:24)]; % Matrix of radial distances and magnetic
flux

%=====
% Calculating Induced voltage // Secondary turns // Output Voltage
%=====

% Core Parameters
%=====
Ac = 1.11; % Cross sectional area of core in cm.sq, AMCC-4 Core.

```

```

%Operating Parameters
%=====
Np = 1; % Number of turns of primary conductor ~1
f = 60; % output frequency in Hz
Kf = 4.44; % Waveform factor, sinewave.

% Magnetic field strength at (,6,7,8,9,10mm)from current carrying...
% conductor is used for calculation ~ approx distance from magnetic
path...
% length(lm or MPL)
%=====
D = [Bac(201,:) ' Bac(241,:) ' Bac(281,:) ' Bac(321,:) ' Bac(361,:) '];

%=====
% Calculating induced voltages for various number of magnetic wire
windings
% around core. Ns = 50, 100, 150, 200, 250, 300, 350, 400, 450, 500.
%=====
Ns = (50:50:500);
Vs = zeros(24,5);
for w = 1:5,
    for g = 1:24,
        for m = 1:10,
            Vs (g,w,m) = Ac * Kf * D(g,w) * f * Ns(m)/(1e4);
        end
    end
end
Vs%;

%=====
%Plotting Induced Voltages against Primary Load (W) for 200, 300, 400,
%500... turns
%=====
clf
figure (1)
% jp = figure('Color',[1 1 1]);
subplot(2,2,1)
plot1=plot (Rp, Vs(:, :, 4));
set(plot1(1), 'LineWidth',1.0, 'Marker', 'o');
set(plot1(2), 'LineWidth',1.0, 'Marker', 'square')
set(plot1(3), 'LineWidth',2.0, 'LineStyle', '--');
set(plot1(4), 'LineWidth',1.0, 'Marker', 'diamond');
set(plot1(5), 'LineWidth',1.0, 'Marker', '^');
set(gca, 'XTick',200:200:2400)

grid on
xlabel({'Primary Load (W)'}, 'FontWeight', 'bold', 'FontSize',12);

ylabel({'Induced Voltage (Vrms)'}, 'FontWeight', 'bold', 'FontSize',12);

title({'Induced Voltage Vrs Primary Load (200 turns, #25 AWG)'},...
'FontWeight', 'bold', 'FontSize',12);
legend('6mm from MPL', '7mm from MPL', '8mm from MPL', '9mm from MPL',...
'10mm from MPL')

```

```

set(legend,...
    'Position',[0.146979166666665 0.750053049452929 0.113125...
    0.144132653061225],'FontSize',10);

subplot(2,2,2)
plot1=plot (Rp, Vs(:, :, 6));
set(plot1(1),'LineWidth',1.0,'Marker','o');
set(plot1(2),'LineWidth',1.0,'Marker','square')
set(plot1(3),'LineWidth',2.0,'LineStyle','--');
set(plot1(4),'LineWidth',1.0,'Marker','diamond');
set(plot1(5),'LineWidth',1.0,'Marker','^');
set(gca,'XTick',200:200:2400)

grid on
xlabel({'Primary Load (W)'},'FontWeight','bold','FontSize',12);

ylabel({'Induced Voltage (Vrms)'},'FontWeight','bold','FontSize',12);

title({'Induced Voltage Vrs Primary Load (300 turns, #25 AWG)'},...
    'FontWeight','bold','FontSize',12);
legend('6mm from MPL','7mm from MPL','8mm from MPL','9mm from
MPL','10mm from MPL')

set(legend,'Position',[0.602916666666662 0.758343865779456 0.09625
0.125]);

subplot(2,2,3)
plot1=plot (Rp, Vs(:, :, 8));
set(plot1(1),'LineWidth',1.0,'Marker','o');
set(plot1(2),'LineWidth',1.0,'Marker','square')
set(plot1(3),'LineWidth',2.0,'LineStyle','--');
set(plot1(4),'LineWidth',1.0,'Marker','diamond');
set(plot1(5),'LineWidth',1.0,'Marker','^');
set(gca,'XTick',200:200:2400)

grid on
xlabel({'Primary Load (W)'},'FontWeight','bold','FontSize',12);

ylabel({'Induced Voltage (Vrms)'},'FontWeight','bold','FontSize',12);

title({'Induced Voltage Vrs Primary Load (400 turns, #25 AWG)'},...
    'FontWeight','bold','FontSize',12);
legend('6mm from MPL','7mm from MPL','8mm from MPL','9mm from
MPL','10mm from MPL')

set(legend,'Position',[0.159166666666666 0.282578559657006 0.09625
0.125]);

subplot(2,2,4)
plot1=plot (Rp, Vs(:, :, 10));
set(plot1(1),'LineWidth',1.0,'Marker','o');
set(plot1(2),'LineWidth',1.0,'Marker','square')
set(plot1(3),'LineWidth',2.0,'LineStyle','--');

```

```

set(plot1(4), 'LineWidth', 1.0, 'Marker', 'diamond');
set(plot1(5), 'LineWidth', 1.0, 'Marker', '^');
set(gca, 'XTick', 200:200:2400)

grid on
xlabel({'Primary Load (W)'}, 'FontWeight', 'bold', 'FontSize', 12);

ylabel({'Induced Voltage (Vrms)'}, 'FontWeight', 'bold', 'FontSize', 12);

title({'Induced Voltage Vrs Primary Load (500 turns, #25 AWG)'}, ...
      'FontWeight', 'bold', 'FontSize', 12);
legend('6mm from MPL', '7mm from MPL', '8mm from MPL', '9mm from
MPL', '10mm from MPL')

set(legend, 'Position', [0.6091666666666654 0.294058151493739 0.09625
0.125]);

ha = axes('Position', [0 0 1 1], 'Xlim', [0 1], 'Ylim', [0
1], 'Box', 'off', 'Visible', 'off', 'Units', 'normalized', 'clipping' ,
'off');

text(0.5, 1, '\bf Induced Voltage for AMCC - 4
Core', 'HorizontalAlignment'...
, 'center', 'VerticalAlignment', 'top', 'FontWeight', 'bold', ...
      'FontSize', 14);

figure (2)
jpm = figure('Color', [1 1 1]);
subplot(2,2,1)
surf(Vs(:, :, 4), 'MarkerEdgeColor', 'none', 'LineWidth', 0.1, ...
      'LineStyle', 'none', ...
      'FaceColor', 'interp', ...
      'EdgeColor', 'none');
colorbar([0.0723362878896467 0.596376914225015 0.0076637121103533...
0.340686022837922]);
set(gca, 'XTick', 1:1:5)
set(gca, 'YTick', 0:5:25)
set(gca, 'ZTick', 0:0.5:5)

xlabel({'Dists., D1-D5 (6mm, 7mm, 8mm, 9mm, and
10mm)'}, 'FontWeight', 'bold', ...
      'FontSize', 8, 'Rotation', 9);

ylabel({'Primary Load
(W)'}, 'FontWeight', 'bold', 'FontSize', 8, 'Rotation', -16);

zlabel({'Induced Voltage (Vrms)'}, 'FontWeight', 'bold', 'FontSize', 8);

title({'Induced Voltage Vrs Primary Load (200 turns, #25 AWG)'}, ...
      'FontWeight', 'bold', 'FontSize', 10);

subplot(2,2,2)
surf(Vs(:, :, 6), 'MarkerEdgeColor', 'none', 'LineWidth', 0.1, ...

```



```

        'LineStyle','none',...
        'FaceColor','interp',...
        'EdgeColor','none');
colorbar([0.937336287889647 0.573649641497743 0.00641371211035334...
0.345930778082677]);
set(gca,'XTick',1:1:5)
set(gca,'YTick',0:5:25)
set(gca,'ZTick',0:0.5:5)

xlabel({'Dists., D1-D5 (6mm, 7mm, 8mm, 9mm, and
10mm)'}, 'FontWeight', 'bold', ...
'FontSize', 12, 'Rotation', 9);

ylabel({'Primary Load
(W)'}, 'FontWeight', 'bold', 'FontSize', 12, 'Rotation', -16);

zlabel({'Induced Voltage (Vrms)'}, 'FontWeight', 'bold', 'FontSize', 12);

title({'Induced Voltage Vrs Primary Load (300 turns, #25 AWG)'}, ...
'FontWeight', 'bold', 'FontSize', 14);

subplot(2,2,3)
surf(Vs(:, :, 8), 'MarkerEdgeColor', 'none', 'LineWidth', 0.1, ...
'LineStyle', 'none', ...
'FaceColor', 'interp', ...
'EdgeColor', 'none');
colorbar([0.0717112878896468 0.106643356643357 0.00828871211035319...
0.339160839160839]);
set(gca,'XTick',1:1:5)
set(gca,'YTick',0:5:25)
set(gca,'ZTick',0:0.5:5)

xlabel({'Dists., D1-D5 (6mm, 7mm, 8mm, 9mm, and
10mm)'}, 'FontWeight', 'bold', ...
'FontSize', 8, 'Rotation', 9);

ylabel({'Primary Load
(W)'}, 'FontWeight', 'bold', 'FontSize', 8, 'Rotation', -16);

zlabel({'Induced Voltage (Vrms)'}, 'FontWeight', 'bold', 'FontSize', 8);

title({'Induced Voltage Vrs Primary Load (400 turns, #25 AWG)'}, ...
'FontWeight', 'bold', 'FontSize', 10);

subplot(2,2,4)
surf(Vs(:, :, 10), 'MarkerEdgeColor', 'none', 'LineWidth', 0.1, ...
'LineStyle', 'none', ...
'FaceColor', 'interp', ...
'EdgeColor', 'none');
colorbar([0.937961287889648 0.134838452686554 0.00703871211035268...
0.340686022837922]);
set(gca,'XTick',1:1:5)
set(gca,'YTick',0:5:25)
set(gca,'ZTick',0:0.5:5)

```

```

xlabel({'Dists., D1-D5 (6mm, 7mm, 8mm, 9mm, and
10mm) '}, 'FontWeight', 'bold', ...
'FontSize', 12, 'Rotation', 9);

ylabel({'Primary Load
(W) '}, 'FontWeight', 'bold', 'FontSize', 12, 'Rotation', -16);

zlabel({'Induced Voltage (Vrms) '}, 'FontWeight', 'bold', 'FontSize', 12);

title({'Induced Voltage Vrs Primary Load (500 turns, #25 AWG) '}, ...
'FontWeight', 'bold', 'FontSize', 14);

ha = axes('Position', [0 0 1 1], 'Xlim', [0 1], 'Ylim', [0
1], 'Box', 'off', 'Visible', 'off', 'Units', 'normalized', 'clipping' ,
'off');

text(0.5, 1, '\bf Induced Voltage for AMCC - 4
Core', 'HorizontalAlignment'...
, 'center', 'VerticalAlignment', 'top', 'FontWeight', 'bold', ...
'FontSize', 14);

%=====
%%%%%%%%%%%%%%%%%%%%%%%%%%%%%%%%%%%%%%%%%%%%%%%%%%%%%%%%%%%%%%%%%%%%%%%%%%%%%% End %%%%%%%%%%%%%%%%%%%%%%%%%%%%%%%%%%%%%%%%%%%%%%%%%%%%%%%%%%%%%%%%%%%%%%%%%%%%%%%
%=====

%%%%%%%%%%%%%%%%%%%%%%%%%%%%%%%%%%%%%%%%%%%%%%%%%%%%%%%%%%%%%%%%%%%%%%%%%%%%%%
%%Title: Electromagnetic Harvesting to power Energy Management Sensors%
%%%%%%%%%%%%%%%%%%%%%%%%%%%%%%%%%%%%%%%%%%%%%%%%%%%%%%%%%%%%%%%%%%%%%%%%%%%%%%

%This MATLAB code is used to determine the following:

% 1. Plot experimental measurements of induced Open Circuit Voltages
% 2. Plot experimental measurements of short circuit currents

%*****
% Electromagnetic Harvesting to power Energy Management Sensors
clear all
close all
clc

% parameters for current carrying conductor
L = 15; % length (mm) copper #12 AWG conductor
C = 2.05/2; % conductor average radius (mm), NEC Table 8

%=====

P1 = [75; 150; 650; 725; 800; 1500; 1650; 2150; 2300]; % Primary Load

% Induced voltage #25 AWG wire - 200 turns, AMCC-4 Core (Open circuit
% voltage, Vso, V rms) and short circuit current Iso (mA)

Vso_a = [0.03; 0.05; 0.34; 0.35; 0.40; 0.82; 0.88; 1.17; 1.23];

```

```

Iso_a = [3.02; 4.58; 24.88; 26.41; 29.64; 57.7; 62.2; 82.3; 86.9];

% Induced voltage #25 AWG wire - 300 turns, AMCC-4 Core (Open circuit
% voltage, Vso, V rms) and short circuit current Iso (mA)

Vso_b = [0.05; 0.08; 0.52; 0.56; 0.62; 1.27; 1.37; 1.82; 1.92];

Iso_b = [1.98; 3.02; 16.40; 17.36; 19.45; 37.80; 40.80; 53.90; 56.9];

% Induced voltage #25 AWG wire - 400 turns, AMCC-4 Core (Open circuit
% voltage, Vso, V rms) and short circuit current Iso (mA)

Vso_c = [0.07; 0.1; 0.7; 0.75; 0.84; 1.7; 1.83; 2.43; 2.55];

Iso_c = [1.49; 2.28; 12.42; 13.10; 14.67; 28.5; 30.8; 40.6; 42.9];

% Induced voltage #25 AWG wire - 500 turns, AMCC-4 Core (Open circuit
% voltage, Vso, V rms) and short circuit current Iso (mA)

Vso_d = [0.08;0.13; 0.89; 0.93; 1.05; 2.12; 2.28; 3.04; 3.19];

Iso_d = [1.20; 1.82; 10.09; 10.53; 11.80; 23.0; 24.7; 33.01; 34.5];

%Plots of Lab results
figure(1)
jpp = figure('Color',[1 1 1]);
subplot(2,2,1)
plot(P1,Vso_a,'LineWidth',2)
set(gca,'XTick',200:200:2400)

xlabel({'Primary Load (W)'},'FontWeight','bold','FontSize',12);

ylabel({'Induced Voltage (Vrms)'},'FontWeight','bold','FontSize',12);

title({'Induced Voltage Vrs Primary Load (200 turns, #25 AWG)'},...
'FontWeight','bold','FontSize',12);
grid on

subplot(2,2,2)
plot(P1,Iso_a,'LineWidth',2)
set(gca,'XTick',200:200:2400)

xlabel({'Primary Load (W)'},'FontWeight','bold','FontSize',12);

ylabel({'Short Circuit Current (mA)'},'FontWeight','bold','FontSize',12);

title({'Short Circuit Current Vrs Primary Load (200 turns, #25 AWG)'},...
'FontWeight','bold','FontSize',12);
grid on
subplot(2,2,3)

```

```

plot(P1,Vso_b,'LineWidth',2)
set(gca,'XTick',200:200:2400)

xlabel({'Primary Load (W)'},'FontWeight','bold','FontSize',12);

ylabel({'Induced Voltage (Vrms)'},'FontWeight','bold','FontSize',12);

title({'Induced Voltage Vrs Primary Load (300 turns, #25 AWG)'},...
      'FontWeight','bold','FontSize',12);
grid on
subplot(2,2,4)
plot(P1,Iso_b,'LineWidth',2)
set(gca,'XTick',200:200:2400)

xlabel({'Primary Load (W)'},'FontWeight','bold','FontSize',12);

ylabel({'Short Circuit Current
(mA)'},'FontWeight','bold','FontSize',12);

title({'Short Circuit Current Vrs Primary Load (300 turns, #25
AWG)'},...
      'FontWeight','bold','FontSize',12);
grid on

ha = axes('Position',[0 0 1 1],'Xlim',[0 1],'Ylim',[0
1],'Box','off','Visible','off','Units','normalized','clipping' ,
'off');

text(0.5, 1,'\bf Experimental Induced Open Cct Voltage and Equivalent
Short cct Current with AMCC - 4 Core',...
     'HorizontalAlignment','center','VerticalAlignment','top',...
     'FontWeight','bold','FontSize',14);

figure(2)
jp = figure('Color',[1 1 1]);
subplot(2,2,1)
plot(P1,Vso_c,'LineWidth',2)
set(gca,'XTick',200:200:2400)

xlabel({'Primary Load (W)'},'FontWeight','bold','FontSize',12);

ylabel({'Induced Voltage (Vrms)'},'FontWeight','bold','FontSize',12);

title({'Induced Voltage Vrs Primary Load (400 turns, #25 AWG)'},...
      'FontWeight','bold','FontSize',12);
grid on
subplot(2,2,2)
plot(P1,Iso_c,'LineWidth',2)
set(gca,'XTick',200:200:2400)

xlabel({'Primary Load (W)'},'FontWeight','bold','FontSize',12);

```

```

ylabel({'Short Circuit Current
(mA) '}, 'FontWeight', 'bold', 'FontSize', 12);

title({'Short Circuit Current Vrs Primary Load (400 turns, #25
AWG) '}, ...
'FontWeight', 'bold', 'FontSize', 12);
grid on
subplot(2,2,3)
plot(P1,Vso_d, 'LineWidth', 2)
set(gca, 'XTick', 200:200:2400)

xlabel({'Primary Load (W) '}, 'FontWeight', 'bold', 'FontSize', 12);

ylabel({'Induced Voltage (Vrms) '}, 'FontWeight', 'bold', 'FontSize', 12);

title({'Induced Voltage Vrs Primary Load (500 turns, #25 AWG) '}, ...
'FontWeight', 'bold', 'FontSize', 12);
grid on
subplot(2,2,4)
plot(P1,Iso_d, 'LineWidth', 2)
set(gca, 'XTick', 200:200:2400)
xlabel({'Primary Load (W) '}, 'FontWeight', 'bold', 'FontSize', 12);

ylabel({'Short Circuit Current
(mA) '}, 'FontWeight', 'bold', 'FontSize', 12);

title({'Short Circuit Current Vrs Primary Load (500 turns, #25
AWG) '}, ...
'FontWeight', 'bold', 'FontSize', 12);
grid on

ha = axes('Position', [0 0 1 1], 'Xlim', [0 1], 'Ylim', [0
1], 'Box', 'off', 'Visible', 'off', 'Units', 'normalized', 'clipping' ,
'off');

text(0.5, 1, '\bf Experimental Induced Open Cct Voltage and Equivalent
Short cct Current with AMCC - 4 Core', 'HorizontalAlignment'...
, 'center', 'VerticalAlignment', 'top', 'FontWeight', 'bold', ...
'FontSize', 14);

%=====
% End %
%=====

%%%%%%%%%%%%%%%%%%%%%%%%%%%%%%%%%%%%%%%%%%%%%%%%%%%%%%%%%%%%%%%%%%%%%%%%%%%%%%
%%Title: Electromagnetic Harvesting to power Energy Management Sensors%
%%%%%%%%%%%%%%%%%%%%%%%%%%%%%%%%%%%%%%%%%%%%%%%%%%%%%%%%%%%%%%%%%%%%%%%%%%%%%%

%This MATLAB code is used to determine the following:

% 1. Plot experimental measurements of induced Voltages across 470 ohms
% 2. Plot experimental measurements of current through 470 ohms load

```

```

%*****
% Electromagnetic Harvesting to power Energy Management Sensors
clear all
close all
clc

% parameters for current carrying conductor
L = 15; % length (mm) copper #12 AWG conductor
C = 2.05/2; % conductor average radius (mm), NEC Table 8

%=====
Pl = [75; 150; 650; 725; 800; 1500; 1650; 2150; 2300];% Primary Load

% Induced voltage #25 AWG wire - 200 turns, AMCC-4 Core (connected load
=
% 470ohms) and short circuit current Iso (mA)

Vso_aa = [0.02; 0.06; 0.35; 0.39; 0.42; 0.83; 0.89; 1.18; 1.25];

Iso_aa = [1.54; 4.59; 24.95; 28.03; 29.69; 57.6; 62.3; 81.6; 87.2];

% Induced voltage #25 AWG wire - 300 turns, AMCC-4 Core (connected load
=
% 470ohms) and short circuit current Iso (mA)

Vso_bb = [0.06; 0.08; 0.53; 0.6; 0.63; 1.27; 1.37; 1.82; 1.92];

Iso_bb = [1.01; 3.02; 16.32; 17.34; 19.32; 37.80; 40.80; 53.60; 56.8];

% Induced voltage #25 AWG wire - 400 turns, AMCC-4 Core (connected load
=
% 470ohms) and short circuit current Iso (mA)

Vso_cc = [0.04; 0.12; 0.69; 0.78; 0.83; 1.68; 1.81; 2.40; 2.52];

Iso_cc = [1.49; 2.27; 12.37; 13.13; 14.62; 28.87; 31.15; 40.5; 43.1];

% Induced voltage #25 AWG wire - 500 turns, AMCC-4 Core (connected load
=
% 470ohms) and short circuit current Iso (mA)

Vso_dd = [0.05;0.14; 0.87; 0.97; 1.03; 2.05; 2.22; 2.94; 3.09];

Iso_dd = [1.19; 1.82; 9.87; 11.09; 11.73; 23.18; 25.02; 32.9; 34.8];

%Plots of Lab results
figure(1)
subplot(2,2,1)
plot(Pl,Vso_aa,'LineWidth',2)
set(gca,'XTick',200:200:2400)

xlabel({'Primary Load (W)'},'FontWeight','bold','FontSize',12);

```

```

ylabel({'Induced Voltage (Vrms)'}, 'FontWeight', 'bold', 'FontSize', 12);

title({'Induced Voltage Vrs Primary Load (200 turns, #25 AWG)'}, ...
      'FontWeight', 'bold', 'FontSize', 12);
grid on

subplot(2,2,2)
plot(P1,Iso_aa, 'LineWidth', 2)
set(gca, 'XTick', 200:200:2400)

xlabel({'Primary Load (W)'}, 'FontWeight', 'bold', 'FontSize', 12);

ylabel({'Sec. Load Current (mA)'}, 'FontWeight', 'bold', 'FontSize', 12);

title({'Sec. Load Current Vrs Primary Load (200 turns, #25 AWG)'}, ...
      'FontWeight', 'bold', 'FontSize', 12);
grid on
subplot(2,2,3)
plot(P1,Vso_bb, 'LineWidth', 2)
set(gca, 'XTick', 200:200:2400)

xlabel({'Primary Load (W)'}, 'FontWeight', 'bold', 'FontSize', 12);

ylabel({'Induced Voltage (Vrms)'}, 'FontWeight', 'bold', 'FontSize', 12);

title({'Induced Voltage Vrs Primary Load (300 turns, #25 AWG)'}, ...
      'FontWeight', 'bold', 'FontSize', 12);
grid on
subplot(2,2,4)
plot(P1,Iso_bb, 'LineWidth', 2)
set(gca, 'XTick', 200:200:2400)

xlabel({'Primary Load (W)'}, 'FontWeight', 'bold', 'FontSize', 12);

ylabel({'Sec. Load Current (mA)'}, 'FontWeight', 'bold', 'FontSize', 12);

title({'Sec. Load Current Vrs Primary Load (300 turns, #25 AWG)'}, ...
      'FontWeight', 'bold', 'FontSize', 12);
grid on

ha = axes('Position', [0 0 1 1], 'Xlim', [0 1], 'Ylim', [0
1], 'Box', 'off', 'Visible', 'off', 'Units', 'normalized', 'clipping' ,
'off');

text(0.5, 1, '\bf Experimental Induced Voltage and Equivalent Current
with AMCC - 4 prototype Core (Rs = 470 ohms)', ...
     'HorizontalAlignment', 'center', 'VerticalAlignment', ...
     'top', 'FontWeight', 'bold', 'FontSize', 14);

figure(2)
subplot(2,2,1)
plot(P1,Vso_cc, 'LineWidth', 2)
set(gca, 'XTick', 200:200:2400)

```

```

xlabel({'Primary Load (W)'}, 'FontWeight', 'bold', 'FontSize', 12);

ylabel({'Induced Voltage (Vrms)'}, 'FontWeight', 'bold', 'FontSize', 12);

title({'Induced Voltage Vrs Primary Load (400 turns, #25 AWG)'}, ...
      'FontWeight', 'bold', 'FontSize', 12);
grid on
subplot(2,2,2)
plot(P1,Iso_cc, 'LineWidth', 2)
set(gca, 'XTick', 200:200:2400)

xlabel({'Primary Load (W)'}, 'FontWeight', 'bold', 'FontSize', 12);

ylabel({'Sec. Load Current (mA)'}, 'FontWeight', 'bold', 'FontSize', 12);

title({'Sec. Load Current Vrs Primary Load (400 turns, #25 AWG)'}, ...
      'FontWeight', 'bold', 'FontSize', 12);
grid on
subplot(2,2,3)
plot(P1,Vso_dd, 'LineWidth', 2)
set(gca, 'XTick', 200:200:2400)

xlabel({'Primary Load (W)'}, 'FontWeight', 'bold', 'FontSize', 12);

ylabel({'Induced Voltage (Vrms)'}, 'FontWeight', 'bold', 'FontSize', 12);

title({'Induced Voltage Vrs Primary Load (500 turns, #25 AWG)'}, ...
      'FontWeight', 'bold', 'FontSize', 12);
grid on
subplot(2,2,4)
plot(P1,Iso_dd, 'LineWidth', 2)
set(gca, 'XTick', 200:200:2400)
xlabel({'Primary Load (W)'}, 'FontWeight', 'bold', 'FontSize', 12);

ylabel({'Sec. Load Current (mA)'}, 'FontWeight', 'bold', 'FontSize', 12);

title({'Sec. Load Current Vrs Primary Load (500 turns, #25 AWG)'}, ...
      'FontWeight', 'bold', 'FontSize', 12);
grid on

ha = axes('Position', [0 0 1 1], 'Xlim', [0 1], 'Ylim', [0
1], 'Box', 'off', 'Visible', 'off', 'Units', 'normalized', 'clipping' ,
'off');

text(0.5, 1, '\bf Experimental Induced Voltage and Equivalent Current
with AMCC - 4 prototype Core (Rs = 470 ohms)', ...
     'HorizontalAlignment', 'center', 'VerticalAlignment', ...
     'top', 'FontWeight', 'bold', 'FontSize', 14);

%=====
% End %
%=====

```



```

%*****

%%%%%%%%%%%%%%%%%%%%%%%%%%%%%%%%%%%%%%%%%%%%%%%%%%%%%%%%%%%%%%%%%%%%%%%%%%%%%%
%%Title: Electromagnetic Harvesting to power Energy Management Sensors%
%%%%%%%%%%%%%%%%%%%%%%%%%%%%%%%%%%%%%%%%%%%%%%%%%%%%%%%%%%%%%%%%%%%%%%%%%%%%%%

%This MATLAB code is used to determine the following:

%1. Compare simulated voltages with measured voltages from experiment
%*****

clear all
close all
clc

% parameters for current carrying conductor
L = 15; % length (mm) copper #12 AWG conductor
C = 2.05/2; % conductor average radius (mm), NEC Table 8

%=====
% Core properties
%=====
lm = 12.2e-2; % (m), Magnetic path length (from core data), AMCC-4 Core
lg = 120e-6; % (m), Air gap between cut cores (range 25-150 micro meter)
mu_m = 3000; % (H/m), permeability of core material (Amorphous, 2605)
mur = mu_m / (1 + mu_m * (lg / (lm))); % relative permeability of core
mu0 = 4e-7 * pi; % Magnetic permeability of free space or vacuum
mu = mu0 * mur; % (H/m), Effective permeability of core

%=====
% Calculating Magnetic Strength around current carrying conductor
%=====
% Primary Load (Watts)
Rp = 100:100:2400;

%Primary Voltage (V rms)
Vp = 120;

Ip = Rp/Vp;

r = (C:.025:30); % radial distances from current carrying
conductor, 0.025...
           % increments

B = zeros(1160,1);
for p = 1:24;
    for i = 1:1160;
        B(i,p) = (mu * Ip(p) * L * 1e-3) / (2*pi*r(i)*1e-3 * ...
            sqrt(4*(r(i)*1e-3)^2 + (L*1e-3)^2));
    end
end

%=====

```

```

% Selecting magnetic field strength values at radial distances from...
% current carrying conductor (1, 2, 3, 4, 5, 6, 7, 8, 9, 10mm ).
%Current range for #12 AWG conductor is 1 to 20A.
%=====

r1 =r(41:1160)'; % radial distances
Bac = B(41:1160,1:24); % Corresponding magnetic field strength
% H = [r1 B(41:1160,1:24)]; % Matrix of radial distances and magnetic
flux

%=====
% Calculating Induced voltage//Secondary turns//Output Voltage
%=====

% Core Parameters
%=====
Ac = 1.11;% Cross sectional area of core in cm.sq, AMCC-4 Core.

%Operating Parameters
%=====
Np = 1; % Number of turns of primary conductor ~1
f = 60; % output frequency in Hz
Kf = 4.44; % Waveform factor, sinewave.

% Magnetic field strength at (,6,7,8,9,10mm)from current carrying...
% conductor is used for calculation ~ approx distance from magnetic
path length(lm or MPL)
%=====
D = [Bac(201,:) ' Bac(241,:) ' Bac(281,:) ' Bac(321,:) ' Bac(361,:) '];

%=====
% Calculating induced voltages for various number of magnetic wire
windings around core. Ns = 50, 100, 150, 200, 250, 300, 350, 400, 450,
500.
%=====
Ns = (50:50:500);
Vs = zeros(24,5);
for w = 1:5,
    for g = 1:24,
        for m = 1:10,
            Vs (g,w,m) = Ac * Kf * D(g,w) * f * Ns(m)/(1e4);
        end
    end
end
Vs%;

%=====
%Comparing simulated and experimental voltages
%=====
Pl = [75; 150; 650; 725; 800; 1500; 1650; 2150; 2300];% Primary Load

% Induced voltage #25 AWG wire - 200 turns, AMCC-4 Core (Open circuit
% voltage, Vso, V rms) and short circuit current Iso (mA)

Vso_a = [0.03; 0.05; 0.34; 0.35; 0.40; 0.82; 0.88; 1.17; 1.23];

```

```

Iso_a = [3.02; 4.58; 24.88; 26.41; 29.64; 57.7; 62.2; 82.3; 86.9];

% Induced voltage #25 AWG wire - 300 turns, AMCC-4 Core (Open circuit
% voltage, Vso, V rms) and short circuit current Iso (mA)

Vso_b = [0.05; 0.08; 0.52; 0.56; 0.62; 1.27; 1.37; 1.82; 1.92];

Iso_b = [1.98; 3.02; 16.40; 17.36; 19.45; 37.80; 40.80; 53.90; 56.9];

% Induced voltage #25 AWG wire - 400 turns, AMCC-4 Core (Open circuit
% voltage, Vso, V rms) and short circuit current Iso (mA)

Vso_c = [0.07; 0.1; 0.7; 0.75; 0.84; 1.7; 1.83; 2.43; 2.55];

Iso_c = [1.49; 2.28; 12.42; 13.10; 14.67; 28.5; 30.8; 40.6; 42.9];

% Induced voltage #25 AWG wire - 500 turns, AMCC-4 Core (Open circuit
% voltage, Vso, V rms) and short circuit current Iso (mA)

Vso_d = [0.08;0.13; 0.89; 0.93; 1.05; 2.12; 2.28; 3.04; 3.19];

Iso_d = [1.20; 1.82; 10.09; 10.53; 11.80; 23.0; 24.7; 33.01; 34.5];

clf
figure (1)
jp = figure('Color',[1 1 1]);
subplot(2,2,1)
plot1=plot (Rp, Vs(:, :, 4));
hold on
plot(P1,Vso_a, 'LineWidth',2, 'Color',[0 0 0])

annotation('textarrow',[0.34125 0.394375],...
    [0.843387755102041 0.767857142857143], 'TextEdgeColor','none',...
    'String',{'Experimental plot'}, 'FontWeight','bold', 'FontSize',12);
% grid on
set(plot1(1), 'LineWidth',1.0, 'Marker','o');
set(plot1(2), 'LineWidth',1.0, 'Marker','square')
set(plot1(3), 'LineWidth',2.0, 'LineStyle','--');
set(plot1(4), 'LineWidth',1.0, 'Marker','diamond');
set(plot1(5), 'LineWidth',1.0, 'Marker','^');
set(gca, 'XTick',200:200:2400)

xlabel({'Primary Load (W)'}, 'FontWeight', 'bold', 'FontSize',12);

ylabel({'Induced Voltage (Vrms)'}, 'FontWeight', 'bold', 'FontSize',12);

title({'Induced Voltage Vrs Primary Load (200 turns, #25 AWG)'},...
    'FontWeight', 'bold', 'FontSize',12);
legend('6mm from MPL', '7mm from MPL', '8mm from MPL', '9mm from MPL',...
    '10mm from MPL')

```

```

set(legend,...
    'Position',[0.1469791666666665 0.750053049452929 0.113125...
    0.144132653061225],'FontSize',10);

subplot(2,2,2)
plot1=plot (Rp, Vs(:, :, 6));
hold on
zz=plot (Pl,Vso_b, 'LineWidth',2, 'Color',[0 0 0]);

annotation('textarrow',[0.790625 0.836875],...
    [0.856142857142857 0.775510204081632],'TextEdgeColor','none'...
    , 'String',{'Experimental plot'}, 'FontWeight','bold', 'FontSize',12);

set(plot1(1), 'LineWidth',1.0, 'Marker','o');
set(plot1(2), 'LineWidth',1.0, 'Marker','square')
set(plot1(3), 'LineWidth',2.0, 'LineStyle','--');
set(plot1(4), 'LineWidth',1.0, 'Marker','diamond');
set(plot1(5), 'LineWidth',1.0, 'Marker','^');
set(gca, 'XTick',200:200:2400)

xlabel({'Primary Load (W)'}, 'FontWeight','bold', 'FontSize',12);

ylabel({'Induced Voltage (Vrms)'}, 'FontWeight','bold', 'FontSize',12);

title({'Induced Voltage Vrs Primary Load (300 turns, #25 AWG)'},...
    'FontWeight','bold', 'FontSize',12);
legend('6mm from MPL','7mm from MPL','8mm from MPL','9mm from
MPL','10mm from MPL')

set(legend, 'Position',[0.6029166666666662 0.758343865779456 0.09625
0.125]);

% grid on

subplot(2,2,3)
plot1=plot (Rp, Vs(:, :, 8));
hold on
plot (Pl,Vso_c, 'LineWidth',2, 'Color',[0 0 0])

annotation('textarrow',[0.34 0.37875],...
    [0.374810318664643 0.288315629742033],'TextEdgeColor','none',...
    'String',{'Experimental plot'}, 'FontWeight','bold', 'FontSize',12);

set(plot1(1), 'LineWidth',1.0, 'Marker','o');
set(plot1(2), 'LineWidth',1.0, 'Marker','square')
set(plot1(3), 'LineWidth',2.0, 'LineStyle','--');
set(plot1(4), 'LineWidth',1.0, 'Marker','diamond');
set(plot1(5), 'LineWidth',1.0, 'Marker','^');
set(gca, 'XTick',200:200:2400)

% grid on
xlabel({'Primary Load (W)'}, 'FontWeight','bold', 'FontSize',12);

ylabel({'Induced Voltage (Vrms)'}, 'FontWeight','bold', 'FontSize',12);

```

```

title({'Induced Voltage Vrs Primary Load (400 turns, #25 AWG)'},...
      'FontWeight','bold','FontSize',12);
legend('6mm from MPL','7mm from MPL','8mm from MPL','9mm from
MPL','10mm from MPL')

set(legend,'Position',[0.159166666666666 0.282578559657006 0.09625
0.125]);

subplot(2,2,4)
plot1=plot (Rp, Vs(:, :, 10));
hold on
plot(P1,Vso_d,'LineWidth',2,'Color',[0 0 0])

annotation('textarrow',[0.79 0.82875],...
           [0.378362670713202 0.295902883156297],'TextEdgeColor','none',...
           'String',{'Experimental plot'},'FontWeight','bold','FontSize',12);

set(plot1(1),'LineWidth',1.0,'Marker','o');
set(plot1(2),'LineWidth',1.0,'Marker','square')
set(plot1(3),'LineWidth',2.0,'LineStyle','--');
set(plot1(4),'LineWidth',1.0,'Marker','diamond');
set(plot1(5),'LineWidth',1.0,'Marker','^');
set(gca,'XTick',200:200:2400)

% grid on
xlabel({'Primary Load (W)'}, 'FontWeight','bold','FontSize',12);

ylabel({'Induced Voltage (Vrms)'}, 'FontWeight','bold','FontSize',12);

title({'Induced Voltage Vrs Primary Load (500 turns, #25 AWG)'},...
      'FontWeight','bold','FontSize',12);
legend('6mm from MPL','7mm from MPL','8mm from MPL','9mm from
MPL','10mm from MPL')

set(legend,'Position',[0.609166666666665 0.294058151493739 0.09625
0.125]);

ha = axes('Position',[0 0 1 1],'Xlim',[0 1],'Ylim',[0
1],'Box','off','Visible','off','Units','normalized','clipping' ,
'off');

text(0.5, 1, '\bf Comparison between Simulated and Experimental Induced
Voltage with AMCC - 4 Core','HorizontalAlignment'...
, 'center','VerticalAlignment', 'top','FontWeight','bold',...
'FontSize',14);

%=====
% End %
%=====

```

REFERENCES

- [1] <<<http://world-nuclear.org/info/inf16.html>>>.
- [2] U.S. Department of Energy Brochure, "The Smart grid: An Introduction," Office of Electricity Delivery and Energy Reliability, Sep. 2008.
- [3] U.S. Environmental Protection Agency, "INVENTORY OF U.S. GREENHOUSE GAS EMISSIONS AND SINKS: 1990 – 2009", Washington, DC, April, 2011.
- [4] http://www.eia.gov/cneaf/electricity/epm/epm_sum.html
- [5] S. Fred Singer, "HOT TALK, COLD SCIENCE: Global Warming's Unfinished Debate", The Independent Institute, CA, 1999.
- [6] Jarret Wollstein, "Global Warming: Myths and Reality",
<<<http://www.isil.org/resources/fnn/2007june/global-warming-hoax.html>>>.
- [7] "What Really Happened",
<<<http://whatreallyhappened.com/WRHARTICLES/globalwarming.html>>>.
- [8] Wisam Nader, "Real-time Monitoring, Home Automation and Sustainability," Master of Science Thesis, UNL, May 2011.
- [9] Frank Lambert et. al, "A Scoping Study of Electric and Magnetic Field Energy Harvesting for Wireless Sensor Networks in Power System Applications", ECCE 2009, IEEE, CA, 2009.
- [10] Guangming et. al. "A Wireless Power Outlet System for Smart Homes" IEEE Transactions on Consumer Electronics, Vol. 54, No. 4, 2008.
- [11] NFPA 70. "National Electrical Code 2011", Massachusetts, 2010.
- [12] Shenzhen Sailwider Electronics Co., Ltd, <<<http://www.sailwider-smartpower.com/>>>.
- [13] Microstrain, <<<http://www.microstrain.com/>>>.
- [14] Crossbow, << <http://www.xbow.com/>>>.
- [15] Digi International, <<<http://www.digi.com/>>>.
- [16] Starman Electric, <<[http:// www.starmanelectric.com](http://www.starmanelectric.com)>>.
- [17] LS Research, <<<http://www.lsr.com>>>.
- [18] Linx Technologies, <<<http://www.linxtechnologies.com>>>.
- [19] Silicon Labs, <<<http://www.silabs.com>>>.

- [20] Daniele Davino, Alessandro Guistiniani, and Ciro Visone, "A Two-Port Nonlinear Model for Magnetoelastic Energy-Harvesting Devices", IEEE Transactions on Industrial Electronics, Vol. 58, No.6, pp. 2556-2564, June 2011.
- [21] Sichuan Ma, et al. "Energy Harvesting and Its Challenges in Smart Grid" unpublished.
- [22] Laurence O'Sullivan, <<<http://laurenceosullivan.suite101.com/worlds-largest-producers-of-alternative-energy-a210170>>>. 2010.
- [23] Greenshine,<< <http://www.streetlamp-solar.com/wide-installation-of-solar-street-lights-remains-to-be-research.html>>>.
- [24] James P. Dunlop, "Photovoltaic Systems", Orland Park, IL, USA, 2010.
- [25] Faruk Yildiz, "Potential Ambient Energy-Harvesting Sources and Techniques." Journal of Technology Studies, Vol. 35, No. 1, pp. 40-48, 2009. S. P.
- [26] Beeby, M. J. Tudor and N. M. White, "Energy harvesting vibration sources for microsystems applications," Measurement Science and Technology, Vol. 17, pp. 175–195, 2006.
- [27] J.W. Judy, "Microelectromechanical Systems (MEMS): Fabrication, Design and Applications," *Smart Mater. Struct.*, Vol. 10, pp. 1115–1134, 2001.
- [28] A.-L. Annala and I. Oy and U. Friedrich, "Passive long distance multiple access UHF RFID System (RFID)," Nov. 2002, Palomar Project, European Commission, Public Report, Project No. IST 1999-10339.
- [29] N. S. Shenck and J. A. Paradiso, "Energy Scavenging with Shoe-mounted Piezoelectrics," *IEEE Micro.*, Vol. 21, pp. 30–41, 2001.
- [30] T. Starner, S. Mann, B. Rhodes, J. Levine, J. Healey, D. Kirsch, R. W. Picard, and A. Pentland, "Augmented Reality Through Wearable Computing", MIT Media Laboratory Perceptual Computing Section Technical Report, No. 397, 1997.
- [31] C. Alippi and C. Galperti, "An Adaptive System for Optimal Solar Energy Harvesting in Wireless Sensor Network Nodes," IEEE Transactions on Circuits and Systems, vol. 55, no. 6, Jul. 2008.
- [32] <<<http://www.roachman.com/thermic/>>>.
- [33] Piezo Patch, "Energy harvesting with piezo patch transducers."
<<<http://www.peizo.com>>>.
- [34] The Piezoelectric Effect, <<<http://www.aurelienr.com/electronique/piezo/piezo.pdf>>>.

- [35] César Meneses Ghiglino, “ Ultra-Wideband (UWB) rectenna design for Electromagnetic Energy Harvesting” Engineering Degree Thesis, UNIVERSITAT POLITÉCNICA DE CATALUNYA, Oct. 2010.
- [36] James O. McSpadden, Lu Fan and Kai Chang, "Design and Experiments of a High-Conversion-Efficiency 5.8-GHz Rectenna", IEEE TRANSACTIONS ON MICROWAVE THEORY AND TECHNIQUES, VOL. 46, No. 12, DEC. 1998.
- [37] USI, <<<http://www.usi-power.com>>>.
- [38] Protura,<< <http://www.protura.no>>>.
- [39] Torkiat Taithongchai and Ekachai Leelarasmee, "Adaptive Electromagnetic Energy Harvesting Circuit for Wireless Sensor Application" IEEE, ECTI-CON 2009. 6th International Conference, 2009.
- [40] D. Pimentel and P. Musilek, "POWER MANAGEMENT WITH ENERGY HARVESTING DEVICES",Electrical and Computer Engineering (CCECE), 2010 23rd Canadian Conference.
- [41] Rohit Moghe,Yi Yang, Frank Lambert and Deepak Divan "A Scoping Study of Electric and Magnetic Field Energy Harvesting for Wireless Sensor Networks in Power System Applications", Energy Conversion Congress and Exposition, IEEE 2009.
- [42] R. H. Bhuiyan, R. A. Dougal, and M. A. Ali, “A miniature energy harvesting device for wireless sensors in electric power system,” IEEE, Sensors Journal, vol. 10, no. 7, pp. 1249–1258, Jul. 2010.
- [43] Metglas POWERLITE C-Cores, available: www.metglas.com.
- [44] Fawwaz T, Ulaby et al., Fundamentals of Applied Electromagnetics , 6th ed, Prentice Hall, Boston, 2010.
- [45] Hugh D. Young et al, University Physic, 6th ed, Addison Wesley, Massachusetts, 1984.
- [46] Nathan Ida, “Engineering Electromagnetics” 2ed, Springer, New York, 2004.
- [47] U.S. Department of the Interior, " Transformers: Basics, Maintenance, and Diagnostics", Bureau of Reclamation April 2005.
- [48] <<http://www.physics.sjsu.edu/becker/physics51/ac_circuits.htm>>.
- [49] R. W. Erickson, "Fundamentals of Power Electronics", New York: Chapman and Hall, May 1997.

- [50] Colonel Wm. T. McLyman, “Transformer and Inductor Design Handbook”, Marcel Dekker Inc, New York, 2004.
- [51] Magnetic Properties METGLAS Powerlite Cores, << <http://www.metglas.com>>>.
- [52] NFPA 70. “National Electrical Code 2008”, Massachusetts, 2007.
- [53] Larbi Hakimi, Soft Magnetic Materials, Hitachi Metals America, Ltd. Jan. 2012.
- [54] << http://www.jr.com/rca/pe/rca_wp2uwr/>>.
- [55] << <http://www.zdnet.com/blog/gadgetreviews/usb-power-outlets-for-the-home-why-didnt-we-think-of-this/9901>>>.
- [56] <<<http://www.blamza.com/usb-wall-socket-for-your-home/>>>.
- [57] U-Socket, <<<http://fastmac.com/usocket.php>>>, 2008.